AN ASSESSMENT OF FUTURE COASTAL LAND LOSS IN GALVESTON, CHAMBERS, AND JEFFERSON COUNTIES, TEXAS

APPROVED:

John M Sharp

W. E. Galloway

R a Morton

AN ASSESSMENT OF FUTURE COASTAL LAND LOSS IN GALVESTON, CHAMBERS, AND JEFFERSON COUNTIES, TEXAS

by

Steven John Germiat, B.S.

THESIS

Presented to the Faculty of the Graduate School of

The University of Texas at Austin

in Partial Fulfillment

of the Requirements

for the Degree of

MASTER OF ARTS

THE UNIVERSITY OF TEXAS AT AUSTIN

December, 1988

Acknowledgements:

This thesis is the result of many people's time and effort. Thanks first and foremost to my family for all the support and encouragement throughout my life. Thank you Mom and Dad, you're the greatest. Thanks also to my brother, Tom. Rock n Roll.

Special gratitude to my advisor, Dr. John M. Sharp, Jr. (Jack), for offering technical insight, unending enthusiasm for the project, and undying patience with me when it seemed this culmination might never arrive. Committee members Dr. Robert Morton and Dr. William Galloway generously gave their time and editing expertise to mend scientific loopholes and make this thesis more concise. Discussions with Dr. Morton provided numerous insights into shoreline processes and dynamics of the study area and of the entire Texas Coast .

Sincere thanks to all the great people I've known during my three years at UT. The list is very long, and certainly incomplete. Thank you to Bob "Fr. Flanagan" Roback for taking me into rehabilitation at the Driftwood Home for Wayward Boys. Gracias and adios to the other wayward souls: Dan-o, Dante the Inferno, Chuck, and the newest Boy, Lars. Thanks to Wham-o, Ozone, the Cow (et al), and Dub...you're animals. This place would be hard to take if not for the many friends you make: Jennifer G., Drew D., Tim R., Peter H. & Celia C., Randy L., Carl F., Will S., Becky C., Kiki B., Danny B., Bill D., Joe G. and Jeff R., the Ogres (don't be weak), Ether Bunnies, and umpteen other folks, thanks for the fun times. Jim Durrett, Bob Asgian and Jerry "Swiss cheese" McNeish - the Black Cat memories are legend. To Harris, for teaching me the art of nerf while helping me

break the monotony of making progress. To Tod Sutherland...it's not too late to say Thanks.

Gratitude is extended to Ron Neighbors and Bud Holzschuh (Harris-Galveston Coastal Subsidence District), R.K. Gabrysch (USGS-Houston), Alex Williamson (USGS-Austin), Samuel Reese (National Geodetic Survey), Karen Ramsey et al (LA GS), all of whom contributed to this research. Special thanks to Dr. Kenneth Foote of the UT Dept. of Geography for allowing me generous access to the computer cartography lab. Sincere thanks to Dennis Trombatore for going well out of his way for me and for all Geo grads.

My appreciation is extended to the Gulf Coast Association of Geological Societies for partial financial support of this project.

My love and gratitude to Kay Allison Higgins for helping me live beyond the drudgery.

Thanks to myself for not putting my fist through the screen of a Macintosh on more than one occasion.

ABSTRACT

An Assessment of Future Coastal Land Loss
in Galveston, Chambers, and Jefferson Counties,
Texas

by

Steven John Germiat, B.S.

Supervising Professor: Dr. John M. Sharp, Jr.

Loss of coastal land has been occurring along the Upper Texas Gulf Coast over the historical record. This loss of land will continue into the future, probably at increasing rates due to accelerated sea-level rise caused by global warming (i.e. the "greenhouse effect"). Three scenarios for shoreline retreat and land loss to the year 2050 are developed for the uppermost 200 km of the Texas Coast, between Sabine Pass and the mouth of the Trinity River. The scenarios (baseline, low-rise and high-rise) integrate best available estimates of sea-level rise in the next century with empirical relations between relative sea-level rise and shoreline movement during a baseline period (1930-1974 or 1982, depending on the availability of shoreline movement data) for each of 10 shoreline segments.

Loss of coastal land results from both erosion and submergence of the coastline due to relative sea-level rise. Relative sea-level (RSL) rise, in turn, encompasses eustatic rise and land-surface subsidence. Baseline rates of RSL rise at

Pier 21 on Galveston are 6.9 mm/yr (1930-1974) and 7.6 mm/yr (1930-1982). Data from nonsubsiding tidal gages along the Florida Gulf Coast are used to define a 2.2 mm/yr baseline rate of eustatic rise within the Gulf of Mexico. Land-surface subsidence accounts for the residual 4.7 and 5.4 mm/yr. Land-surface subsidence within the study area is the result of undifferentiated natural consolidation of clay-rich sediments and regional subsurface depressurization caused by production of oil and gas. Groundwater pumpage is minimal within the area and is not considered a cause of subsidence, although large-scale pumping in the metropolitan Houston area has probably caused subsidence along the eastern shore of Trinity Bay.

The baseline scenario assumes a constant rate of RSL rise, resulting in a rise of 0.45-0.49 m by 2050. At 2050, RSL rises of 0.66-0.70 m in the low-rise scenario and 0.88-0.92 m in the high-rise scenario are predicted by combining low- and high-rise estimates of eustatic rise developed from a synthesis of nine recently-published projections with a constant baseline rate of subsidence. The multiplicative factors of approximately 1.5 for the low-rise and 2.0 for the high-rise scenario are calculated from the ratios of projected RSL rise to baseline RSL rise at 2050. These factors are integrated into the baseline relation between RSL rise and shoreline movement to estimate shoreline displacement and subsequent loss of land by 2050 in each of the 10 shoreline segments. The estimated net change of land area by 2050 for the entire study area coastline is -17.2 km^2 (4248 acres) in the baseline scenario, -25.2 km^2 (6224 acres) in the low-rise scenario, and -33.8 km^2 (8349 acres) in the high-rise scenario.

Shoreline retreat and land loss scenarios developed in this study represent conservative estimates. Recent rates of relative sea-level rise (between 1958 and the

mid-1980s) at Pier 21 and at Sabine Pass exceed 11 mm/yr, 50-60% higher than the calculated long-term rates of 6.9 and 7.6 mm/yr, used as the baseline for this analysis. Therefore projected RSL rise by 2050 are conservative and may underestimate shoreline displacement and coastal land loss. These projections should be considered in the future development of and use of the Texas Coast.

TABLE OF CONTENTS

TABLE OF CONTENTS (continued)

List of Tables

List of Figures

List of Figures (continued)

plate 1 pocket

1.0 Introduction:

1.1 General Statement:

The shoreline along most of the Texas Gulf Coast has been generally retreating over the historical record, resulting in a continual loss of coastal land. Loss of land is occurring at present and will continue, probably at accelerated rates, into the future. Coastal land loss is the result of two major processes: submergence due to relative sea-level rise, and erosion.

Relative sea-level rise can be divided into two components: (1) land-surface subsidence, the vertical sinking of the land surface with respect to a stable datum,usually mean sea level, and (2) eustatic sea-level rise, the worldwide rise in 'absolute' sea level. Land-surface subsidence can be the result of several processes. In the Texas Gulf Coast, the principal processes are the withdrawal of subsurface fluids (water, oil, and gas), and consolidation caused by natural loading and dewatering of clay-rich sedimentary sequences. In addition, we now know that mean sea level can not be considered a stable datum. Generally, eustatic sea level has been rising since the final retreat of Pleistocene glaciers approximately 18,000 years ago (Fisher and others, 1973). Furthermore, accelerated sea-level rise is anticipated over the next century as a result of global warming induced by increased concentrations of carbon dioxide, methane, chlorofluorocarbons, nitrous oxide, and other trace gases. This phenomenon is termed the "greenhouse effect". Relative sea-level changes are important because a small vertical rise in sea level can cause a large landward displacement of the shoreline in low-lying coastal areas. Land-surface subsidence coupled with eustatic rise can cause permanent inundation, increased

severity of coastal erosion and storm flooding, and intrusion of saltwater into coastal aquifers.

Erosion of the Texas Coast has caused major losses of land during the past century. Long-term trends indicate that rates of erosion and the total length of eroding shoreline are increasing, perhaps in response to rising relative sea level. There is no evidence to suggest that these trends will reverse (Morton, 1977).

1.2 Objectives and Methodology:

The principal objective of this study is to develop reasonable scenarios for coastal land loss within the study area to the year 2050. The three scenarios, baseline, low-rise, and high-rise, are based on future projections of shoreline recession caused by the undifferentiated effects of submergence and erosion. This is the most realistic approach of making projections since it is extremely difficult to separate the components of submergence and erosion for a measured shoreline displacement. The generation of future projections for land loss involves calculating a "multiplicative acceleration factor" for shoreline retreat. The factor is equal to the ratio of projected future relative sea-level rise to historical relative sea-level rise, determined for a "baseline" period. The acceleration factor is multiplied by baseline rates of shoreline movement to estimate shoreline displacements in accelerated sea-level rise scenarios, assuming that higher rates of relative sea-level rise will cause proportionally higher rates of shoreline movement. This analysis assumes that the rate of land-surface subsidence will be constant over the projection period, therefore accelerated relative sea-level rise will be caused solely by accelerated eustatic rise. Three projections of future eustatic rise (low, middle, and high) are generated from a

simple statistical synthesis of nine projections published in the past three years by four scientific organizations. The four organizations are the National Research Council, combining the 1983 results of the Carbon Dioxide Assessment Committee (National Research Council, 1983) and the 1985 results of the Polar Research Board (National Research Council, 1985); the U.S. Environmental Protection Agency (Hoffman and others, 1986); the Scientific Committee on Problems of the Environment (Robin,1986); and the Marine Board of the National Research Council (Marine Board, 1987). Land-loss scenarios begin at the year 1985 in order to remain consistent with the eustatic projections, which use 1985 as year zero. A summary of the four organizations' methodologies for generating eustatic sea-level rise projections is presented in Appendix 1.

An empirical relation between historical rates of shoreline movement and relative sea-level rise is developed for discrete segments of the shoreline of the study area. The relation is developed using data for a baseline period: 1930 to 1974 or 1982, depending on the availability of shoreline-movement data for a given segment. The shoreline is discretized on the basis of differences in shoreline type and general uniformity in movement within a segment over the historical record. Past trends of shoreline movement are obtained from published reports (Morton, 1975; Paine and Morton, 1986) that relied on analysis of aerial photographs and, for times prior to 1930, vintage topographic maps and coastal charts. Past trends of relative sea-level rise are calculated by linear regression analysis of tidal gage data for selected stations along the Gulf of Mexico. Tidal stations at Sabine Pass, on the eastern edge of the study area, and at Pier 21 on Galveston, on the western edge, are used to define relative sea-level trends for the study area. The eustatic component of relative sea-

level rise for the Gulf of Mexico is estimated from tidal stations along the Florida Gulf Coast since subsidence there is assumed to be negligible relative to the subsidence of the Texas Coast (Swanson and Thurlow, 1973). The component of land-surface subsidence for the study area is determined by subtracting the eustatic component from the rate of relative sea-level rise measured at stations bordering the study area.

1.2.1 Key assumptions:

This study focuses on relative sea-level rise as the principal cause of increased rates of both submergence and erosion, which together produce shoreline retreat and loss of coastal land. Clearly, other factors contribute to shoreline changes. These factors include altered precipitation and wind patterns associated with climatic changes, storm frequency and intensity, sediment budget, and human activities (Paine and Morton, 1986). It is not possible, at present, to separate and quantify the effects of these factors on shoreline movement, although each is directly or indirectly involved in historical rates of relative sea-level rise and shoreline movement. Therefore, a key assumption of this study is that all other contributing factors are accounted for within the empirical relation between historical rates of relative sea-level rise and shoreline movement for a given segment of shoreline.

A second key assumption is that the baseline rate of land-surface subsidence (1930 to 1974 or 1982) will be constant into the future. This may be an overestimate because subsidence due to groundwater withdrawal in the Houston area may be a significant component of the measured relative sea-level rise at the Pier 21 and Pleasure Pier gages on Galveston. However, subsidence due to groundwater

withdrawal in the Houston-Galveston area has been declining since the late-1970s due to pumping restrictions (Williams and Ranzau, 1985). On the other hand, very little groundwater has been pumped near the gage at Sabine Pass, yet the rate of relative sea-level rise between 1958 and the mid-1980s is nearly identical at both the Sabine Pass gage and the Pier 21 gage (fig. 1). The land-surface subsidence occurring at Sabine Pass, and to a lesser extent at Galveston, may be the result of natural consolidation of thick sequences of poorly-consolidated Holocene muddy sediment within buried Pleistocene river valleys. It is reasonable to consider this rate of subsidence constant over a sixty-year projection period. Regional subsurface depressurization resulting from widespread production of oil and gas may also cause subsidence within the study area.

An alternate method of dealing with the projection of rates of land-surface subsidence would be to maintain a constant proportion (equal to the inferred proportion during the baseline period) of subsidence to eustatic rise. By this method, the rate of subsidence would increase as the rate of eustatic rise increased, resulting in rates of rise more than double those calculated by assuming a constant rate of subsidence. I believe this method is unreasonable, however, because there is no evidence to suggest that land-surface subsidence will accelerate at the same rate as eustatic rise.

The third assumption is that the historical rate of relative sea-level rise has been approximately constant across the study area. The rate of relative sea-level rise between 1958 and the mid-1980s is approximately equal at the Sabine Pass and Pier 21 gages (11.4 mm/yr and 11.1 mm/yr, respectively) (fig.1). The similarity in annual sea-level fluctuations, as well as the nearly identical overall rate of rise,

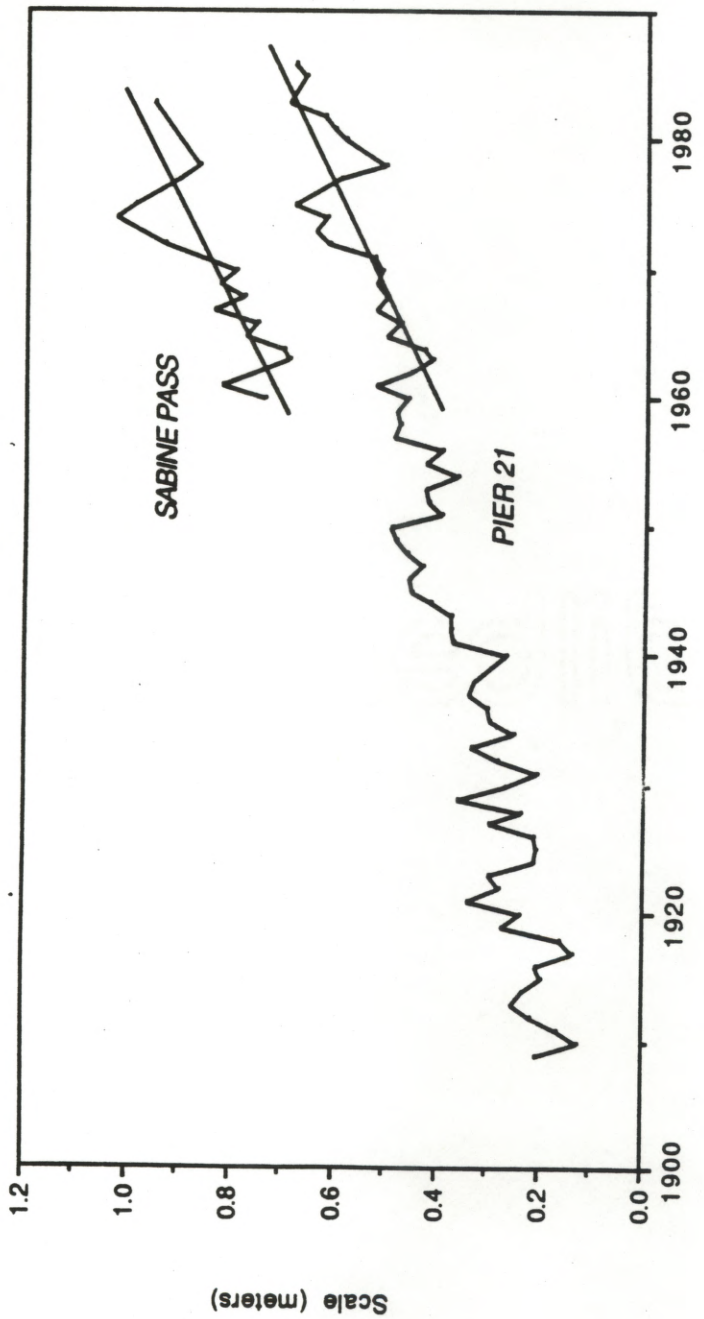

Figure 1. Tidal records (annual means of tide height) with lines of regression for Sabine Pass and Pier 21 tidal stations. Rate of rise = 11.4 mm/yr at Sabine Pass (1958-1983), and 11.1 mm/yr at Pier 21 (1958-1986) (Data from the National Ocean Service, NOAA).

indicate that the assumption is reasonable. The rates of relative sea-level rise for the baseline period are calculated from the Pier 21 data because it is the gage with the longest record on the Texas Gulf Coast (1908-1986), and the only Texas gage with a record preceding 1930.

A fourth assumption is that the rate of relative sea-level rise measured at tidal stations along the Florida Coast represents eustatic rise in the Gulf of Mexico over the period of record. The validity of this assumption is discussed further in section 3.1.2.2.

1.2.2 Development of scenarios:

Baseline, low-rise, and high-rise scenarios for land loss by the year 2050 are developed in this study. A projection target year of 2050 was chosen since coastal developments generally have associated infrastructure, such as roads and utilities, that are usually planned to endure for periods in excess of 50 years. Sixty-five years (1985-2050) is a long enough period of projection for significant changes to occur, yet not so long that the scenarios lose validity.

The baseline scenario is generated by linear extrapolation of the trend for shoreline movement for the baseline period 1930 to 1974 or 1982, depending on the available shoreline movement data for a particular segment. The baseline rise in relative sea level is also calculated. An empirical relation between shoreline retreat and relative sea-level rise is developed for each shoreline segment from these baseline rates. The baseline rise in eustatic sea level is estimated from tidal gages on the Florida Gulf Coast, and the baseline rate of land-surface subsidence is the difference between the rate of relative sea-level rise and the rate of eustatic rise.

The low-rise scenario for relative sea level at 2050 is generated by adding the middle eustatic-rise projection and the component of subsidence (the baseline subsidence rate times 65 years). A low-rise multiplicative factor for relative sea-level rise is the ratio of the low-rise estimate to the baseline rate. The low-rise rate of movement for an individual shoreline segment is then calculated by multiplying the factor by the baseline rate of shoreline retreat.

The high-rise scenario for relative sea-level is generated in a similar manner, using the high estimate of relative sea-level rise calculated by adding the high-eustatic-rise projection at 2050 to the subsidence component at 2050. The high-rise multiplicative factor is then used to calculate a rate of shoreline displacement for each segment.

1.3 Significance of Study:

The combination of relative sea-level rise and removal of coastal sediment by erosion presents a number of economically-significant problems for coastal regions. The most obvious problems are the submergence of land in low-lying areas and the potential subjection of more land to the temporary flooding resulting from storm surge and/or high tides. These two hazards account for most of the costs and losses in property value that have been historically associated with relative sea-level rise (Jones, 1976). The Houston-Galveston area has experienced severe subsidence-related flooding in the past decade. For example, subsidence at the San Jacinto Battlefield State Park resulted in the permanent inundation of more than 0.4 km^2 (100 acres) of park land by 1974, with losses estimated at $4.5 million (Jensen, 1985). Brownwood, a subdivision of Baytown, has subsided nearly 2.5 m since

1915 (Gabrysch, 1984). In both 1979 and 1983, Brownwood flooded seriously, causing extensive property damage. Many homes have been permanently inundated. The U.S. Army Corps of Engineers has recommended that the entire subdivision, consisting of 448 homes occupied by 1550 residents, be purchased by the federal government and the inhabitants be relocated at an estimated cost of $40 million (Gabrysch, 1984). Most homes in the subdivision have been abandoned. The present study focuses on permanent loss of low-lying coastal land as the primary effect of rising relative sea level combined with continuing shoreline erosion.

The development of future projections necessarily involves a certain amount of speculation. A scenario analysis is a reasonable way of dealing with the inherent uncertainty since scenario development allows the generation of a range of future realities for coastal configuration. Coastal management efforts must be cognizant of the past and present changes and, most importantly, must anticipate future changes in order to intelligently plan for future development of coastal resources.

2.0 Study Area:

2.1 Geographic Setting:

The study area comprises the northernmost portion of the Texas Gulf Coast, including portions of Galveston, Chambers, and Jefferson counties (fig. 2). The area extends from the Galveston Bay complex approximately 100 km northeastward to the Texas-Louisiana border (Sabine Pass), and approximately 30 km inland to a line drawn between the junction of the Trinity River with Trinity Bay on the northwest, to the junction of the Neches River with Sabine Lake on the northeast. The area is bordered on the west by Trinity Bay and East Bay, on the south by the Gulf of Mexico, and on the east by Sabine Lake. Port Arthur is the only major city within the study area. Galveston Island lies immediately adjacent to the southwestern corner of the study area.

2.2 Climate:

The climate of the area is characterized by hot summers and mild winters. Mean annual precipitation ranges between 110-140 cm (44-55 in.) per year and is distributed fairly uniformly throughout the year. The average annual low temperature ranges between 14-18 °C (58-64 °F) and the average annual high temperature ranges between 24-26 °C (75-78 °F). Tropical storms originating in the Gulf of Mexico are common in the area.

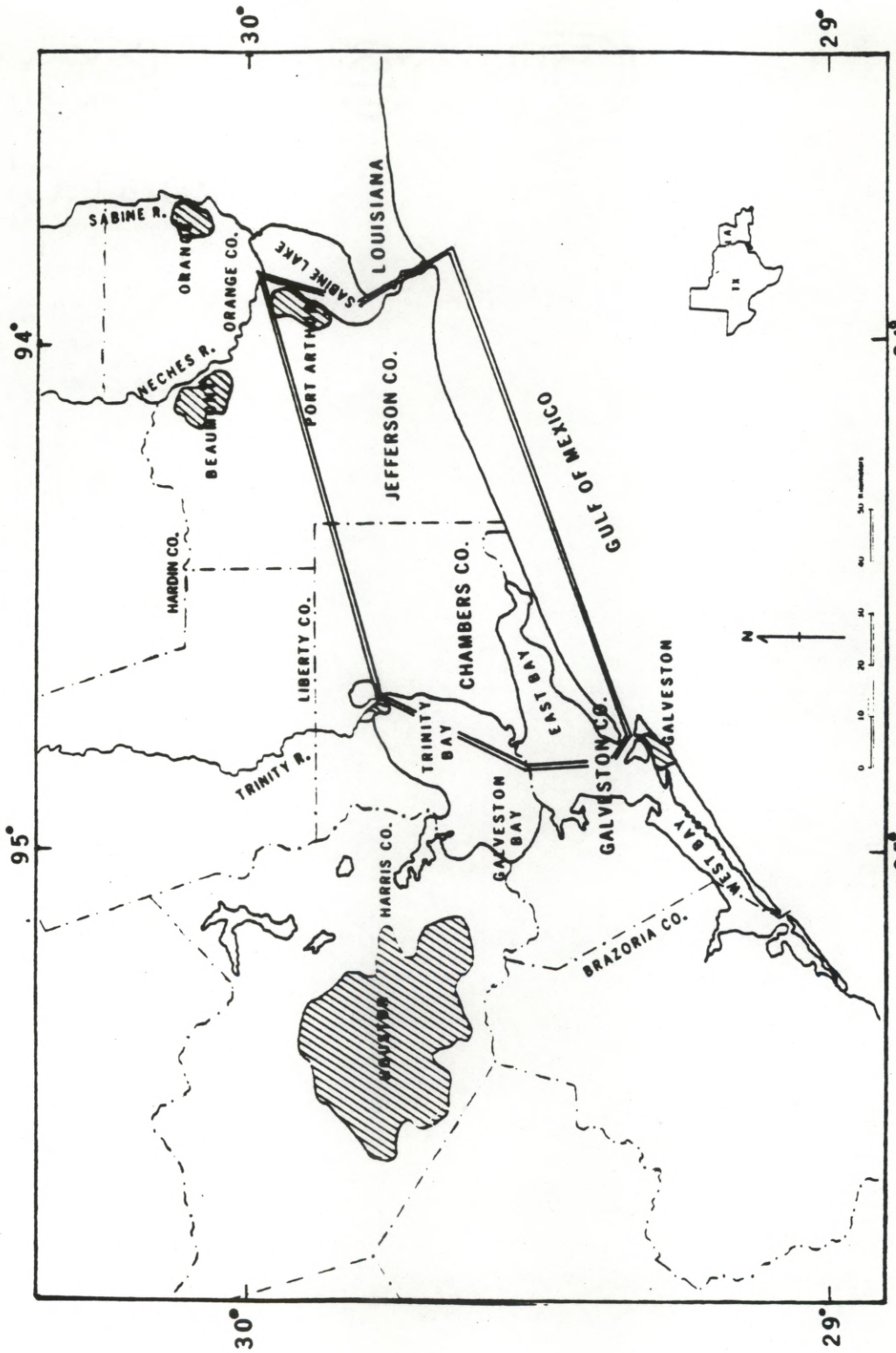

Figure 2. Location map of study area (delineated by double line).

2.3 Susceptibility to Land Loss:

The study area is especially susceptible to loss of land for three principal reasons: low land-surface elevation, low inland slope, and low sediment input.

Plate 1 is a topographic map of the study area digitized from topographic maps in the Environmental Geologic Atlas of the Texas Coastal Zone (Fisher and others, 1972; 1973). The map shows the large percentage (approximately 50%) of the study area at or below 5 feet elevation. About 75-80% of the area is at or below an elevation of 10 feet.

Like most areas along the Texas Coast, the land surface of the study area dips gently toward the Gulf. The Pleistocene Beaumont Formation, which crops out at the surface, has a seaward dip on the order of 0.2-0.4 m/km (Bernard and LeBlanc, 1965). Much of the coastline within the study area is characterized by a relatively steep and narrow beach zone that grades inland to marshland with negligible topography. Therefore, even a small rise in relative sea level can cause a large landward displacement of the shoreline.

Like most of the Texas Coast, the study area is sediment-starved, thus providing little opportunity for coastal accretion. The major rivers bordering the study area, the Trinity and Sabine-Neches system (fig. 2), do not contribute significant amounts of sediment to the shoreline. Reservoir development has severely decreased the sediment load carried by the Trinity River over the past 20-30 years (Paine and Morton, 1986). Much of the remaining sediment is deposited in the Trinity River delta. Most of the sediment transported by the Sabine and Neches Rivers is trapped in Sabine Lake and does not enter the Gulf (Fisher and others, 1973). In addition, the Mississippi River has shown a substantial decrease in

sediment discharge to the Gulf of Mexico since the beginning of the century (Meade and Parker, 1985). The lack of sediment being delivered to the Gulf by the Sabine-Neches and Mississippi River systems diminishes the sediment available for transport by longshore currents traveling from east to southwest. The longshore supply of sediment is further hampered by jetties at Sabine Pass and Bolivar Roads (fig. 3), which were built in the early 1900s.

2.4 Quaternary Geology and Geologic History:

All sediments outcropping within the study area are of Pleistocene and Holocene age. The Beaumont Formation comprises all exposed Pleistocene sediments within the study area. The Beaumont is the youngest of four Pleistocene interglacial depositional surfaces in the upper Texas Coastal Plain. From oldest to youngest, the surfaces are the Willis, Bentley, Montgomery, and Beaumont. Each plain unconformably overlies the next older plain, separated by a surface of erosion developed during lower sea-level substages of each interglacial stage (Bernard and LeBlanc, 1965). Each successively younger plain dips seaward at progressively smaller rates. Along the shoreline, the Beaumont Formation is unconformably overlain by thin Holocene marsh, beach, and chenier plain deposits.

Quaternary geologic history:

Pleistocene: During the Pleistocene Epoch, sea level dropped in response to continental glaciation. At maximum glaciation, sea level was approximately 140 m (450 ft.) below present mean sea level and the shoreline along the Texas Coast extended 80-225 km (50-140 mi.) seaward of present positions (LeBlanc and

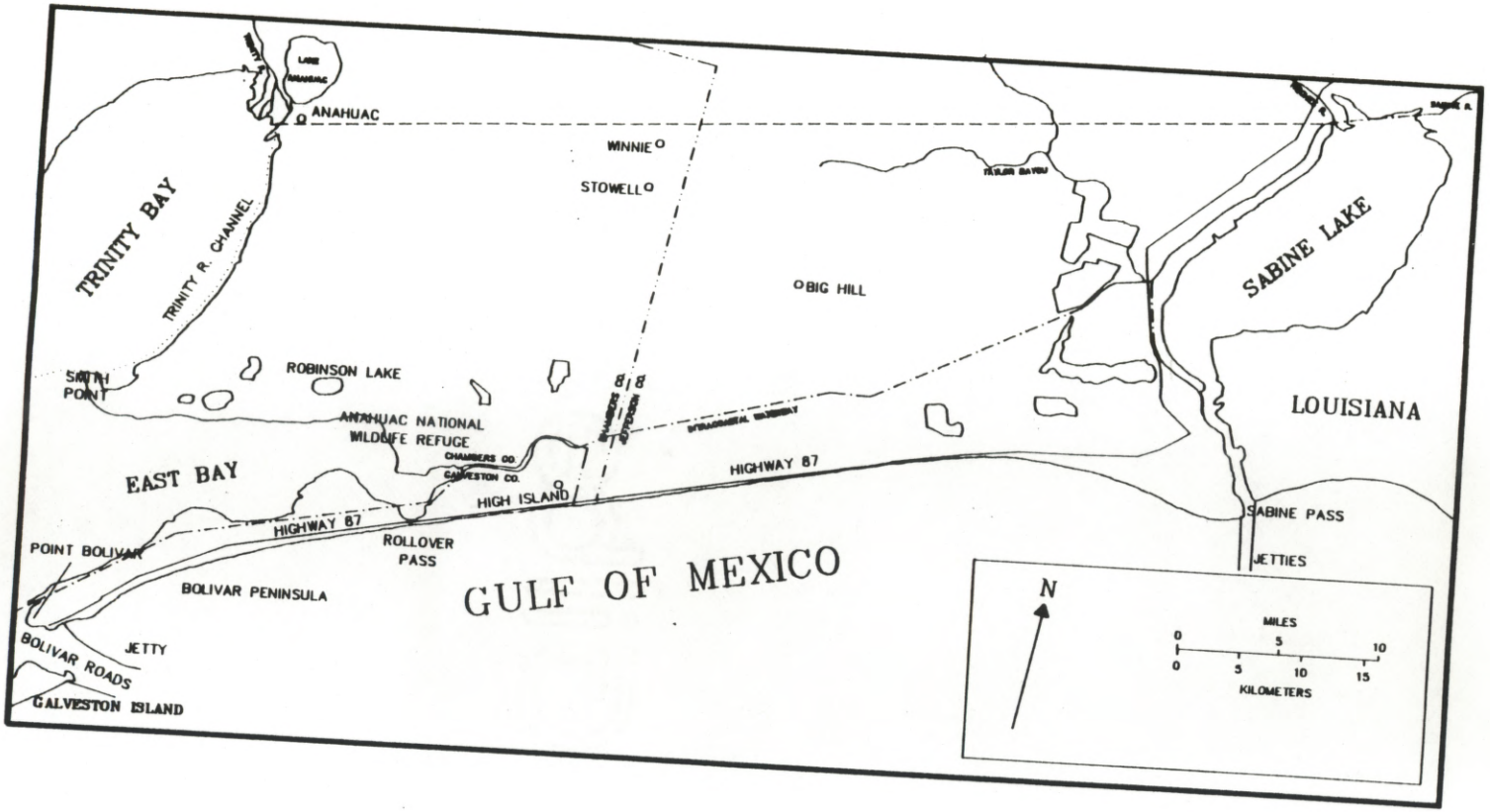

Figure 3. Map of localities referred to in text.

Hodgson, 1959). During one or more of the last interglacial episodes, when the sea was near its present level, rivers traversing the study area transported large quantities of sand and mud to deltas along the ancient shoreline. Aronow (in Wesselman and Aronow, 1971) indicates that four northwest-to-southeast-trending meander belts can be mapped within the study area, in addition to a fifth west of the present Trinity River. Each of these meander belts terminated in small deltas similar in size to the present-day Trinity River delta. This is in contrast to Barton's (1930) hypothesis that the meandering sand bodies were a relict group of distributaries within a birdsfoot delta, analogous to the present-day Mississippi River delta. Barton's conclusion suggests that the Pleistocene Trinity River delta was as large or larger than the present Mississippi delta.

Sandy sediments were deposited as point bars and crevasse splays along these meandering Pleistocene rivers. Overbank silts and muds were deposited during flood stages. Overbank and interdistributary muds and muddy sands comprise the majority of the exposed Pleistocene sediments within the study area (Wesselman and Aronow, 1971; Fisher and others, 1973). As the meandering rivers reached the delta, the transported sediment was deposited at the distributary mouths, causing delta progradation. Some of the mud, silt, and sand was redistributed by littoral currents, but most of it remained and was compacted (and is still compacting) beneath the prograding delta lobe(s) (Fisher and others, 1973).

The Late Pleistocene fluvial-deltaic sediments belong to the clay-rich Beaumont Formation (Beaumont Clay). The Beaumont Formation has been subaerially exposed, causing dewatering of the clay and oxidation of its upper surface. Mapping of the unconformable Holocene-Pleistocene contact relies on

recognition of this surface (Kane, 1959; Nelson and Bray, 1970) as well as differences in consolidation. The Pleistocene clays are very stiff and resist penetration (Kane, 1959; Bentley, 1980). This characteristic suggests that the Beaumont Clay is overconsolidated, therefore further consolidation should be minimal during the period of projection (to 2050). In contrast, the Holocene sediments are primarily poorly-consolidated silts and clays with a high moisture content, and are therefore highly susceptible to further consolidation.

Pleistocene (Ingleside) barrier island/strandplain deposits extending from Smith Point northeastward across the study area (fig. 4) are evidence of an earlier shoreline, indicating that the delta-building process was discontinuous, in response to fluctuating sea level. These strike-oriented sand bodies, first mapped by W.A. Price (1933; 1947), were named for their occurrence at Ingleside, near Corpus Christi. Winker (1979) states that the Ingleside represents the maximum transgression during deposition of the Beaumont Formation. Later-stage distributary and deltaic sedimentation partially buried the barrier island deposits within the study area.

During the final stage of Wisconsinan glaciation, which began about 50,000-60,000 B.P., sea level dropped approximately 140 m (450 ft.). The Trinity, Neches, and Sabine Rivers incised deeply into older fluvial and deltaic sediments. The buried valleys of the Sabine and Neches Rivers join under present-day Sabine Lake. According to Nelson and Bray (1970), the combined Sabine-Neches river valley extended approximately 25 km (15 mi.) south of the present shoreline at Sabine Pass where it joined the Calcasieu River, which flows from southwest Louisiana. The combined Sabine-Neches-Calcasieu River valley then veered to the

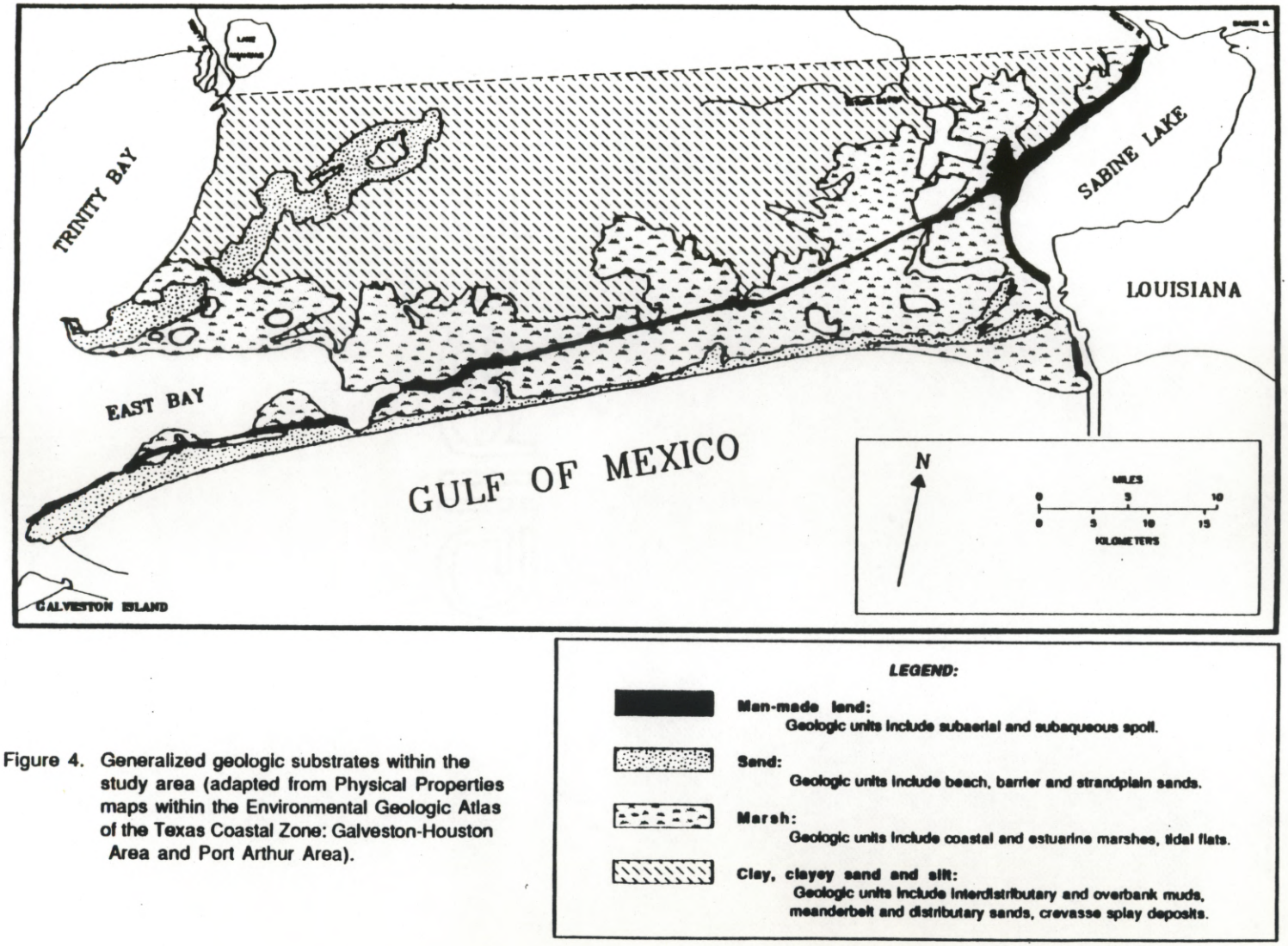

Figure 4. Generalized geologic substrates within the study area (adapted from Physical Properties maps within the Environmental Geologic Atlas of the Texas Coastal Zone: Galveston-Houston Area and Port Arthur Area).

southwest, paralleling the coastline, to join the Trinity River, probably some 30 km (19 mi.) gulfward of the present shoreline at Galveston.

Holocene: The final glacial retreat, accompanied by a rise of sea level that continues to present (fig. 5), began approximately 18,000 B.P. (Fisher and others, 1973). Holocene sands and overbank muds were deposited as rivers continued to meander within the filling valleys. As the sea transgressed, the deeply incised Trinity, Sabine, and Neches River valleys gradually filled with marine water, producing estuarine systems in present-day Trinity Bay and Sabine Lake (Kane, 1959; Fisher and others, 1972). Sabine Lake was formed when the estuary was partially restricted by later chenier deposition. The Holocene sediment sequence within the Sabine Lake area is fluvial-deltaic sands, overlain by peat representing transient marshes, overlain by estuarine muds (Nelson and Bray, 1970). At least 35 m (120 ft.) of Holocene sediment overlie the oxidized Pleistocene surface (Beaumont Formation) within the buried Sabine-Neches valley at Sabine Pass (Kane, 1959; Nelson and Bray, 1970). Within the buried Trinity River valley at Bolivar Roads, the maximum thickness of Holocene sediment is approximately 30 m (100 ft.), of which 10-20 m are estuarine muds (Morton and Price, 1987). Moving laterally away from the axis of the buried valleys, the Holocene thickness diminishes quickly.

Coastal marshes are the most extensive Holocene deposits within the study area. The marshes are formed by continual submergence of low-lying coastal land, and the subsequent development of adaptable vegetation. The vegetation traps much of the sediment that may be transported to the marsh from inland, and decomposition of the vegetation produces an organic-rich muddy substrate. The marsh sediments

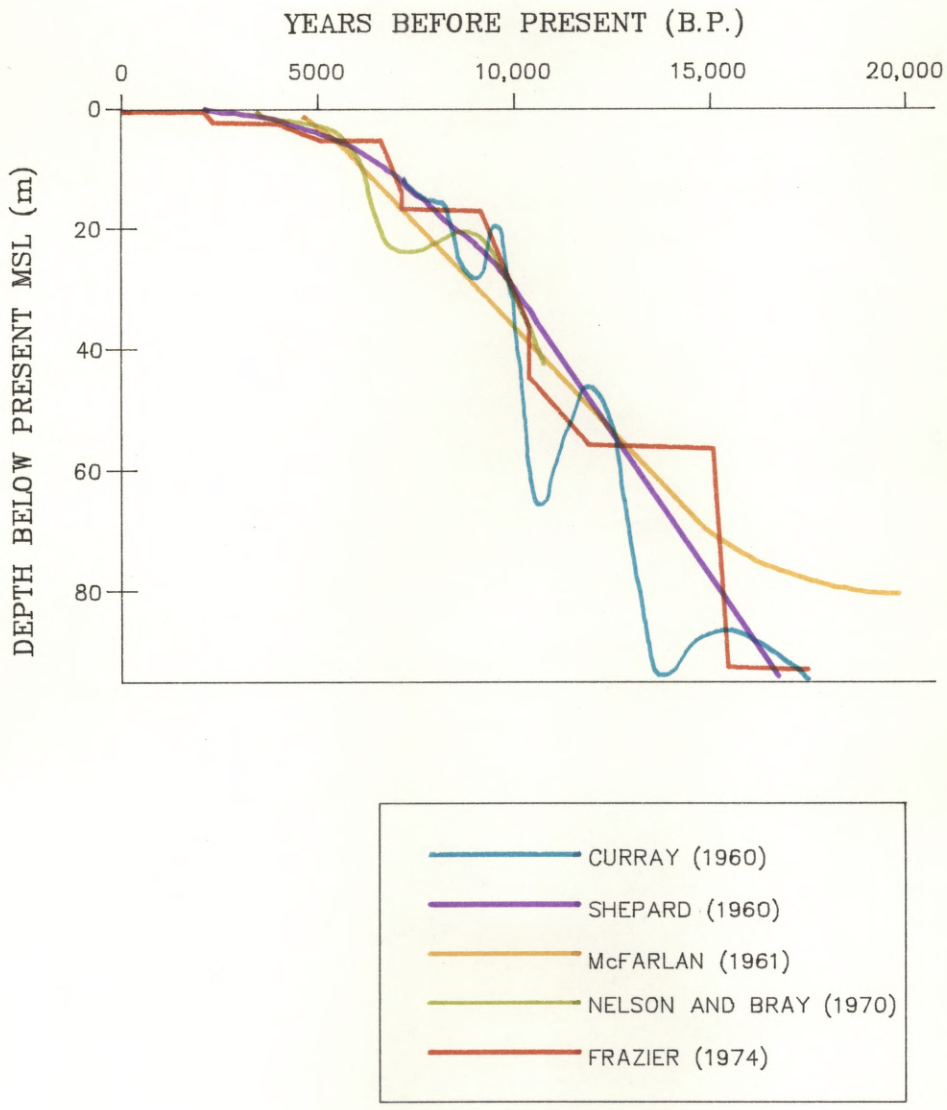

Figure 5. Inferred sea-level rise during the past 18,000 years (modified from Fisher and others, 1973).

are generally not more than 1 m thick (Wesselman and Aronow, 1971; Morton and Nummedal, 1982).

Chenier accretion has occurred during the past 3000 years. The Chenier Plain extends along more than 175 km of the western Louisiana Gulf Coast to approximately 15-20 km west of Sabine Pass. The plain consists of a series of thin shore-parallel ridges of sand and shell ("cheniers" or "chenier ridges") upon a muddy substrate. The entire Holocene sequence is generally 7-8 m thick at the present shoreline (Morton and Nummedal, 1982). The generally-accepted explanation for the development of the Chenier Plain is that extensive coastal mudflats were deposited when the Mississippi River was discharging its sediment to the west. When the sediment dispersal shifted to the east, the muddy sediments were reworked by wave action, removing the fines and leaving a sandy beach deposit called a chenier ridge (Gould and McFarlan, 1959). Alternating reversals in the Mississippi River discharge over the past 3000 years has resulted in repetitive accumulation of chenier ridges separated by mudflats, forming the chenier plain.

2.5 Hydrogeology:

Upper Texas Gulf Coastal Plain: The aquifers of the northern Texas Gulf Coastal Plain consist of interbedded layers of sand, silt, and clay of fluvial-deltaic origin (Kreitler and others, 1977). The sand and clay layers are not uniform in either lithology or thickness, and they grade both laterally and vertically, making differentiation of formal geological formations on the basis of drillers' logs and electrical logs very difficult. The formations that form important hydrologic units in the upper Texas Coast, from oldest to youngest, are: the Fleming Formation of

Miocene age; the Goliad Sand of Pliocene (Late Miocene?) age; the Willis Sand, Bentley Formation, Montgomery Formation, and Beaumont Formation of Pleistocene age, and alluvium of Holocene age (fig. 6). Presently, the Texas Water Development Board groups all formations from the Catahoula (Oligocene-Miocene age) upward to the surface into the Gulf Coast Aquifer.

With the exception of the alluvium in and near stream valleys and the subsurface Goliad Sand, the formations crop out in bands that approximately parallel the coastline. The younger formations crop out closer to the coast, and the more-steeply-dipping older ones crop out farther inland. Locally, faults and salt structures have reversed regional dips and caused thickening or thinning of individual beds.

Several different classifications exist for Tertiary stratigraphic units of the Texas Coastal Plain. Similarly, several different classification schemes have been developed for hydrologic units within these Tertiary stratigraphic units. Jorgenson (1975) developed an accepted convention for classifying hydrostratigraphic units in the area by use of both the logs and the hydraulic properties of the aquifers (fig. 6). The subsurface units are divided into three aquifer systems and one major confining unit. The deepest aquifer containing fresh water is the Jasper aquifer of Miocene age, which is separated from the overlying aquifers by the Burkeville confining unit, which is part of the Fleming Formation. Little is known about the hydraulic properties of the Jasper aquifer since it is generally undeveloped in the region. The two principal aquifers for the upper Texas Coast are the Evangeline Aquifer of Pliocene age and the Chicot Aquifer of Pleistocene-Holocene age. The basis for separating the Chicot Aquifer from the underlying Evangeline Aquifer is primarily a difference in average hydraulic conductivity: 5×10^{-3} cm/s in the Evangeline and 1 x

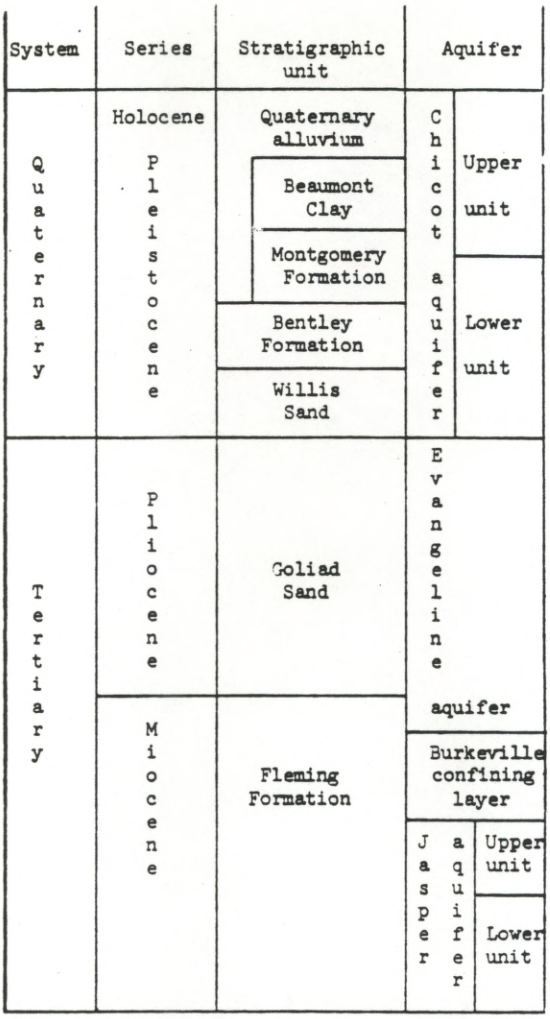

Figure 6. Geologic and hydrologic units of Upper Texas Coastal Plain (from Jorgenson, 1975).

10^{-2} cm/s in the Chicot (Gabrysch, 1984). In areas without significant groundwater production, the difference in hydraulic conductivity may cause potentiometric levels in the Evangeline to be 5-15 m higher than in the Chicot (Jorgenson, 1975). Locally, however, either the presence of a prominent clay layer or higher sand-clay ratios in the Chicot relative to the Evangeline have been used to define a Chicot-Evangeline boundary (Baker, 1979).

Study area: Both the Chicot and Evangeline Aquifers provide vast quantities of good-quality groundwater for the Houston area as well as for northern portions of Chambers and Jefferson counties. Within the study area however, the upper unit of the Chicot Aquifer provides the sole source of potable groundwater. Texas Water Commission records of wells in Galveston, Chambers, and Jefferson counties indicate that all groundwater pumpage within the study area is from the Chicot Aquifer, upper unit or undifferentiated. The lower unit of the Chicot Aquifer and the Evangeline Aquifer contain highly mineralized water with total dissolved solids (TDS) generally greater than 3000 mg/l. A more detailed discussion of groundwater quality is provided in section 3.1.3.2.

Chicot Aquifer: The Chicot Aquifer, defined and named in southwestern Louisiana by Jones and others (1954), is the youngest aquifer in the Texas Coastal Plain. The aquifer is composed of the Willis Sand, Bentley Formation, Montgomery Formation, and the Beaumont Formation. Usually the Holocene alluvium is also included so that the Chicot Aquifer includes all deposits from the land surface down to the top of the Evangeline Aquifer (Gabrysch, 1984). Within the study area, the base of the Chicot

Aquifer is at a depth of approximately 400 m (1200 ft.) at the coastline. The aquifer thins updip, pinching out approximately 150 km inland near the northern borders of Hardin and Liberty counties (Baker, 1979). Over most of the study area, the Chicot Aquifer can be divided into an upper sand section and lower sand section, separated by a thick clay unit. There are significant differences in water levels within wells completed in the upper and lower units in eastern Jefferson county.

Lower unit: The lower unit of the Chicot Aquifer can be divided into two or more thick sands separated by clay units. The lowermost of these sands is the Alta Loma Sand, as defined by Rose (1943). The Alta Loma Sand is a massive, highly transmissive, laterally extensive sand that is part of the "heavily-pumped layer" described by Wood and Gabrysch (1965) for the Houston area. In the Houston-Galveston area, Jorgenson (1975) defines the base of the Chicot Aquifer as the base of the Alta Loma Sand. In northwestern Chambers and Jefferson counties, the lower unit thins considerably, losing much of the sand that is present downdip (Wesselman and Aronow, 1971). In this updip area, the lower and upper units often can not be differentiated. Wesselman and Aronow (1971) provide a range of values for transmissivity (T), hydraulic conductivity (K), and storativity (S) for the lower unit of the Chicot based on 10 pump tests in Jefferson and Chambers counties:

lower unit:

$T = 7.5 \times 10^{0} - 5.8 \times 10^{2}$ cm^2/s

$K = 5.1 \times 10^{-3} - 7.8 \times 10^{-2}$ cm/s

$S = 4.0 \times 10^{-4} - 3.7 \times 10^{-3}$

Upper unit: The upper unit of the Chicot Aquifer consists of a highly-transmissive sand unit of the Montgomery Formation overlain by a thick clayey unit belonging to the Beaumont Formation (Beaumont Clay). The range of values for hydraulic characteristics of the upper unit of the Chicot, based on 9 pump tests, are (Wesselman and Aronow, 1971):

upper unit:

$T = 1.6 \times 10^{1} - 4.3 \times 10^{1}$ cm^2/s

$K = 8.2 \times 10^{-5} - 2.8 \times 10^{-4}$ cm/s

$S = 2.0 \times 10^{-4} - 7.0 \times 10^{-4}$

Average hydraulic characteristics of the Chicot Aquifer: Based on a more extensive data base compiled primarily from the Houston-Galveston area, Gabrysch (1984) determined that, for the Chicot Aquifer as a whole, the horizontal hydraulic conductivity (K) averages 9.3 m/d (0.01 cm/s), and the storativity (S) ranges from 4 x 10^{-5} to more than 0.20 in the updip region where the aquifer is under water-table conditions. The transmissivity of the aquifer ranges from near zero to approximately 1860 m^2/d (215 cm^2/s), depending on the thickness.

3.0 Causes of Coastal Land Loss

3.1 Relative Sea-Level Rise:

Relative sea-level rise is divided into two components: eustatic sea-level rise, the worldwide rise in absolute sea level, and land-surface subsidence, the vertical sinking of the land surface with respect to a stable datum. Relative sea level has been rising from the end of the last glacial epoch, approximately 18,000 B.P., until the present. Past (Holocene) and present (historical) sea-level trends are discussed below.

3.1.1 Holocene sea-level trends:

Eustatic sea level has risen and fallen, perhaps cyclically, throughout geologic time. Vail and others (1977) used seismic stratigraphic data gathered primarily from continental shelves to define seismic sequences with chronostratigraphic significance. They interpreted sea-level histories along several continental margins from these seismic sequences and observed them to be synchronous on a global scale, leading to the development of the "Vail curves" that document cycles of sea level change on a global scale. Within Phanerozoic time, Vail described first, second, and third order eustatic cycles, with durations of 200 to 300 million, 10 to 80 million, and 1 to 10 million years, respectively. Although there is considerable controversy concerning the validity of these Vail curves, long-term cycles of sea-level change are generally accepted.

The Vail curves cover all of Phanerozoic time and therefore show poor definition for the late Holocene, the time period most critical for this study. Other researchers have documented sea-level rise during the past 20,000 years along the

northwest coast of the Gulf of Mexico by use of radiocarbon dating of nearshore organisms and brackish-marsh peats (Curray, 1960; Shepard, 1960; McFarlan, 1961; Nelson and Bray, 1970; Frazier, 1974). A compilation of these various sea-level curves dating from the last glacial stage (Wisconsinan), approximately 18,000 years B.P., to the present is depicted in fig. 5. The curves indicate a eustatic rise of 70-90 meters during this time. Since the last major retreat of continental glaciation, sea-level rise has been punctuated by standstills and minor reversals, correlative with minor advances in continental glaciation (Frazier, 1974). The general trend of the curves shows a high rate of rise (6-8 mm/yr) for the early Holocene, with a decrease in rate of rise beginning approximately 8500 $\pm$ 1000 years B.P., followed by a further significant decrease in the rate of rise at 5000 $\pm$ 500 years B.P. During the past 5000 $\pm$ 500 years, eustatic sea level has probably risen at a rate of approximately 1-3 mm/yr, a rate in accord with historical trends determined by tidal gage records from the past century. Furthermore, the postglacial sea-level curves for the Texas Gulf Coast show general agreement with similar curves from around the world (Shepard, 1963; Jelgersma, 1966).

3.1.2 Historical sea-level trends:

Changes in historical sea-level position are most accurately documented in tidal gage records (mareographs). The length and completeness of record is highly variable. Unfortunately, most tidal records worldwide begin after 1900, making analysis of trends in excess of 100 years impossible.

3.1.2.1 Tidal stations:

Tidal gages provide sea-level data during the present century at various points along the Gulf of Mexico. For this study, tidal gage data for several stations along the Gulf Coast were obtained from the National Ocean Service (NOS). The stations in Texas are located at Sabine Pass, Pier 21 and Pleasure Pier, the latter two on Galveston; stations in Florida are located at Pensacola, Cedar Keys, St. Petersburg, and Key West (fig. 7). The data consist of monthly means of hourly measurements of tide height. Tidal records from Sabine Pass, on the eastern edge of the study area, and Galveston Island (both Pier 21 and Pleasure Pier), on the western edge of the study area, provide the best documentation of historical relative sea-level rise along the coastline of the study area. There are no other tidal gage stations within the study area. Pier 21 provides the longest and most complete record, with data from 1908-1986, inclusive. The records at Sabine Pass and Pleasure Pier, covering 1958-1983 and 1958-1986, respectively, are less complete in terms of years covered and number of missing data points within the record.

3.1.2.2 Linear regression analysis of tidal data:

The rate of relative sea-level rise at a tidal station is determined by linear regression analysis of the tidal data. The rate of relative sea-level rise is obtained by the value of the sample regression coefficent, b. This coefficent represents the slope of the estimated line of regression and is computed by

$$b = \frac{\sum_{i=1}^{N} x_i y_i - (1/N)\left(\sum_{i=1}^{N} x_i \sum_{i=1}^{N} y_i\right)}{\sum_{i=1}^{N} x_i^2 - (1/N)\left(\sum_{i=1}^{N} x_i\right)^2}$$

where x_i is the time in months (x_1 being the first month in the record), y_i is the monthly mean gage height for x_i, and N is the number of months in the time series for that gage. The month numbers at all stations were standardized such that January 1908 was month number 1.

Tidal gage data from four stations along the Florida Gulf Coast (fig. 7) were analyzed in order to determine the regional variability of relative sea-level rise within the Gulf Coast and to make an estimate of the magnitude of the component of land-surface subsidence to relative sea-level rise within the study area. Tidal stations at Pensacola, Cedar Keys, St. Petersburg, and Key West, Florida are located on a carbonate platform and are assumed to be geologically stable (non-subsiding) for the less-than-seventy-five-year period of record of the stations (Swanson and Thurlow, 1973; Ramsey and Moslow, 1987). Therefore, relative sea-level rise measured at these stations represents the best estimate of eustatic sea-level rise for the Gulf of Mexico over the period of record.

Florida stations: The rate of relative sea-level (RSL) rise at Key West, Pensacola, and St. Petersburg is 2.4 mm/yr over the period of record (1913-1986, 1923-1986, and 1947-1986, respectively), whereas at Cedar Keys the rate of rise is 1.8 mm/yr over the period 1914-1986 (Table 1). The data and lines of regression for the four

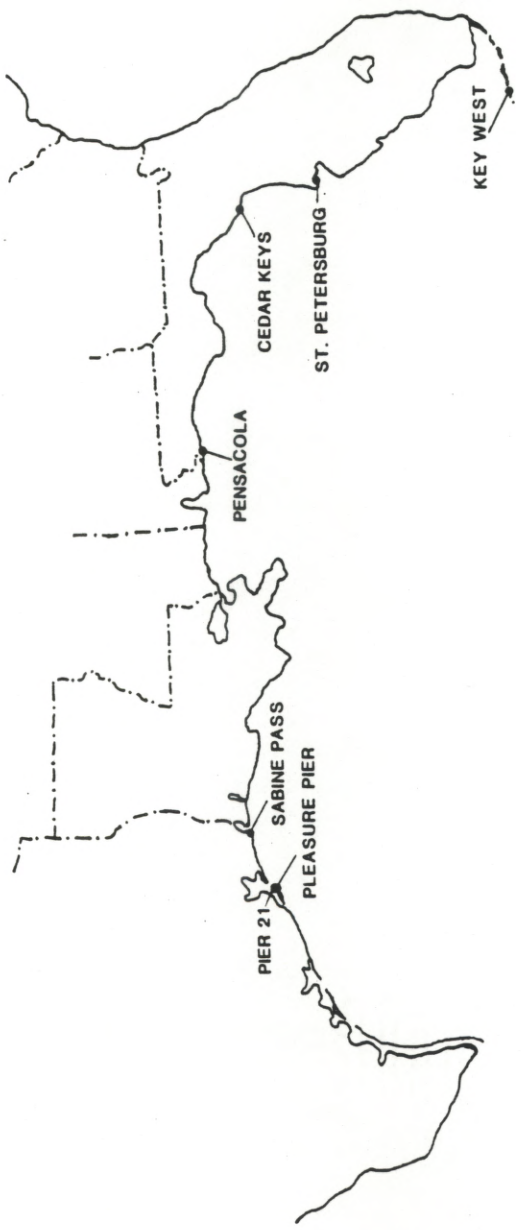

Figure 7. Location of tidal stations.

Station	Length of Series	Entire Series	Pre-1950	Post-1950	1958-1986	1930-1974	1930-1982
Sabine Pass	1958 - 1983	11.4	NA	11.4	11.4**	NA	NA
Pier 21	1908 - 1986	6.3	3.4	6.3	11.1	6.9	7.6
Pleasure Pier	1958 - 1986	7.3	NA	7.3	7.3	NA	NA
Pensacola	1923 - 1986	2.4	2.9	2.6	2.8	2.2	2.2
Cedar Keys	1914 - 1986	1.8	3.1	1.5	1.7	NA	NA
St. Petersburg	1947 - 1986	2.4	NA	2.9	2.8	NA	NA
Key West	1913 - 1986	2.4	2.9	2.3	2.9	2.1	2.2

Note: NA: Length of series precludes regression for this period.
**: Series ends in 1983

Table 1. Relative sea-level rise (mm/yr) for various time periods at seven stations within the Gulf Coast.

Florida stations are presented in figures 8-11. The calculated trend for the Cedar Keys station is less than for the other three, possibly due to localized land-surface movement or disruption of the gage itself. In addition, the tidal record contains an eleven-year-plus (141 month) gap between 1926-1939. Therefore, the Cedar Keys station is not included in the analysis, regardless of the reason for the anomaly.

Rates of RSL rise for the two baseline periods (1930-1974, 1930-1982) are essentially identical at the Pensacola and Key West stations (2.2 mm/yr) (Table 1). This value is considered to be the baseline rate of eustatic rise for the study area. The baseline rate of RSL rise at Pier 21 is 6.9 mm/yr for the period 1930-1974, and 7.6 mm/yr for the period 1930-1982.

The assumption that tidal stations along the Florida coast are not subsiding may not be entirely valid. Analyses of worldwide tidal gage data by independent researchers indicate a global rise in sea level of between 1-1.5 mm/yr over the past century (Table 2). Gornitz and others' (1982) value of 1.2 mm/yr is the most commonly cited value in the recent literature (e.g. Revelle, 1983; Robin, 1986; Ramsey and Moslow, 1987). In a follow-up study, Gornitz and Lebedeff (1987) obtained values of 1.2 ± 0.3 and 1.0 ± 0.1 mm/yr by applying two different averaging methods to worldwide tidal gage data spanning the past century. This indicates that the value for eustatic rise in the Gulf of Mexico determined from the Florida gages is approximately twice the global rate. Although the cause of this discrepency is uncertain, one possible explanation is tectonic downwarping of the Gulf of Mexico basin beneath an exceedingly thick sediment load. The rate of this crustal downwarping can be considered constant over the time period of interest and therefore, for this study, will not be differentiated from 'true' eustatic rise in the Gulf

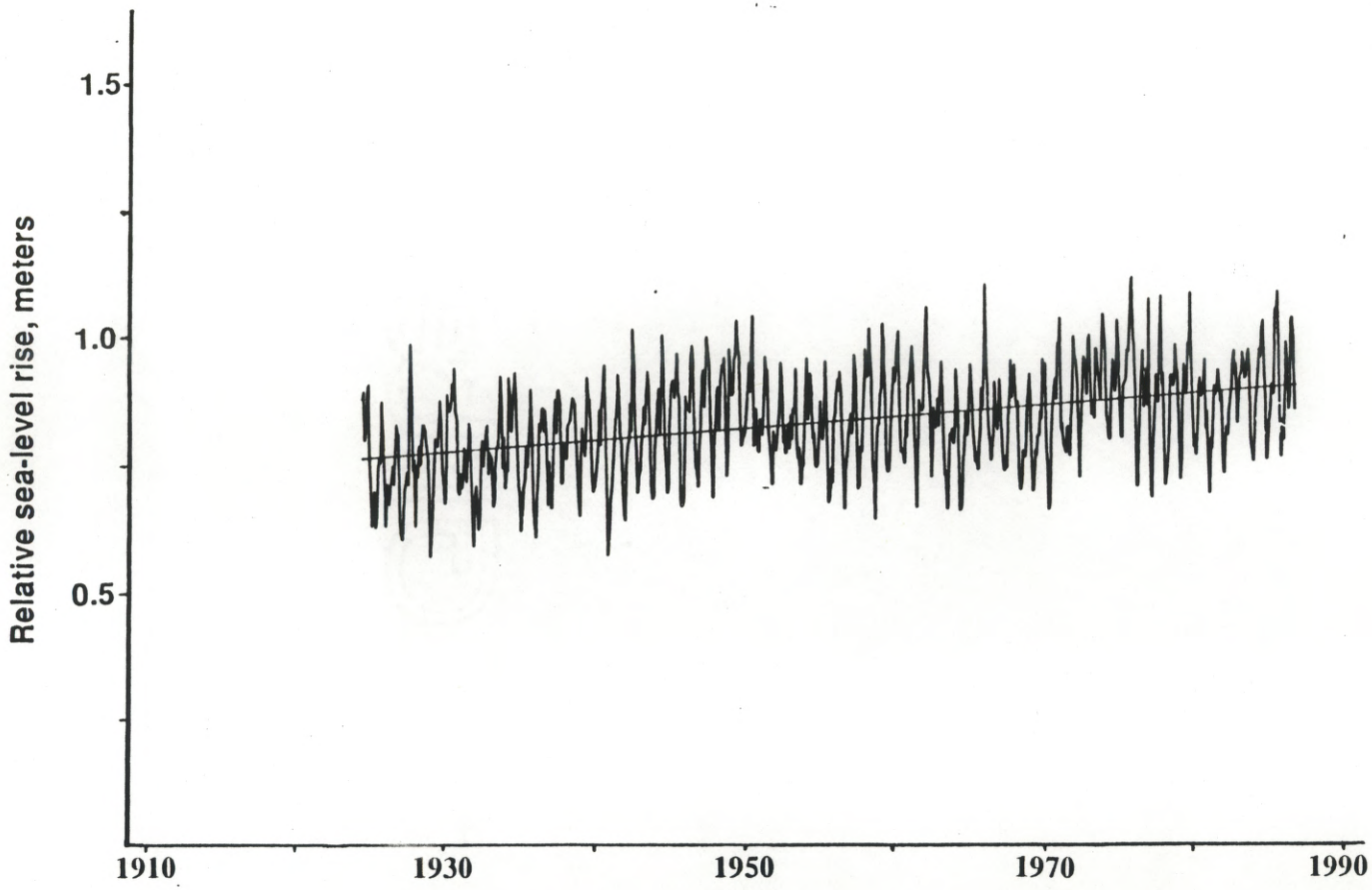

Figure 8. Pensacola, Fla. tidal data and line of regression (slope = 2.4 mm/yr).
Period of record = 1923-1986 (Data from the National Ocean Service, NOAA).

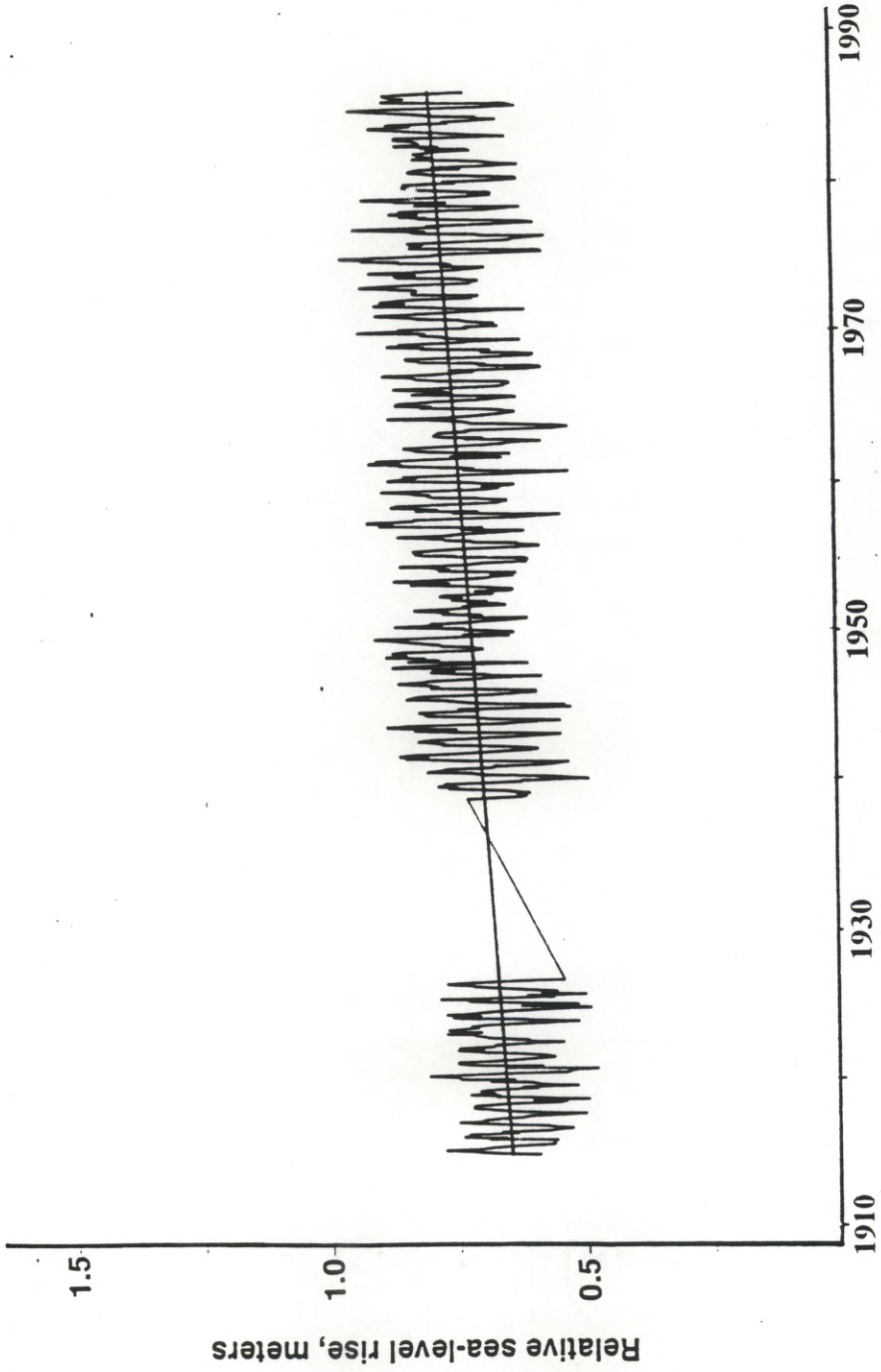

Figure 9. Cedar Keys, Fla. tidal data and line of regression (slope = 1.8 mm/yr).
Period of record = 1914-1986 (Data from the National Ocean Service, NOAA).

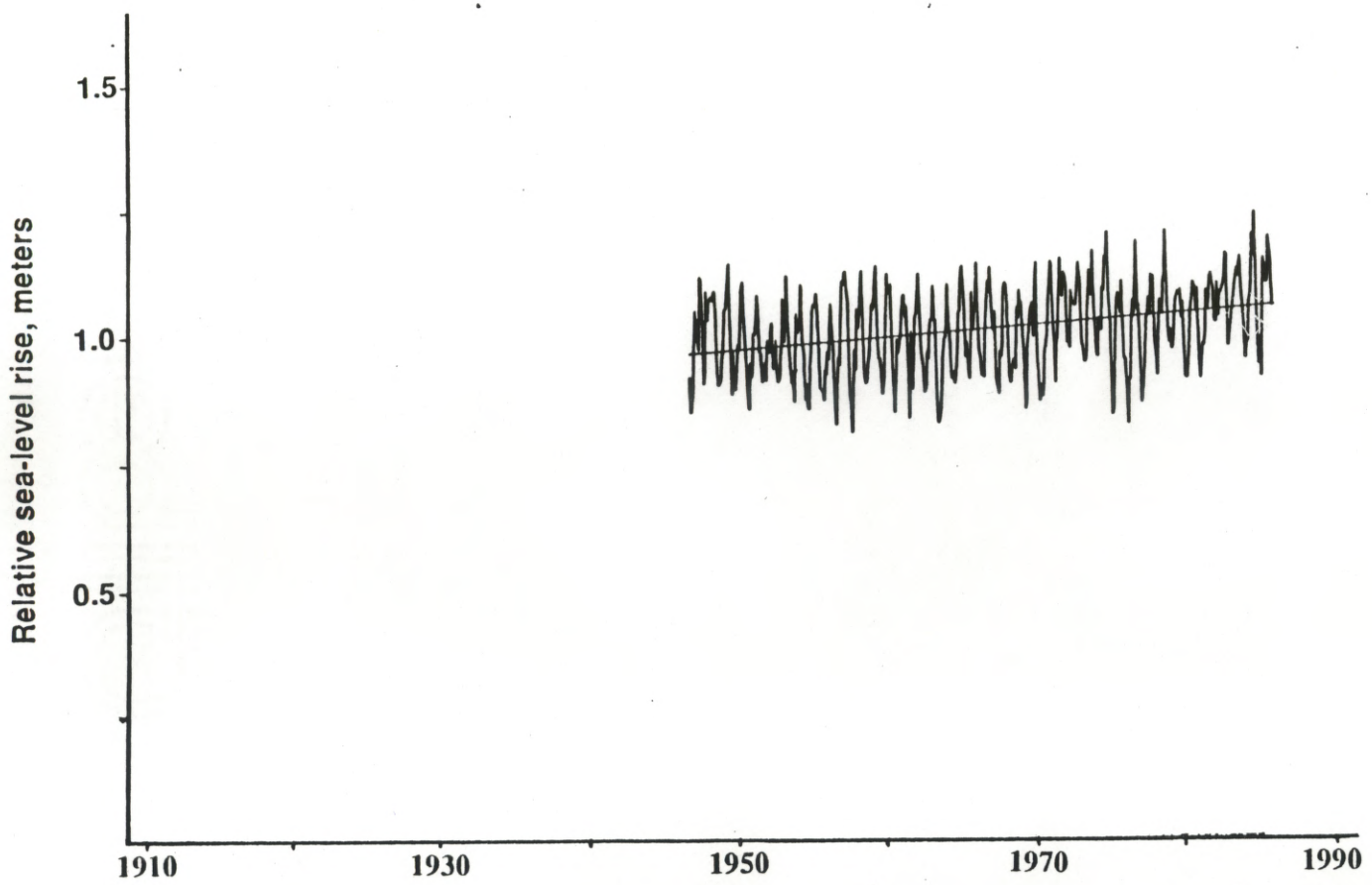

Figure 10. St. Petersburg, Fla. tidal data and line of regression (slope = 2.4 mm/yr). Period of record = 1947-1986 (Data from the National Ocean Service, NOAA).

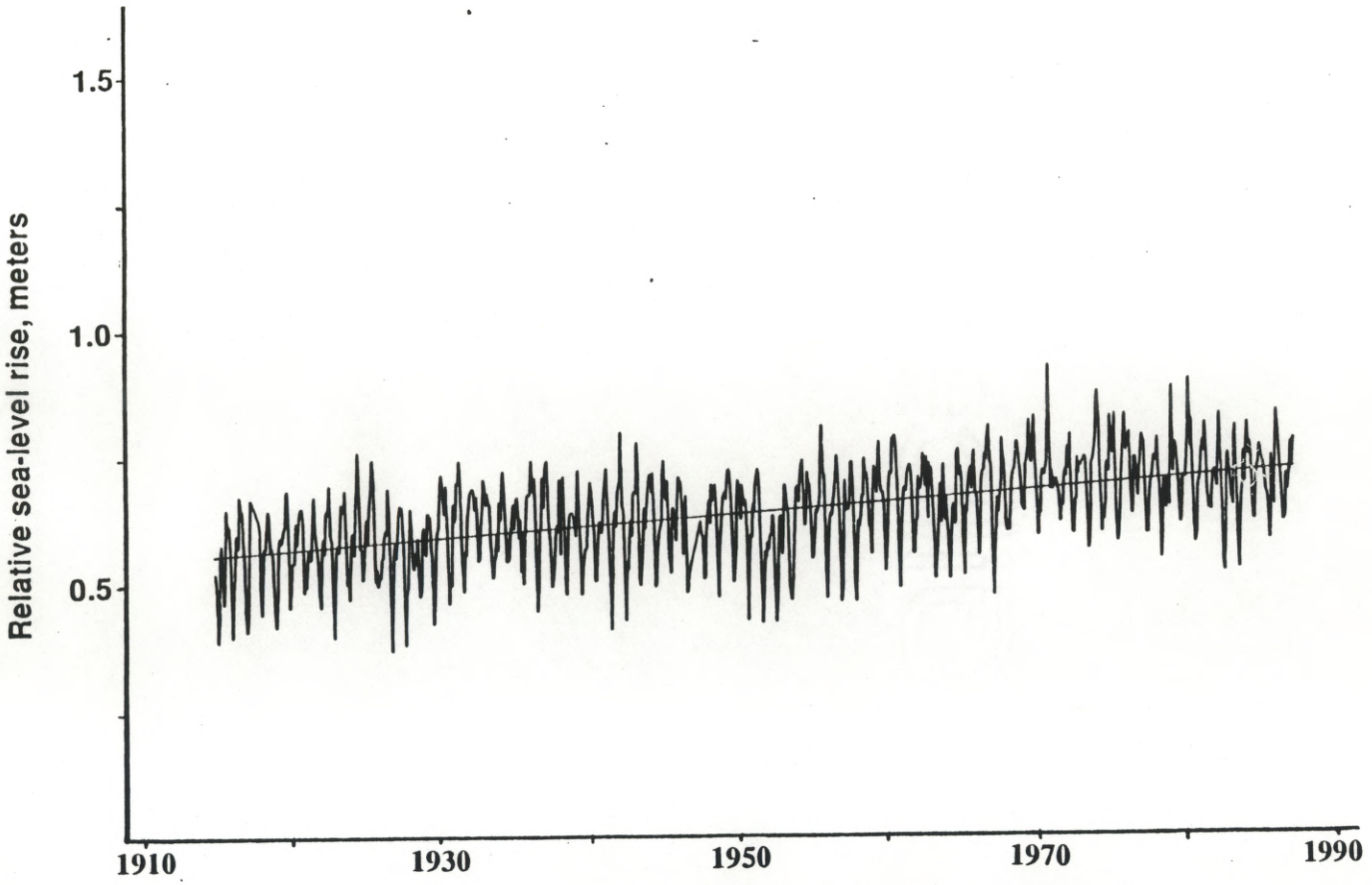

Figure 11. Key West, Fla. tidal data and line of regression (slope = 2.4 mm/yr).
Period of record = 1913-1986 (Data from the National Ocean Service, NOAA).

Researcher	Rate (mm/yr)	Data base
Lisitzen, 1958	1.1 + 0.4	6 stations in Europe 1807-1943
Fairbridge and Krebs, 1962	1.2	Many stations, worldwide 1900-1950
Hicks, 1978	1.5	27 stations in U.S. 1940-1975
Gornitz and others, 1982	1.2	193 stations, worldwide 1880-1980
Barnett, 1984	1.4 + 0.1	155 stations, worldwide 1881-1980
Gornitz and Lebedeff, 1987	1.2 + 0.3 1.0 + 0.1	130 stations, worldwide 1880-1980

Table 2. Estimates of global sea-level rise.

of Mexico. The working assumption is therefore made that the RSL rise of 2.4 mm/yr measured at the Florida stations (excluding the anomalous Cedar Keys trend) represents the best estimate of eustatic rise in the Gulf of Mexico during the past century.

Relative sea-level has been rising at a rate of 6.3 mm/yr over the period 1908-1986 at Pier 21, at a rate of 7.3 mm/yr at Pleasure Pier over the period 1958-1986, and at a rate of 11.4 mm/yr at Sabine Pass over the period 1958-1983 (Table 1). The tidal record at Sabine Pass terminates in 1983. Figures 12, 13 and 14 are plots of the tidal data and lines of regression for the Sabine Pass, Pier 21, and Pleasure Pier stations, respectively.

The magnitude of the component of land-surface subsidence at the Pier 21 gage can be estimated by comparing the rate of RSL rise at that gage (6.3 mm/yr) with the rate determined from the Pensacola, St. Petersburg, and Key West stations (2.4 mm/yr). Assuming the Florida gages represent eustatic rise, the rates suggest that approximately 60% of the observed RSL rise at the Pier 21 gage can be accounted for by land-surface subsidence over the full period of record. Eustatic rise accounts for the remaining 40%.

In order to compare the rate of relative sea-level rise at Sabine Pass and Pleasure Pier to the Florida stations, the trend at the Florida gages must be calculated for the period of record for the Texas gages. For the time period 1958-1983, Sabine Pass shows a rate of rise of 11.4 mm/yr. During the period 1958-1986, relative sea level rose at a rate of 11.1 mm/yr at the Pier 21 gage and at 7.3 mm/yr at the Pleasure Pier gage, whereas the three Florida gages register a rate of rise of 2.8-2.9 mm/yr

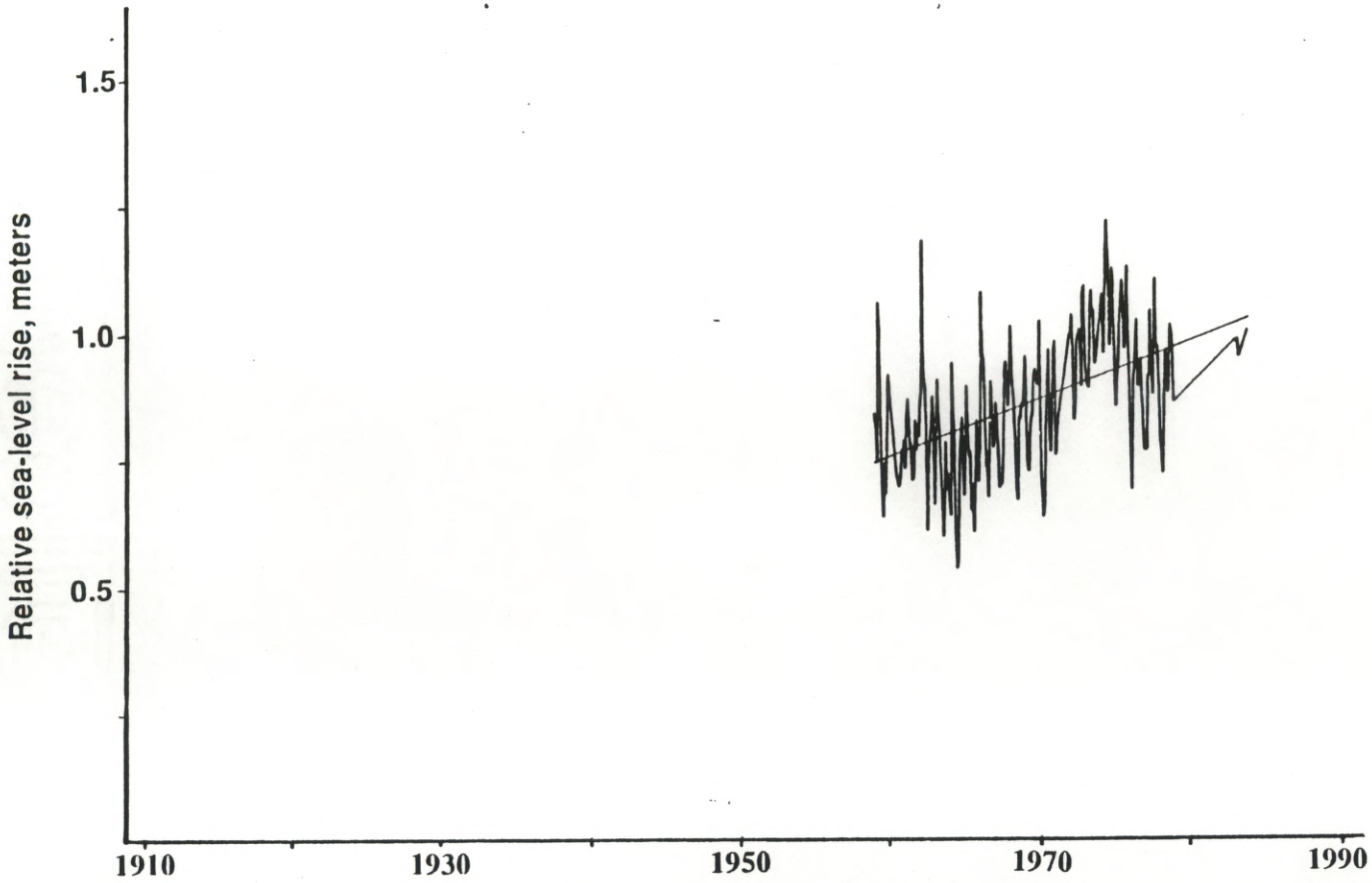

Figure 12. Sabine Pass, TX tidal data and line of regression (slope = 11.4 mm/yr). Period of record = 1958-1983 (Data from the National Ocean Service, NOAA).

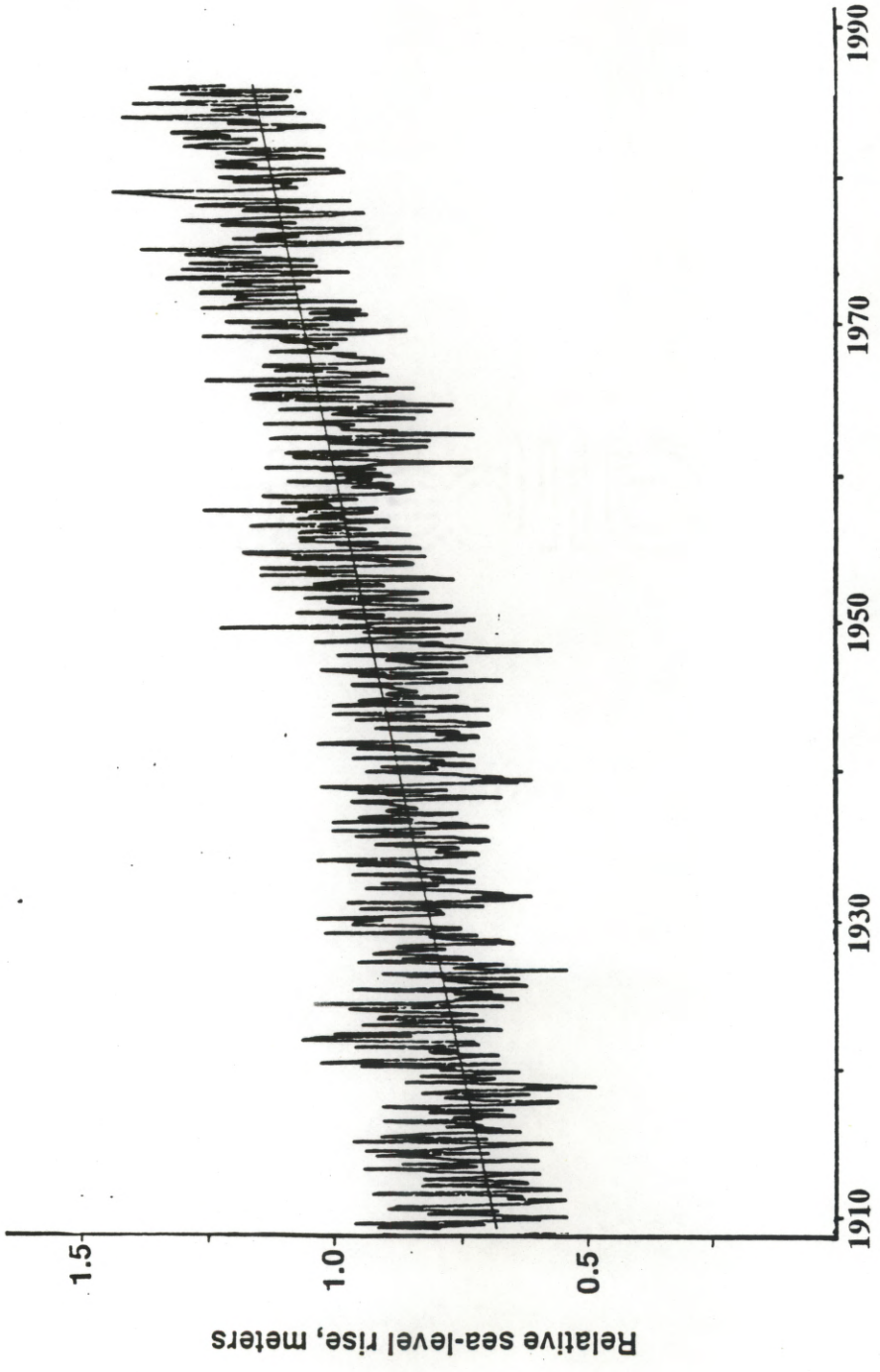

Figure 13. Pier 21, Galveston, TX tidal data and line of regression (slope = 11.1 mm/yr). Period of record = 1908-1986 (Data from the National Ocean Service, NOAA).

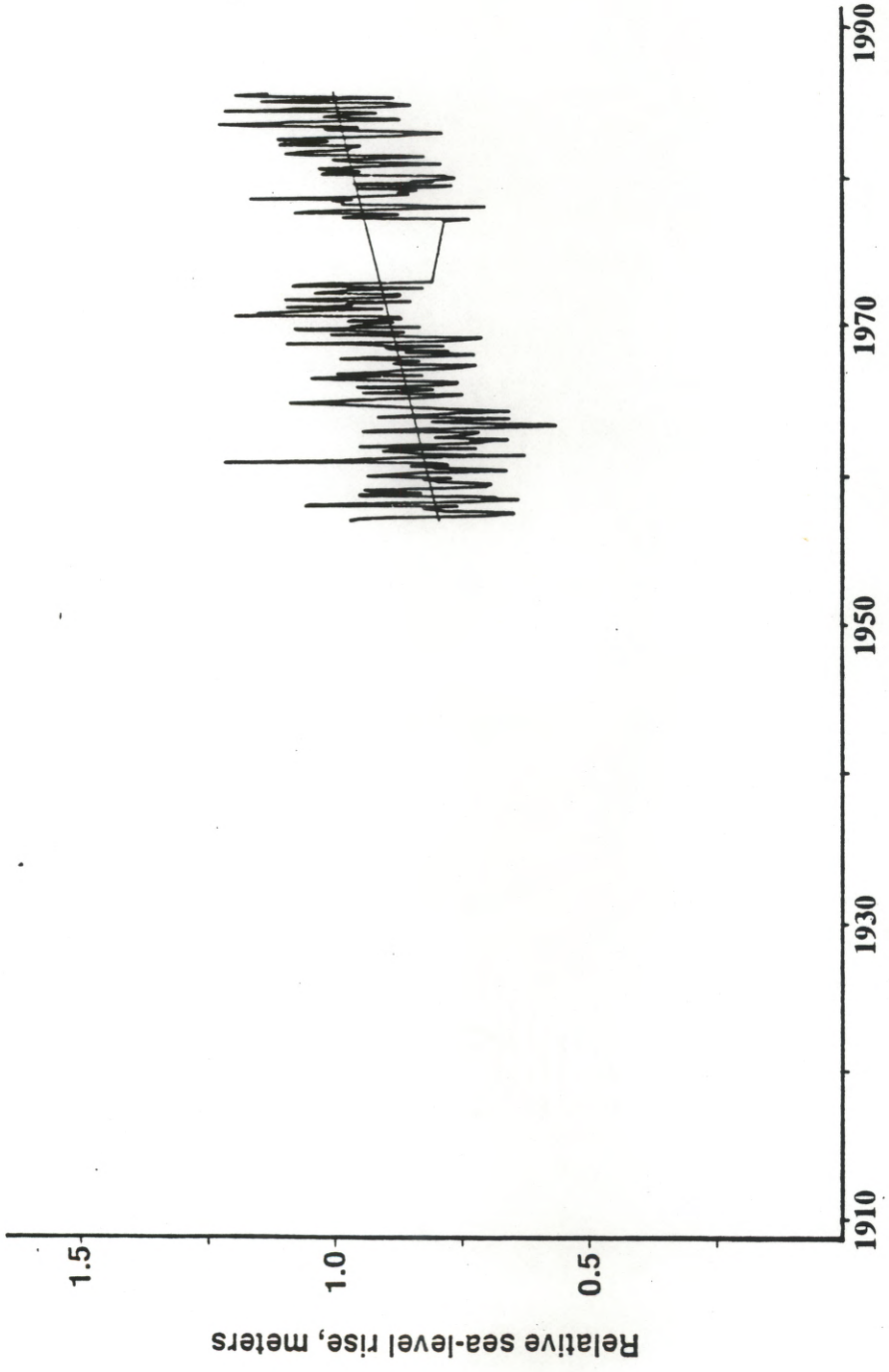

Figure 14. Pleasure Pier, Galveston, TX tidal data and line of regression (slope = 7.3 mm/yr). Period of record = 1958-1986 (Data from the National Ocean Service, NOAA).

(Table 1). The reason for the difference in rate of 3.8 mm/yr between Pier 21 on the landward side of Galveston Island and Pleasure Pier on the Gulfward side is unknown. Although the Pier 21 gage is closer to the focus of groundwater pumping in metropolitan Houston than is the Pleasure Pier gage, the difference in distance is not great enough to account for the discrepency in rates. Fault movement is a possible cause, although additional detailed study is required to reconcile this problem.

These trends suggest that eustatic rise accounts for approximately 25% of the observed RSL rise over the period 1958 to the mid-1980s at the Pier 21 and Sabine Pass stations, which bound the study area. Comparison of the ratio of land-surface subsidence to eustatic rise at the Pier 21 station for the period 1908-1986 (0.60 / 0.40 = 1.5) with the period 1958-1983 (0.75 / 0.25 = 3.0) further suggests that land-surface subsidence has been accelerating more rapidly than eustatic rise over the past century. Although the record at the Sabine Pass station is not long enough to make this comparison, it is probable that the trend is similar.

In order to examine the rate of change of RSL rise over time, pre-1950 and post-1950 regressions, as well as a series of four overlapping 20-year regressions, were performed for each of the stations for which a sufficient length of series is available. Twenty years was chosen because it is the shortest period that can encompass a full 18.6-year lunar cycle. The significance of the lunar cycle is discussed below. The 20-year regressions cover the years 1913-1932, 1931-1950, 1949-1968, and 1967-1986 (all years inclusive). This allows an overlap of 2 years (24 months) of data between each of the regressions. Table 3a shows the rates of RSL rise (in mm/yr) at each of the stations for each of the six epochs. Asterisks (*)

Station	Length of Series	1913-1932	1931-1950	1949-1968	1967-1986
Sabine Pass	1958 - 1983	NA	NA	NA	11.7**
Pier 21	1908 - 1986	3.7	4.1	3.7	9.6
Pleasure Pier	1958 - 1986	NA	NA	5.0*	5.4
Pensacola	1923 - 1986	1.8*	7.3	-0.1	3.5
Cedar Keys	1914 - 1986	1.1*	1.5*	-0.8	1.5
St. Petersburg	1947 - 1986	NA	NA	1.7	4.1
Key West	1913 - 1986	-0.2	4.9	-0.1	4.2

Table 3a. Rates of RSL rise (mm/yr) for 20-yr regressions with 2-yr overlap (time scheme 1)

Station	Length of Series	1916-1935	1933-1952	1950-1969	1967-1986
Sabine Pass	1958 - 1983	NA	NA	NA	11.7**
Pier 21	1908 - 1986	4.8	4.6	3.9	9.6
Pleasure Pier	1958 - 1986	NA	NA	5.4*	5.4
Pensacola	1923 - 1986	2.5*	5.3	0.5	3.5
Cedar Keys	1914 - 1986	2.3*	5.8*	0	1.5
St. Petersburg	1947 - 1986	NA	NA	1.9	4.1
Key West	1913 - 1986	1.3	3.3	0.4	4.2

Table 3b. Rates of RSL rise (mm/yr) for 20-yr regressions with 3-yr overlap (time scheme 2)

Note: NA: Length of series precludes regression for this period.
*: Regression was performed with <150 months of data (20 yr. = 240 mo.).
**: Series ends in 1983.

denote values calculated with an incomplete series of data (less than 150 out of 240 months). Since the data are generally missing from one end of the 20-year series, rather than uniformly distributed throughout the series, the rates are biased either high or low, depending on whether the data are missing from the beginning or the end, respectively, of the series. Therefore, values marked with * should be viewed with caution.

For an individual 20-year series, the rate of rise is variable among the three Florida gages, indicating that there is less consistency among the different stations as the length of series decreases from the full period of record to 20 years. This variability is particularly evident by performing regressions on 20-year series covering only slightly different time periods. Regressions were included for the time periods 1916-1935, 1933-1952, 1950-1969, and 1967-1986 (i.e. three year (36 month) overlap between series) (Table 3b). At all stations, significant differences in the rate of RSL rise exist between the two "time schemes" for any of the epochs (e.g. first epoch: 1913-1932 vs. 1916-1935, etc.).

The variability is likely caused by secular variations, or time-dependent oscillations that have a strong influence on short-term tidal records. An example would be the lunar nodal cycle related to the wobble of the plane of the moon's orbit around the earth. Sea level maxima and minima in tidal records from certain East Coast harbors have been found to correspond closely with the lunar cycle period of ~18.6 yr. (Kaye and Stuckey, 1973). Ramsey and Moslow (1987) suggest that it is necessary to analyze tidal records with records at least twice the lunar cycle (i.e. >37 years) in order to produce meaningful numbers. Other secular variations can be related to seasonal changes and meteorological fluctuations (e.g. droughts). These

short-term variations cause enough noise in the data that trends determined from these 20-year regressions are of little use. Fortunately, the effects of these variations average out when analyzing longer-term records.

Despite the noted variability, the Pier 21 station shows an unmistakable acceleration from a rate of between 3.7-4.8 mm/yr in each of the first three epochs (examining both time schemes) to a rate of 9.6 mm/yr in the fourth epoch (1967-1986). Likewise, the 1908-1950 rate is 3.4 mm/yr while the 1950-1986 trend is 6.3 mm/yr. Sabine Pass shows a rate of rise of 11.7 mm/yr for the period 1967-1983, although the regression was performed with less than 150 data points (months). No regressions could be performed for earlier periods at Pleasure Pier or Sabine Pass for lack of record.

Caution must be exercised in applying the trends for RSL rise determined at Pier 21 and Sabine Pass to the whole coastline of the study area. As discussed in section 2.4, the stations at Pier 21 and Sabine Pass sit atop entrenched Pleistocene valleys of the Trinity River and Sabine-Neches Rivers, respectively. These valleys are filled with sediments deposited as sea level rose following the last glacial retreat 18,000 B.P. The thickness of the Holocene section is approximately 30 m in the buried Trinity River valley near Galveston (Morton and Price, 1987), and at least 35 m in the buried Sabine River valley at Sabine Pass (Kane, 1959; Nelson and Bray, 1970). The thickness of the Holocene section rapidly diminishes away from the buried valleys. The valley-fill sediment is generally clay-rich and still undergoing virginal compaction (normally-consolidated). Therefore, due to consolidation of this thick sequence of sediment, the rates of subsidence, and therefore relative sea-level

rise, recorded at Pier 21 and Sabine Pass may be greater than the rate of rise occurring outside of the entrenched valleys.

3.1.2.3 Bench mark releveling:

This study relies on the assumption that relative sea-level rise has been uniform across the study area and equal to the rate of rise measured at the Pier 21 gage at Galveston (see section 1.2.1). As discussed above, the rate of rise at Pier 21 may be greater than that occurring within the large percentage of the study area outside of the entrenched Pleistocene valleys. The analysis of historical bench mark releveling data is a method to determine land-surface movement within the study area away from the tidal stations.

Bench mark releveling data for the study area are spatially and temporally sparse. Usable data were obtained directly from the National Geodetic Survey for 30 bench marks within the study area. Measured values of land subsidence for an additional 29 bench marks were obtained from two reports published by the National Geodetic Survey (National Ocean Service, 1974; Balazs, 1980). All bench mark locations are shown in fig.15.

The data obtained directly from the Geodetic Survey were in the form of "synthetic" leveling lines constructed specifically for this project, courtesy of Mr. Samuel Moore at the Geodetic Survey. The leveling lines consist of a series of bench marks common to an existing first-order releveling line (called the baseline). For this study, the baselines are L7579 (including bench marks Z167 through R172), constructed in 1936; and L5493 (including benchmarks V309 through Z57), constructed in 1935. Leveling lines for the years 1954 and 1959 are referenced to

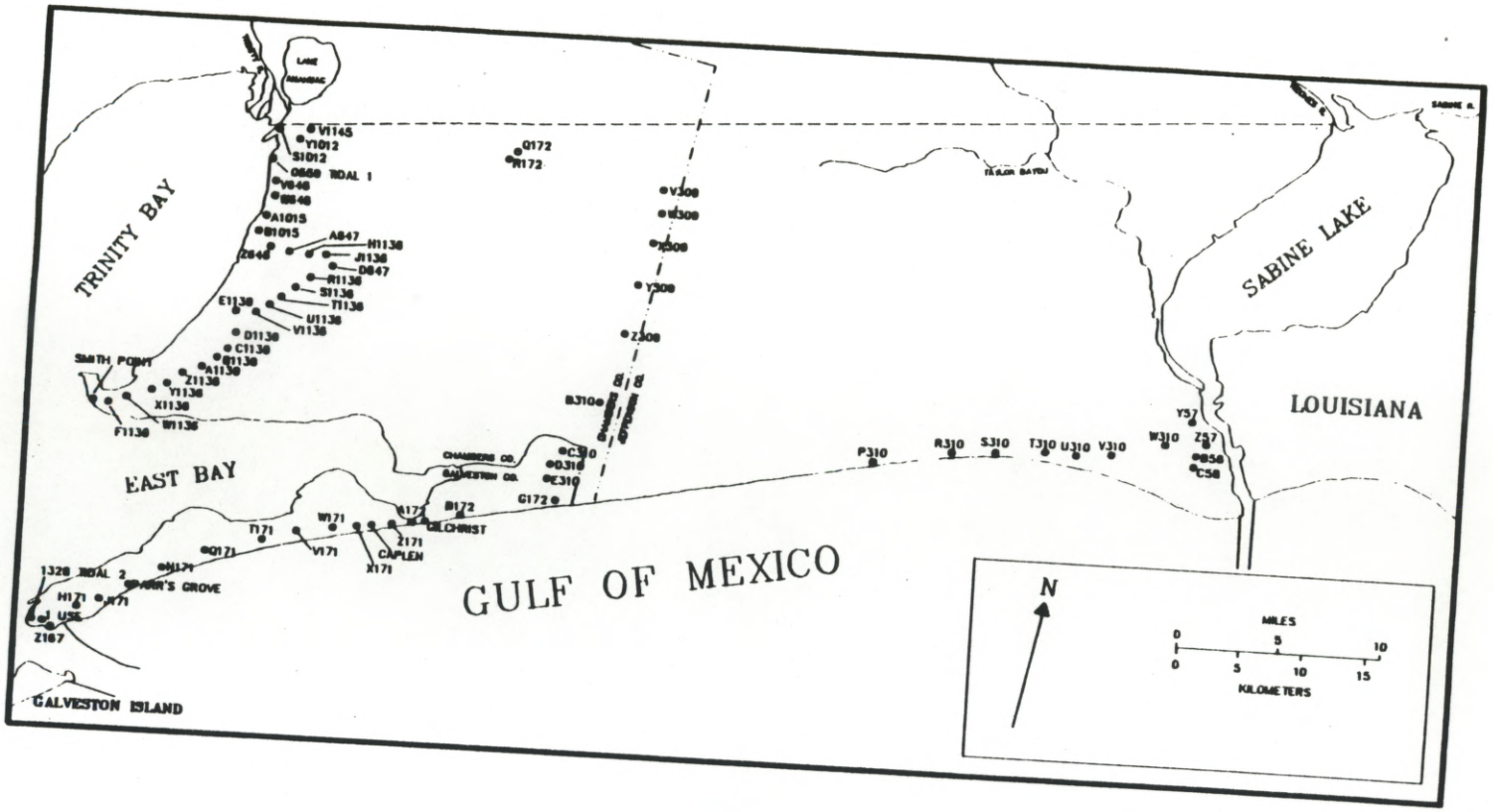

Figure 15. Locations of benchmarks.

Bench mark	Difference in elevation (mm) relative to V309		Rate of movement (mm/yr)	
	1935-1954	1935-1959	1935-1954	1935-1959
V309	0.00	0.00	-9.7	-0.3
W309	49.67	66.56	-7.1	2.5
X309	61.71	-	-6.5	-
Z309	49.24	68.66	-7.1	2.6
B310	47.36	86.34	-7.2	3.3
C310	28.80	64.69	-8.2	2.4
D310	27.41	62.81	-8.3	2.3
E310	45.80	90.77	-7.3	3.5
P310	0.00	0.00	-9.7	-0.3
R310	-10.93	-7.92	-10.3	-0.6
S310	5.25	55.12	-9.5	2.0
T310	10.72	53.96	-9.2	2.0
U310	-3.44	48.21	-9.9	1.7
V310	-2.48	59.05	-9.9	2.2
W310	-4.98	49.90	-10.0	1.8
Y57	-28.36	30.95	-11.2	1.0
C58	-37.70	20.19	-11.7	0.5
B58	-48.40	1.65	-12.3	-0.2
Z57	-41.36	-	-11.9	-

Apparent 'absolute' movement of V309 was -185 mm for 1935-1954 and -7 mm for 1935-1959.

Note: Negative sign indicates subsidence.

Table 4. Unadjusted differences in elevation relative to the first common mark (V309) and calculated rates of movement for the periods 1935-1954 and 1935-1959 at bench marks referenced to baseline L5493 (Data from the National Geodetic Survey).

Bench mark	Difference in elevation (mm) relative to Z167			Rate of movement (mm/yr)		
	1936-1954	1936-1959	1936-1978	1936-1954	1936-1959	1936-1978
Z167	0.00	0.00	0.00	-6.2	-9.4	-5.0
1 USE	13.38	24.69	41.03	-5.4	-8.3	-4.0
877 1328 TIDAL 2	-3.70	7.90	-	-6.4	-9.0	-
H171	31.18	-	-	-4.4	-	-
J171	33.02	-	-	-4.3	-	-
PARRS GROVE	57.02	48.64	196.14	-3.0	-7.3	-0.3
N171	37.83	-	-	-4.1	-	-
Q171	27.60	-	-	-4.6	-	-
PATTON	-43.64	-87.13	35.14	-8.6	-13.2	-4.1
T171	-19.19	-	-	-7.2	-	-
V171	10.67	-	-	-5.6	-	-
W171	31.52	-	-	-4.4	-	-
X171	46.25	-	-	-3.6	-	-
CAPLEN	32.58	-13.87	144.15	-4.4	-10.0	-1.5
Z171	1.79	-	-	-6.1	-	-
A172	108.31	-	-	-0.1	-	-
GILCHRIST	105.57	82.08	-	-0.3	-5.8	-
B172	95.73	-	-	-0.8	-	-
G172	79.13	46.16	195.34	-1.8	-7.4	-0.3
E310	122.82	94.65	290.73	0.7	-5.3	2.0
D310	103.26	65.52	-	-0.4	-6.5	-
C310	107.34	70.09	-	-0.2	-6.3	-
B310	132.52	98.36	-	1.2	-5.1	-
Z309	131.68	77.95	-	1.1	-6.0	-
X309	123.13	-	-	0.7	-	-
W309	99.31	43.05	-	-0.6	-7.5	-
V309	55.22	-17.92	-	-3.1	-10.2	-
Q172	111.17	58.92	-	0.0	-6.8	-
R172	54.34	-12.67	-	-3.1	-9.9	-

Apparent 'absolute' movement of Z167 was -111 mm for 1936-1954, -216 mm for 1936-1959, and -208 mm for 1936-1978.

Note: Negative sign indicates subsidence.

Table 5. Unadjusted differences in elevation relative to the first common mark (Z167) and calculated rates of movement for the periods 1936-1954, 1936-1959, and 1936-1978 at bench marks referenced to baseline L7579 (Data from the National Geodetic Survey).

baseline L5493; separate 1954 and 1959 lines, in addition to a 1978 line, are referenced to baseline L7579 (Tables 4 and 5).

The first common mark in each leveling line is considered equivalent to the elevation of the baseline. Therefore, the value for that first common mark is 0.00. Each subsequent common mark is the difference of the elevation from the first common mark, minus the equivalent difference on the baseline, in millimeters. To illustrate: the second common mark (bench mark 1 USE) in the 1978 leveling line has a value of 41.03 mm (Table 5). To calculate the movement (H) of that bench mark between 1936 (the year of the baseline) and 1978, the following formula is applied:

$$41 = H - (-208)$$

where -208 is the movement, in mm, of the first common mark over the period 1936-1978. A negative value indicates subsidence. From this relation, H equals -167 mm. Dividing H by 42 years gives a subsidence rate of 4.0 mm/yr at bench mark 1 USE between 1936-1978.

This method requires knowing the official height of the first common mark for each year for which a leveling line is available. A height is considered official if it is part of a leveling line that has been adjusted. A line of leveling is considered to be adjusted when the survey is connected to and made consistent with stable bench marks of known elevations (National Ocean Service, 1974). Unfortunately, the data consist of unadjusted elevations. Therefore, the heights for the first common mark are unofficial and calculated differential movements are likely to be inaccurate. This

is evident in examining the vertical movements of bench mark Z167 relative to the 1936 baseline:

1936-1954: -111 mm

1936-1959: -216 mm

1936-1978: -208 mm

These data indicate slight uplift of the bench mark between 1959 and 1978, which is improbable. Similarly, the data indicate that bench mark V309 (the first common mark for L5493) moved -185 mm between 1935-1954, and -7 mm between 1935-1959. Since all other bench marks are referenced to the first common mark, erroneous differential movements will result throughout the entire line of leveling. Regardless, the data can be used to examine spatial, if not temporal, variability in subsidence rates within the study area away from the tidal gages. The calculated rates (mm/yr) of land-surface movement at each benchmark during the different epochs are listed in Tables 4 and 5.

Published reports by the National Ocean Service (1974) and Balazs (1980) present subsidence data based on adjusted heights, which are considered reliable. These reports document releveling done in the Houston-Galveston area in 1973 and 1978. The benchmarks V1145 through SMITH POINT, along the eastern shore of Trinity Bay (fig. 15), were included in these surveys, as well as a 1959 survey. Data for the period 1959-1973 is provided in the 1974 report; the period 1973-1978 is covered in the 1980 report. Unfortunately, these benchmarks were not included in the Houston-Galveston releveling surveys performed in 1983 or 1987.

The data from the two periods were combined to derive a subsidence rate at each bench mark for the period 1959-1978 (Table 6). The rates of subsidence

Bench mark	Movement (mm) 1959-1973	1973-1978	Rate of movement (mm/yr) 1959-1978
V1145	-147.83	-36.58	-9.7
Y1012	-171.91	-47.24	-11.5
S1012	-122.22	-28.96	-8.0
TIDAL 1	-105.46	-49.68	-8.2
V646	-140.82	-34.75	-9.2
W646	-110.03	-43.28	-8.1
A1015	-121.01	-30.48	-8.0
B1015	-119.18	-28.35	-7.8
Z646	-103.02	-26.52	-6.8
A647	-92.05	-44.50	-7.2
H1136	-99.97	-21.95	-6.4
J1136	-97.84	-19.81	-6.2
D647	-92.05	-15.24	-5.6
R1136	-92.96	-16.15	-5.7
S1136	-93.88	-15.54	-5.8
T1136	-93.88	-17.07	-5.8
U1136	-101.80	-18.59	-6.3
V1136	-106.98	-16.76	-6.5
E1139	-119.18	-11.58	-6.9
D1139	-119.18	-13.11	-7.0
C1139	-156.97	-13.72	-9.0
B1139	-224.94	-17.07	-12.7
A1139	-249.94	-24.08	-14.4
Z1136	-217.02	-29.57	-13.0
Y1136	-192.02	-24.99	-11.4
X1136	-176.17	-20.42	-10.3
W1136	-182.88	-15.85	-10.5
F1139	-185.93	-12.50	-10.4
SMITH POINT	-189.89	-10.36	-10.5

Note: Negative sign indicates subsidence.

Table 6. Adjusted differential movements (mm) at bench marks along the east shore shore of Trinity Bay for the periods 1959-1973 and 1973-1978, and rates of subsidence for the period 1959-1978. Data from National Ocean Service (1974) and Balazs (1980).

indicate a general north-to-south trend from higher values (8-11 mm/yr) for marks V1145 through B1015, gradually decreasing to values of 5-6 mm/yr for marks H1136 through V1136, and gradually increasing again to rates higher than 10 mm/yr for marks B1139 through SMITH POINT. The highest rates of subsidence occur at these latter bench marks. The high rates can not be explained by consolidation of soft marsh sediments because the bench marks run adjacent to a road, wisely constructed upon the ridge formed by Ingleside strandplain deposits, which overlie the well-indurated Beaumont Formation. An alternate hypothesis is that the regional subsidence caused by heavy groundwater pumpage in the Houston area extends to these bench marks, although it is still difficult to explain the near doubling of rate over such a short distance. The evidence for the regional effect is discussed in more detail in section 3.1.3.2. Regardless of the reason, the data do suggest higher rates of subsidence near the shore than inland. The rates of movement near the shoreline are in general agreement with rates of movement determined at the Pier 21 and Sabine Pass tidal gages.

3.1.3 Causes of land-surface subsidence:

In order to develop reliable projections of future relative sea-level rise, it is important to assess the contribution of the various components of relative sea-level rise. Historical rates of eustatic rise can be determined and future rates can be estimated from a synthesis of current projections. Past rates of land subsidence can be ascertained from tidal data, but separating the causes of the subsidence is exceedingly difficult. Subsidence of the land surface can be the consequence of both natural and man-induced processes. This study evaluates three possible causes of

land-surface subsidence occurring in the study area: (1) natural consolidation of coastal sediments, (2) consolidation of aquifer systems caused by groundwater withdrawal, and (3) reservoir compaction caused by withdrawal of hydrocarbons and associated water. If it were possible to quantify the contribution of each of these, future projections would be more accurate since future changes in man's activities (e.g. fluid withdrawal) could be considered properly.

Quantification of the various components of land-surface subsidence has not been possible within this study. In a qualitative sense, natural consolidation may account for a major percentage of the subsidence within the study area, although regional depressurization from production of hydrocarbons is also a likely cause. The contributions from these two processes have not been differentiated. Subsidence caused by groundwater withdrawal appears to be negligible within the study area, except along the eastern edge of Trinity Bay, where the effects of pumpage in the Houston area are evident. The three causes of land-surface subsidence within the study area are discussed below.

3.1.3.1 Natural consolidation:

Natural consolidation of Pleistocene and Holocene sediments is a little-researched, and thus poorly-understood, phenomenon. Consolidation is the result of sediment dewatering under the weight of overlying sediments. This process has occurred throughout geologic time and is therefore termed natural consolidation, in contrast to man-induced consolidation caused by withdrawal of subsurface fluids. For the time period of this study, saturated unconsolidated Holocene sediments are of greatest concern since the underlying Pleistocene (Beaumont) sediments have already

undergone considerable consolidation. Unfortunately, the scant information available in the literature does not deal with consolidation of these Holocene sediments, but rather with large scale tilting of Pleistocene depositional surfaces.

Previous investigations: Bernard and LeBlanc (1965) presented an estimated rate of 0.3 mm/yr (1 ft./100,000 yr) for the average rate of tilting of the Beaumont depositional plain. This rate was based on the thickness, age, and present seaward slope of the Beaumont surface.

Winker (1979) provided two methods of estimating a typical rate of subsidence for the Texas Coastal Plain. The first is based on maximum deformation of the Ingleside shoreline assuming continuous tilting since its formation. The subsidence rate is calculated by measuring the difference between geophysically-determined stratigraphic markers (top of clinoform sets) and estimated minimum sea level for small scale eustatic fluctuations (assumed to be 20,000 yrs). Winker calculated a rate of 0.1 m/1000 yrs (0.1 mm/yr) by this method. The second method involves dividing the total sediment thickness for a sedimentary cycle by the duration of that cycle, assuming the rate of sedimentation is constant and equal to the rate of subsidence. This method gives a rate of 0.15 m/1000 years (0.15 mm/yr).

Morton (1979) estimated a subsidence rate for a submerged strandline of the Holocene Brazos-Colorado shoreline. The strandline sits 14 km offshore under 19 m of water. A maximum rate of subsidence was calculated by assuming that depth of scour was negligible during subsequent transgression and that the strandline was 7500 years old. Morton calculated a subsidence rate of 2.5 mm/yr by this method.

I am aware of no studies that measure, directly or indirectly, rates of subsidence in unconsolidated Holocene sediments. These rates are crucial for correct interpretation of rates of relative sea-level rise measured by tidal gages at Galveston and Sabine Pass.

3.1.4.2 Subsidence due to groundwater withdrawal:

Previous investigations: Winslow and Wood (1959) examined subsidence caused by groundwater withdrawal along the upper Texas Gulf Coast from the Brazos River to the Texas-Louisiana border. Using bench mark releveling data, they showed that the area of western Chambers County in the vicinity of Smith Point, as well as the Bolivar Peninsula in Galveston County, subsided between 0.25-0.5 foot between 1918-1954, although no data on potentiometric declines were presented for these areas. Their map indicates that the rest of the study area subsided less than 0.25 foot over this period, except for a small area outlining Sabine Lake. The 0.25 foot contour around Sabine Lake is dashed on their map, however, indicating uncertainty.

The Houston metropolitan area is one of the most spectacular examples anywhere in the world of the direct connection between excessive groundwater withdrawal and land-surface subsidence. Since the late 1960s, R.K. Gabrysch of the USGS in Houston has authored numerous articles on the subsidence in this area. His map of surface subsidence for the period 1908-1978 (Gabrysch, 1982) shows that the regional subsidence is centered at the Pasadena area, where more than 2.7 m (9 ft.) of subsidence occurred (fig. 16). In this region, an area in excess of 12,000 km^2 (4600 $mi.^2$) has subsided greater than 0.3 m (1 ft.). The Harris-Galveston Coastal Subsidence District was created by the Texas Legislature in 1975 to "provide

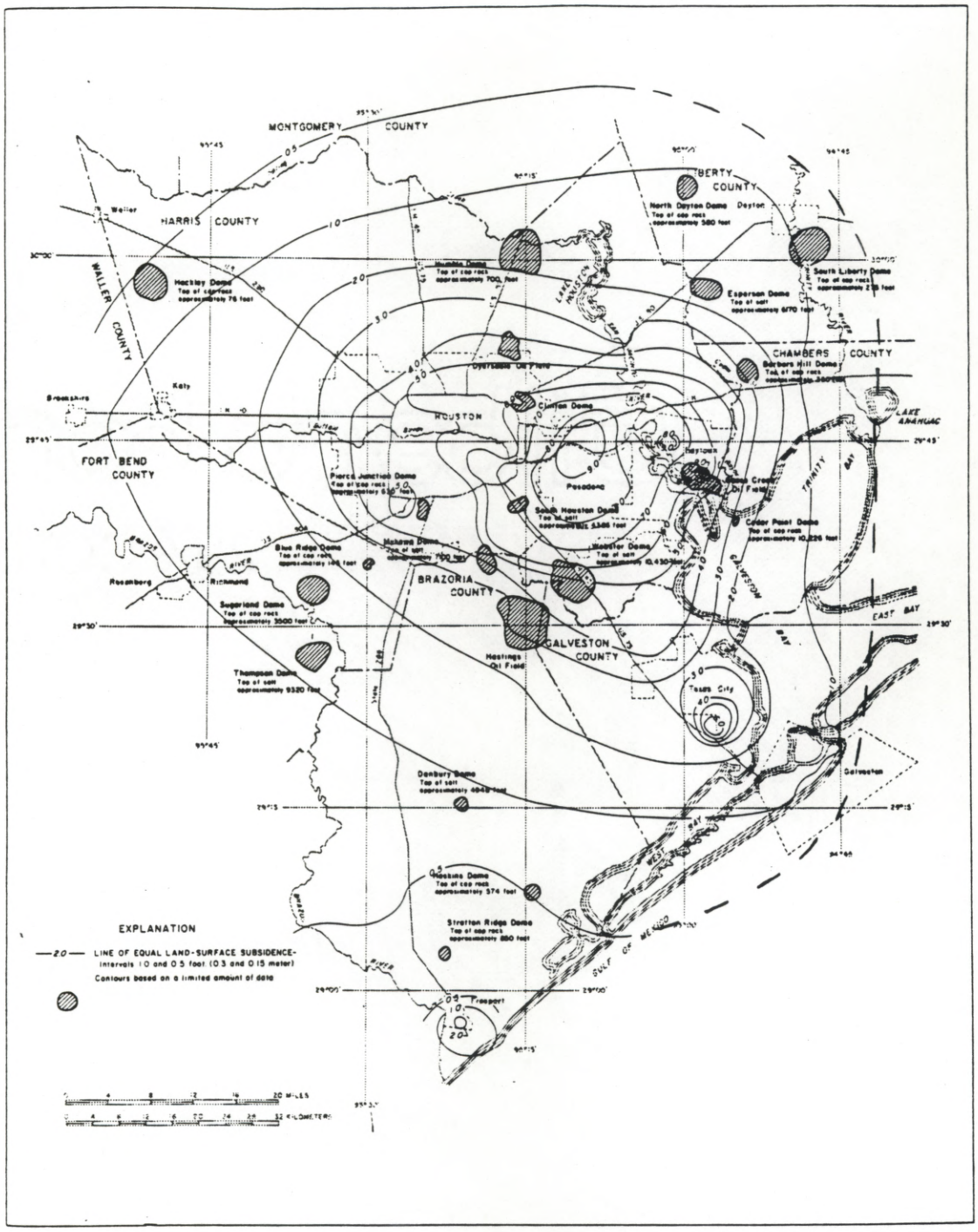

Figure 16. Approximate land-surface subsidence in the Houston-Galveston region, 1906-1978 (from Gabrysch, 1982). Dashed 0.5-foot contour is added by the author (see text).

for the regulation of the withdrawal of ground water within the boundaries of the District for the purpose of ending subsidence..." (Gabrysch, 1984). Records from twelve borehole extensometers (compaction monitors) within the areas of most severe subsidence indicate that subsidence in these areas has generally decreased or ceased since the mid-1970's (Williams and Ranzau, 1985). In these areas of decreasing subsidence, water levels have risen significantly in both the Chicot and Evangeline aquifers, attesting to the success of the District in slowing subsidence by decreasing groundwater pumpage.

Subsidence within the study area caused by groundwater withdrawal:

Figure 16 shows the map of approximate land-surface subsidence in the Houston-Galveston area (1906-1978), adapted from Gabrysch (1982). Although the subsidence contours are approximate, the one-foot contour crosses the tip of the Bolivar Peninsula and almost touches Smith Point. As discussed above, bench marks near Smith Point have subsided nearly twice as much as bench marks to the immediate northeast (section 3.1.2.3). Based on the general shape of the contours, I have drawn on fig. 16 a reasonable extension of the 0.5-foot subsidence contour (dashed line). The position of this contour suggests that the westernmost portion of the study area has subsided in response to the groundwater pumpage in the Houston area. Subsidence of 0.3 m (1.0 ft.) over the 73-year period (1906-1978) equals a rate of land-surface subsidence of 4.1 mm/yr, and a subsidence of 0.15 m (0.5 ft.) equals a rate of 2.1 mm/yr. This suggests that a significant proportion of the observed relative sea-level rise at Pier 21 (6.3 mm/yr, 1908-1986; 11.1 mm/yr, 1958-1986) and Pleasure Pier (7.3 mm/yr, 1958-1986) is caused by land-surface

subsidence caused by groundwater pumpage in the Houston-Galveston area. This hypothesis is supported by the higher rate of rise at Pier 21 than at Pleasure Pier for the period 1958-1986. Pier 21, on the bayward side of Galveston Island, is closer to the areas of concentrated pumpage than is Pleasure Pier on the gulfward side (see fig. 7 for general locations). The causal relationship is further supported by the acceleration in relative sea-level rise during the 1958-1986 epoch. Between 1960-1978, withdrawals of groundwater in the Houston metropolitan area increased over 130% (Gabrysch, 1982), suggesting that a significant increase in groundwater withdrawal has had a direct effect on the rate of relative sea-level rise measured at Pier 21.

Because of poor groundwater quality, pumpage within the study area itself is minor. Historically, most of the groundwater used within the study area has been imported from neighboring Orange, Hardin, and Liberty counties (fig. 2), although surface water from the Trinity and Neches Rivers is the principal source of potable water for the area (Wesselman and Aronow, 1971; Bonnet and Gabrysch, 1982).

The salinity of groundwater within the Chicot aquifer underlying the study area restricts its use. Groundwater with total dissolved solids (TDS) less than 1000 mg/l (the accepted limit for potable water) occurs only in shallow, isolated sand lenses and in alluvium adjacent to streams. Most of the groundwater in the Chicot aquifer underlying the study area contains more than 3000 mg/l TDS (Wesselman and Aronow, 1971). Figures 17b and 18b are cross sections along strike (A-A') and along dip (B-B'), respectively, through the Chicot and Evangeline aquifers in Chambers and Jefferson counties (modified from Wesselman and Aronow, 1971). The locations of the cross sections are shown in figures 17a and 18a. The aquifers

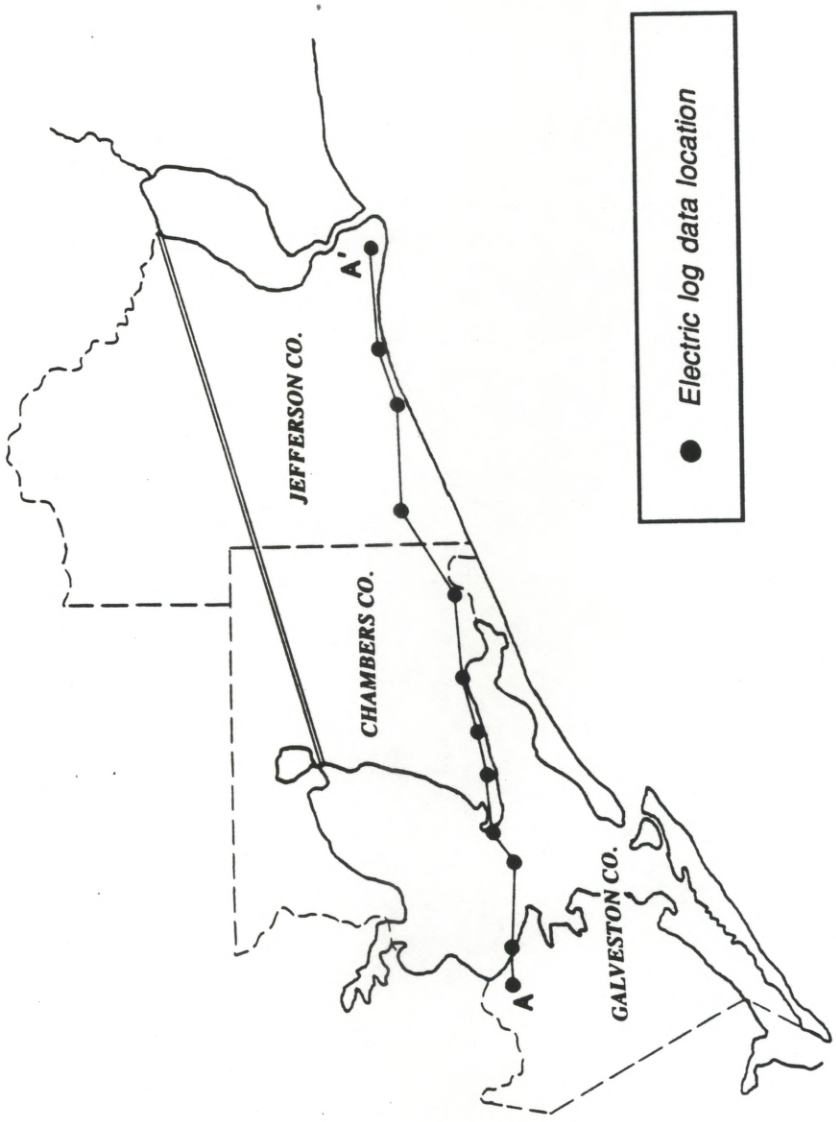

Figure 17a. Location of cross section A-A'. Northern border of study area is delineated by double line.

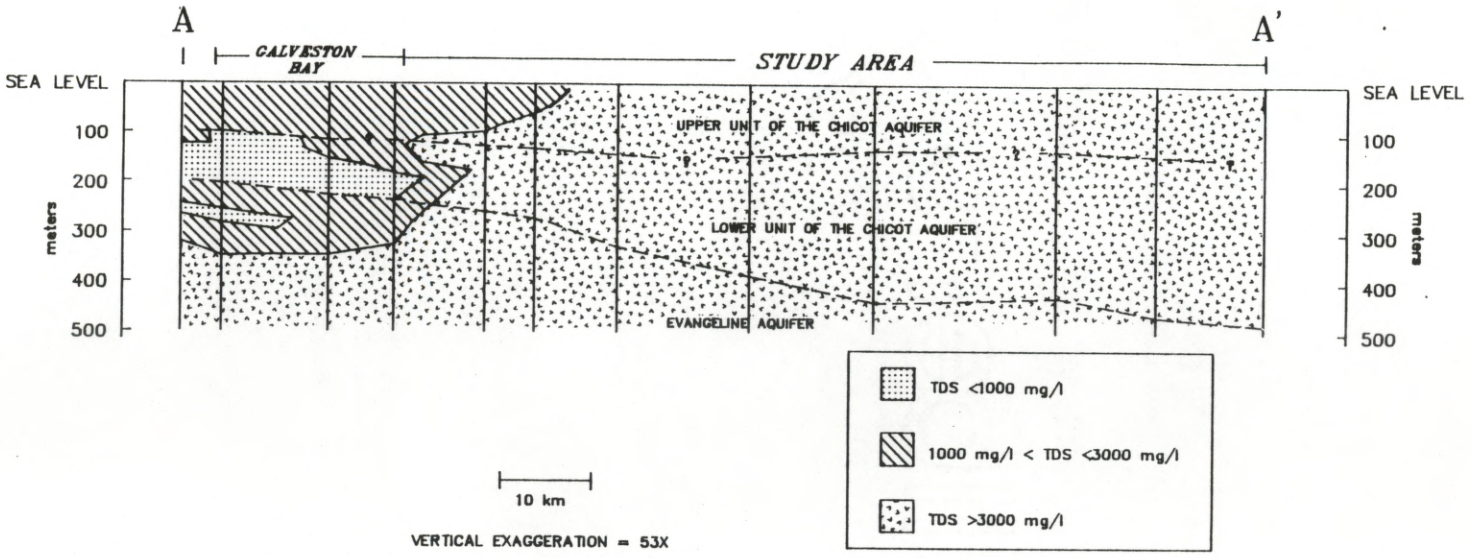

Figure 17b. Cross section A-A'. Vertical lines represent locations of electric log data shown in fig. 17a (modified from Wesselman and Aronow, 1971).

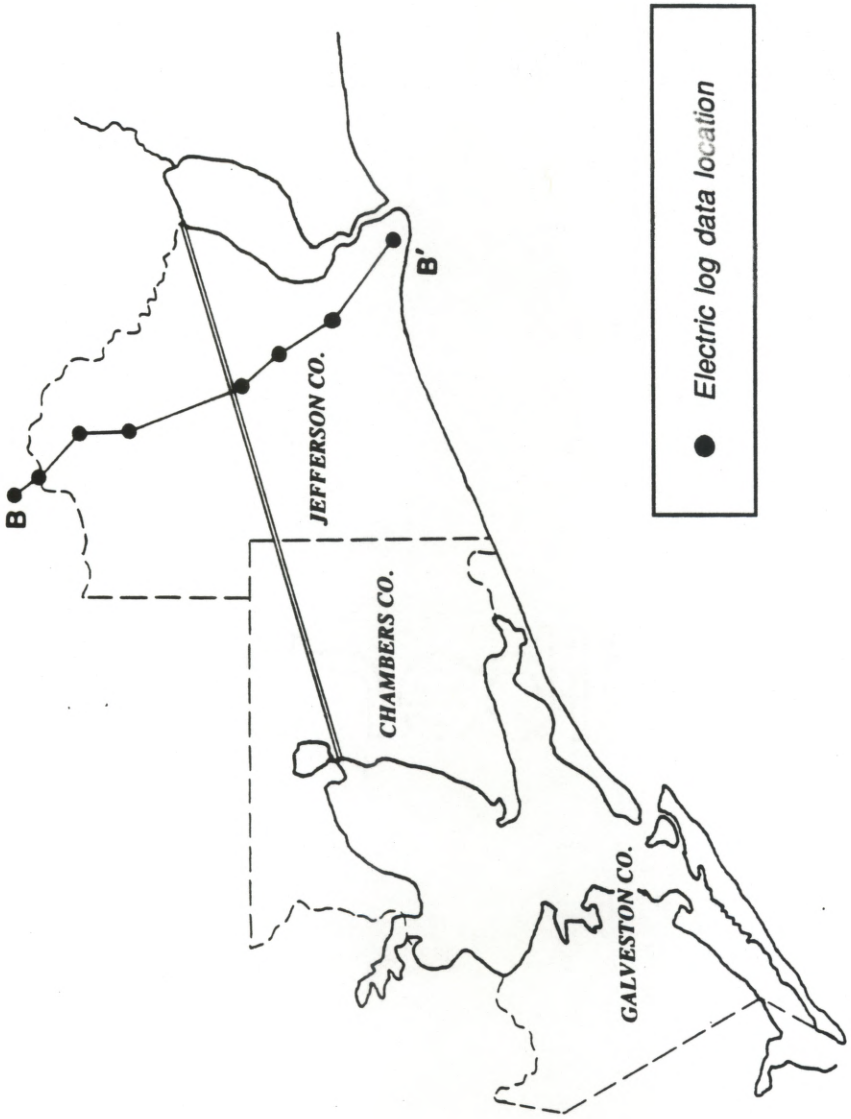

Figure 18a. Location of cross section B-B'. Northern border of study area is delineated by double line.

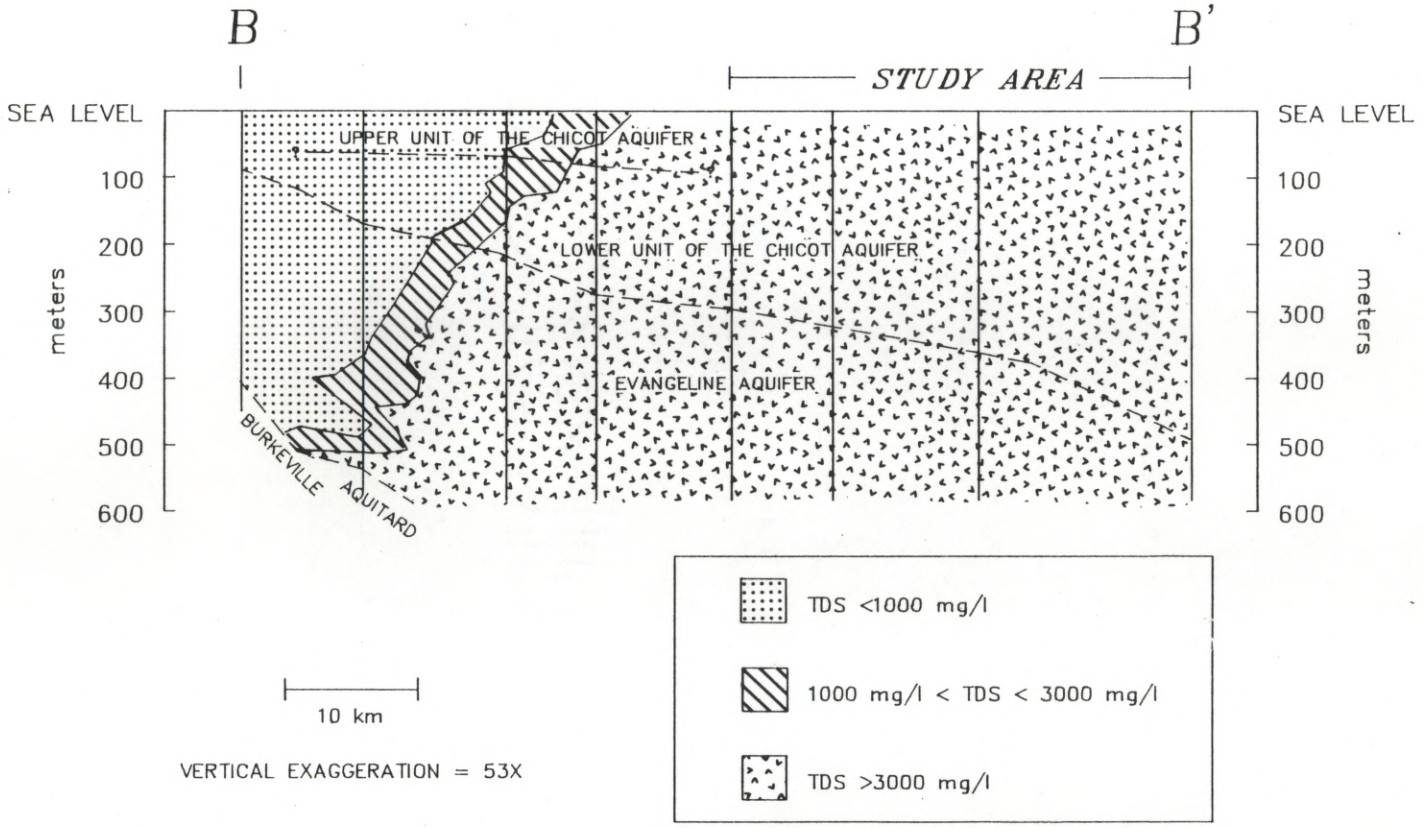

Figure 18b. Cross section B-B'. Vertical lines represent locations of electric log data shown in fig. 18a (modified from Wesselman and Aronow, 1971).

are divided into three categories based on groundwater salinity as interpreted from electric logs: TDS < 1000 mg/l, 1000 mg/l < TDS < 3000 mg/l, and TDS > 3000 mg/l. Cross section A-A' (fig. 17b) shows the eastward deterioration of water quality from the area west of Galveston Bay along strike to the study area. Cross section B-B' (fig. 18b) shows the deterioration of water quality from the recharge area in Hardin County downdip to beneath the study area. The TDS in the westernmost portion of the study area along Trinity Bay varies between 1000-3000 mg/l; however, the majority of sands within the Chicot aquifer underlying the study area contain water with TDS greater than 3000 mg/l, making it unsuitable for most uses.

Land-surface subsidence caused by groundwater withdrawals is not significant within the study area since water-level declines are small throughout the area, except in the westernmost portion as discussed above. A review of all water level data for Galveston, Chambers, and Jefferson counties available from the Texas Water Commission shows no water-level decline in excess of 11 m (36 ft.) for any well within the study area. Appendix 2 shows hydrographs for nine typical water wells across the area. The well locations are shown in fig. 19. These nine hydrographs are representative of the wells in the area and were chosen primarily for their geographic distribution and length of record. The maximum decline, the difference between the highest and lowest levels on record, is 11 m (36 ft.) at well # 64-14-406 near Winnie. A potentiometric decline of 11 m corresponds to a decrease in pore fluid pressure of less than 111 kN/m^2 (16 psi).

By comparison, maximum water level declines in the Houston area were greater than 75 m (250 ft.) in the Chicot aquifer, and greater than 120 m (400 ft.) in

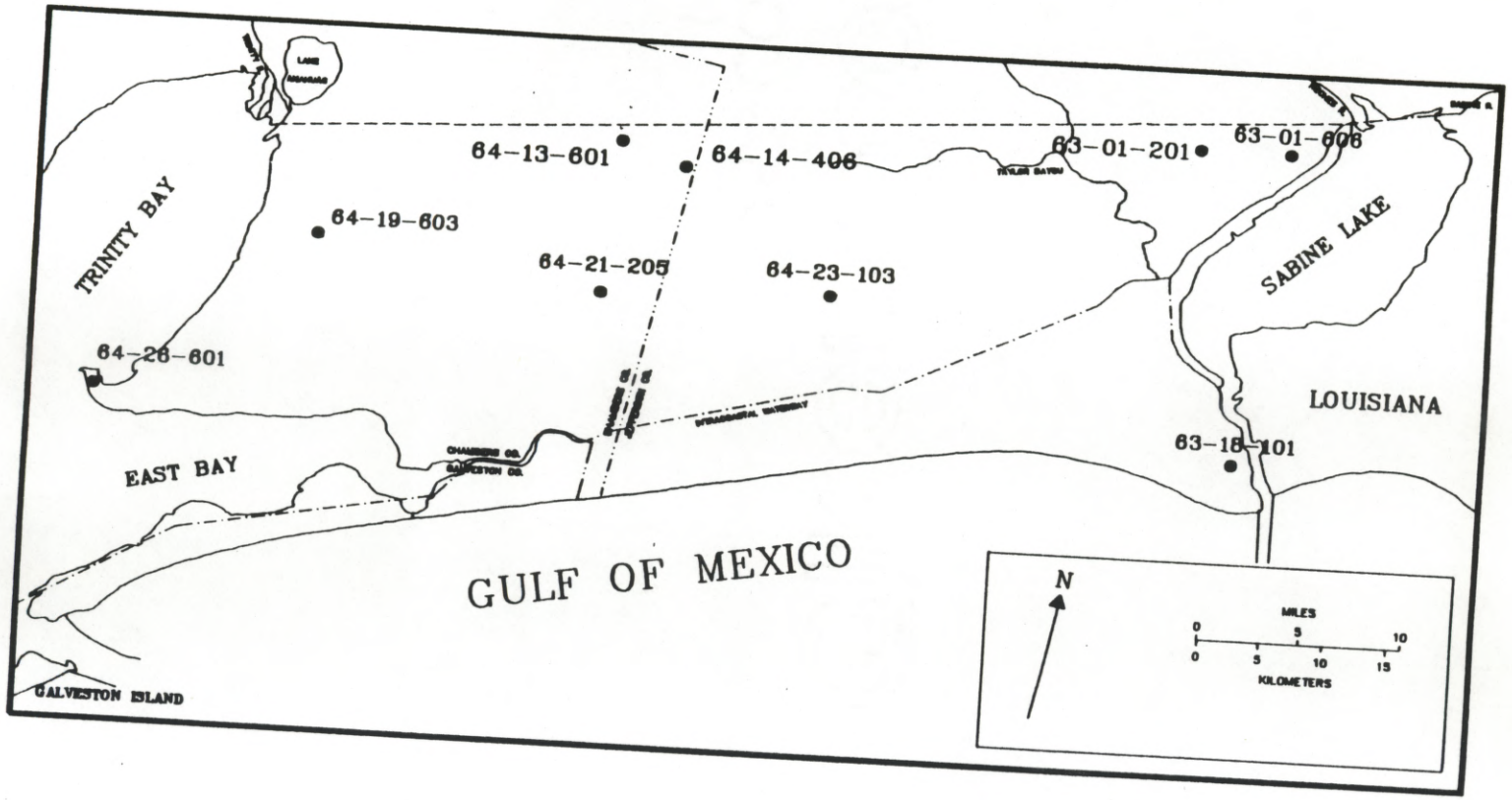

Figure 19. Locations of water wells for which hydrographs are provided in Appendix 2.

the Evangeline aquifer by the mid 1970s (Harris-Galveston Coastal Subsidence District, 1980). In addition, since the pumping within the study area is limited to the Chicot aquifer, primarily the upper unit of the Chicot where water quality is better, there is a small stratigraphic interval, generally less than 75 m (250 ft.), within which compaction will occur. Pumping from the Chicot and Evangeline aquifers in the Houston area occurs over a stratigraphic interval more than 600 m (2000 ft.) thick (Carr and others, 1985). The combination of small pumping stresses and a relatively thin interval of production suggests that compaction, and resulting surface subsidence, should be insignificant within the study area, except in areas where water levels are drawn down in response to pumping beyond the boundaries of the study area. This is also the consensus of Winslow and Wood (1959), Wesselman and Aronow (1971) and Bonnet and Gabrysch (1982).

Groundwater pumpage in the study area is not expected to increase significantly in the future. Water levels should not decline and subsidence caused by aquifer compaction, therefore, should not occur. Water levels are relatively stable at present, as indicated by the hydrographs in Appendix 2. In general, the water level declines have ceased following the initial well development; water levels have even increased over the past 15-20 years in some wells. Water quality in wells producing from isolated fresh-water sands will deteriorate where continued pumping causes intrusion of more saline water from depth. Furthermore, large quantities of fresh groundwater are available in adjoining counties, making continued importation of groundwater practicable. However, most future fresh-water demands within the study area will probably continue to be met by surface water.

3.1.4.3 Subsidence due to oil-and-gas production:

Previous Investigations: Pratt and Johnson (1926) first documented differential subsidence due to oil-and-gas production in the Texas Gulf Coast at the Goose Creek oil field near Baytown (fig. 20). Production began in 1917 and by 1925 subsidence at the center of the field exceeded 1 m and affected an elliptical area of approximately 11 km^2. Pratt and Johnson estimate that the reservoir pressure declined by 7600-8300 kPa (1000-1200 psi) over the eight year period. Normal faults as long as 0.7 km with displacements as great as 40 cm were recorded within the subsiding area. The subsidence caused permanent inundation of low-lying areas adjacent to the area of production.

Kreitler (1976) stated that land-surface subsidence and surface faulting have occurred over six oil-and-gas fields in Harris county, namely the South Houston, Clinton, Mykawa, Blue Ridge, Webster, and Goose Creek fields. Groundwater withdrawals within these fields are not great enough to be responsible for the movements. Kreitler also described the Saxet oil-and-gas field west of Corpus Christi where a two-meter fault scarp developed within the field, coincident with a rapid increase in gas production from shallow sands in the field, but he concluded that, within the general Houston area, groundwater withdrawal is the predominant driving force for land-surface subsidence.

Holzer and Bluntzer (1984), using leveling data from the National Geodetic Survey, generated 29 subsidence profiles crossing 26 oil-and-gas fields within the Houston regional subsidence area. They concluded that subsidence at all but six (the same six listed by Kreitler, 1977) of the 26 fields was not increased by production of hydrocarbons. At four fields -Barbers Hill, Cedar Bayou, Humble, and Pierce

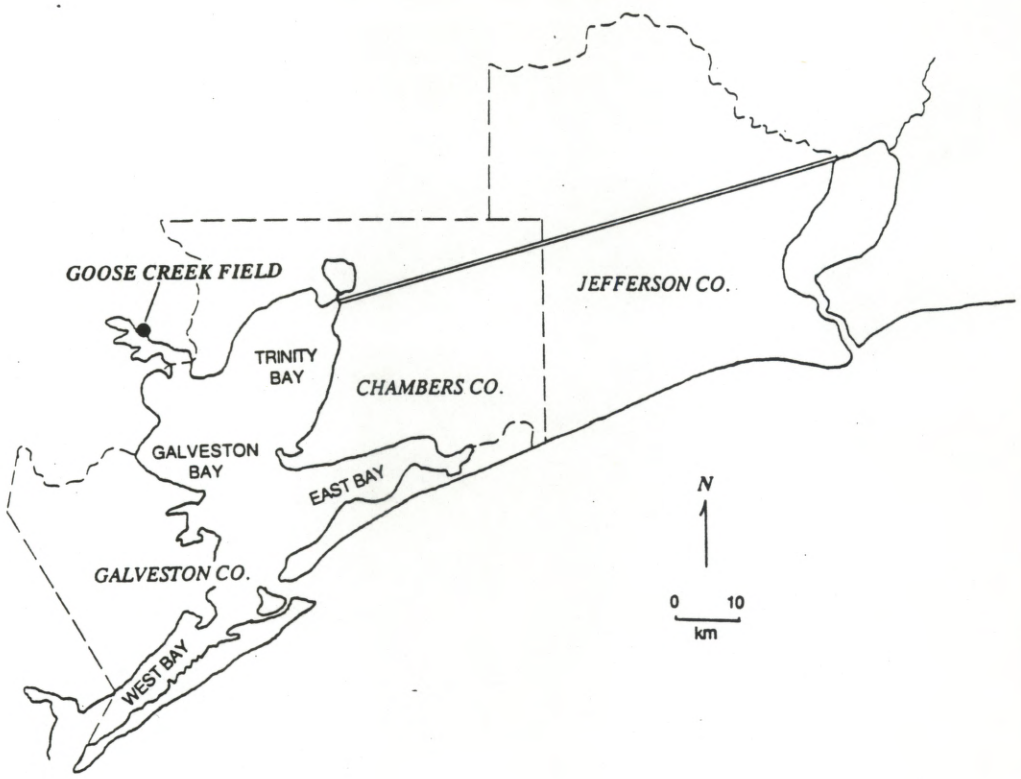

Figure 20. Location of the Goose Creek oil field.

Junction- the observed subsidence was considerably less than in the surrounding area. Holzer and Bluntzer attributed this to a localized decrease in the thickness of the aquifer system caused by shallow salt domes that intrude above the base of the aquifer system. They concluded that the contribution of oil-and-gas withdrawal to localized land subsidence is minimal in the Houston area.

Ratzlaff (1982) presented the only example of localized subsidence over a producing reservoir within the study area. Between 1959-1977 subsidence of at least 0.33 m occurred in a 20 km^2 (4940 acres) area in the Port Acres area, based on releveling data and comparison of 1959 and 1977 topographic maps. Within this 20 km^2 area, two smaller areas subsided in excess of 1 meter. This period of subsidence corresponds closely to the period of discovery and development of the Port Acres Gas Field in 1957. Ratzlaff concluded that withdrawal of oil, gas, and associated water is the most probable cause of this subsidence.

Ewing (1985) presented another example of subsidence and surface faulting probably caused by hydrocarbon production. Surface faulting in the High Island-Caplen area of Chambers and Galveston counties, where groundwater withdrawals are minimal, is observed in 1982 aerial photos but absent in 1930 photos, suggesting that the faulting is man-induced. The faults at Caplen extend to Robinson Lake across East Bay, forming a graben structure that is located above a subsurface structural high. The geometry of the East Bay fault system closely resembles that of the Genoa-Webster fault system southeast of Houston. Ewing hypothesizes that perhaps the two fault systems are responses to production of oil and gas from reservoirs with strong water drive. Large-volume production from such reservoirs could cause a regional depressurization in laterally-continuous aquifer systems, thus

leading to consolidation of interbedded aquitards. This consolidation would create tension resulting in the formation of normal faults. Ewing further states that the depressurization at Caplen might be associated with the production of roughly 83 million cubic meters (400 million bbls) of oil and associated water from Lower Miocene sands at depths of 1200-2400 m (4000-8000 ft.) at the High Island Dome 15 km to the east. These sands show excellent lateral continuity to the Caplen field.

Modeling land subsidence above oil-and-gas reservoirs: In order to have significant land-surface subsidence above producing hydrocarbon reservoirs, four criteria must be met:

1) Large reduction in reservoir pressure
2) Production from a large vertical interval
3) Poorly-consolidated reservoir rock
4) Shallow reservoir depth of burial

Several of the fields within the study area appear to satisfy these four criteria, to differing degrees.

The most straightforward method for determining a relationship between land-surface subsidence and oil-and-gas production is to directly compare histories of differential subsidence with histories of reservoir pressure decline for a number of major oil-and-gas fields within the study area. Fig. 21 shows generalized outlines of major oil-and-gas fields within the study area. Production has been from three primary plays: shallow piercement salt domes, Frio deep-seated salt domes, and Frio

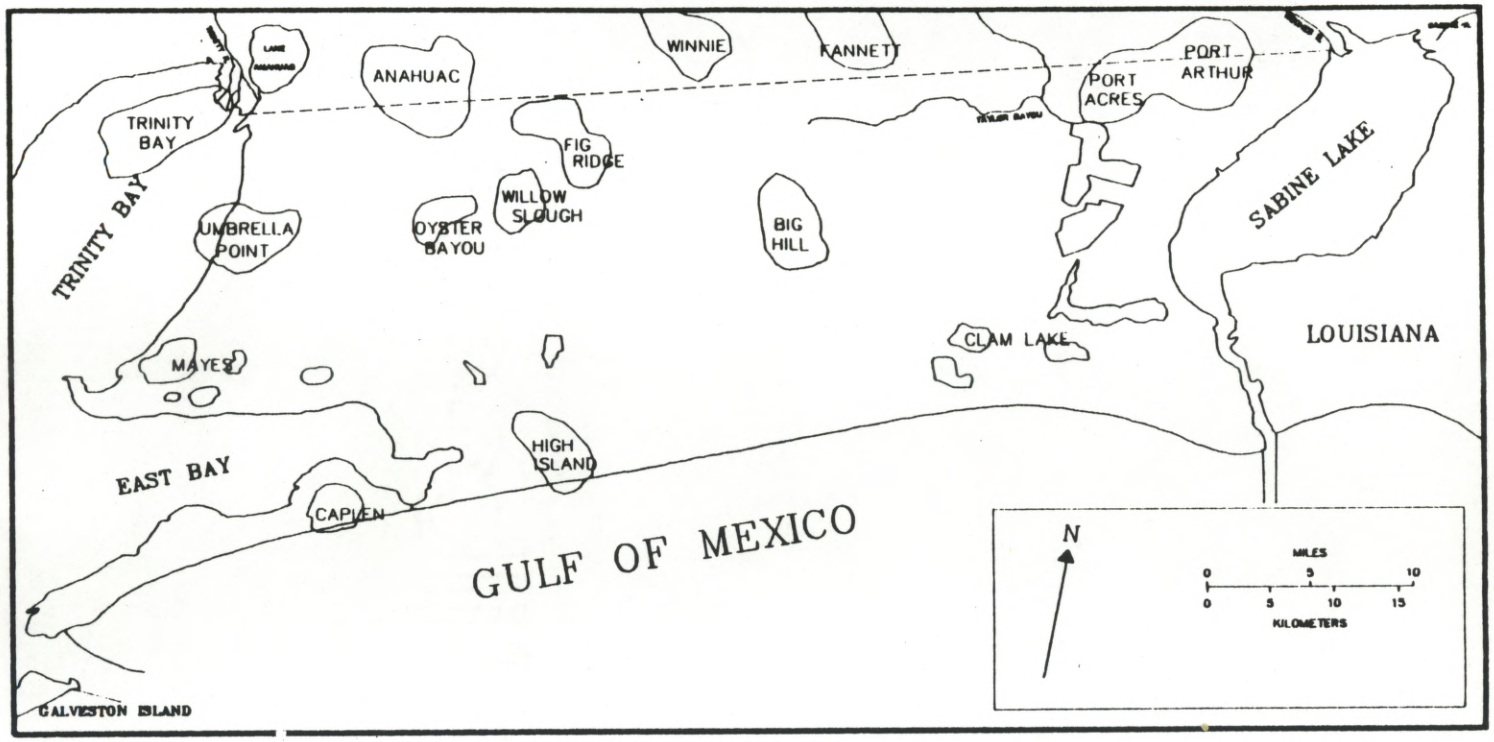

Figure 21. Generalized outlines of major oil-and-gas fields within the study area.

(Buna) barrier/strandplain sandstones (Galloway and others, 1983). Hydrocarbon production has been extensive within the area; however, I am aware of only one report (Ratzlaff, 1982) of localized land-surface subsidence above oil-and-gas fields within the study area. This may be due to the fact that there have been few studies addressing land subsidence in the area.

In addition, although abundant production data are available from the Texas Railroad Commission, data on reservoir pressures for oil-and-gas fields are scarce since bottom-hole pressures are not routinely required to be reported in Texas (Holzer and Bluntzer, 1984). It would be possible to develop a relation between production volume and subsidence, but the relation would be tenuous at best since the large volumes of water produced with the hydrocarbons are rarely reported. Dealing directly with reservoir pressure avoids this problem.

For litigation purposes, oil companies often develop pressure decline curves which are subsequently kept in hearing files at the Texas Railroad Commission. From these files, I found pressure-decline curves for seven fields within, or immediately adjacent to, the study area. The pressure declines generally represent averages for an entire reservoir, or even for an entire field. In addition to these seven fields, I estimated a pressure decline of 7585 kN/m^2 (1100 psi) for the Goose Creek field, based upon Pratt and Johnson's (1926) estimate of a 6895-8275 kN/m^2 (1000-1200 psi) depressurization within the field between 1917-1925. The Goose Creek field is especially useful in this analysis since the land-surface subsidence resulting from oil-and-gas production is well documented, therefore providing a means of calibration between depressurization and land-surface subsidence. The eight fields for which depressurization data are compiled are listed in Table 7.

Field	low Cm (m2/N)	high Cm (m2/N)	Avg. porosity (-)	D (m)	R (m)	h (m)	dP (kN/m2)
Anahuac	4.2E-07	1.5E-06	0.28	2030	2010	110	4964
Clam Lake	6.3E-07	2.1E-06	0.32	1590	800	470	1207
Fig Ridge/Seabreeze	1.2E-07	2.7E-07	0.27	2590	1830	50	7722
Goose Creek	2.1E-06	6.0E-06	0.37	460	1680	30	7585
High Island	6.0E-07	9.0E-07	0.31	1680	950	90	19030
Lovells Lake	3.0E-07	3.9E-07	0.30	2320	2070	60	11722
Oyster Bayou	2.1E-07	3.0E-07	0.29	2500	1390	50	5861
Trinity Bay	3.0E-07	4.5E-07	0.32	2440	2530	30	2275

Table 7. Reservoir parameters and depressurization data for eight fields within and adjacent to the study area. Parameters include: D = depth of burial, R = radius of assumed disc-shaped reservoir, h = reservoir thickness, dP = reservoir pressure decline, Cm = uniaxial compaction coefficient (low and high Cm values from ranges of values presented in Geertsma (1973)).

Geertsma (1973) developed a simple analytical model for making an order-of-magnitude estimate of surface subsidence above compacting oil-and-gas reservoirs. I used this model to determine which fields within the study area have the potential for significant land-surface subsidence based on the field's history of depressurization.

Land-surface subsidence above a reservoir is the result of reservoir compaction caused by an increase in effective stress equal to the decrease in pore-fluid pressure. This simple relation is termed the Terzaghi equation (eq. 1).

$$\sigma = \sigma' + P \qquad (1)$$

where σ = total stress, σ' = effective stress, and P = pore fluid pressure. Provided the lateral dimensions of the reservoir are large compared to the vertical, reservoirs deform predominantly vertically (Geertsma, 1973). Consequently, this model does not consider lateral strains in the reservoirs. The uniaxial compaction coefficient, c_m, is defined as the formation compaction per unit decline in pore pressure (i.e. the ratio of one-dimensional strain to stress)

$$c_m = (1/h)\,\Delta h/\Delta P, \text{ or } \varepsilon = c_m\,\Delta P \qquad (2)$$

where h = reservoir thickness, ΔP = change in pore pressure, and $\varepsilon = \Delta h/h$ is the vertical strain in the reservoir. C_m is a function of effective stress (inversely related), and thus also of the change in pore pressure. However, c_m can be assigned a fixed value over the pressure range occurring during production in most reservoirs

(Geertsma, 1973). Therefore, eq. 2 can be rearranged to solve for reservoir compaction, Δh, caused by a depressurization, ΔP.

$$\Delta h = c_m \, h \, \Delta P \tag{3}$$

Geertsma's model treats the problem of subsidence due to reservoir depressurization as one of an isolated volume of reduced fluid pressure, termed the nucleus of strain, in an elastically-deforming half space with a traction-free surface (fig. 22). The free surface represents the ground surface. The interaction between the compacting nucleus of strain and its surroundings is calculated using methods developed in the theory of thermoelasticity (Geertsma, 1973). The 1-D displacement of the free surface ($z = 0$) above the contracting nucleus of strain is given by

$$u_z(r,0) = -(1/\pi) \, c_m \, (1 - \upsilon) \, (r^2 + D^2)^{-1.5} \, \Delta P \, D \, V \tag{4}$$

where u_z = vertical displacement of the free surface ($z = 0$) at any radius r from the nucleus of strain, c_m = compaction coefficient, υ = Poisson's ratio, ΔP = change in pore pressure, D = vertical distance between the nucleus of strain and free surface, and V = finite volume of the nucleus of strain.

The model assumes a highly simplified geometry: a disc-shaped reservoir of radius R, thickness h, under a depth of burial D (fig. 23). The model further assumes that the reservoir and its surroundings deform homogeneously (i.e. both the compaction coefficent, c_m, and Poisson's ratio, υ, are assumed constant throughout the half space), and that the reservoir volume undergoes uniform depressurization.

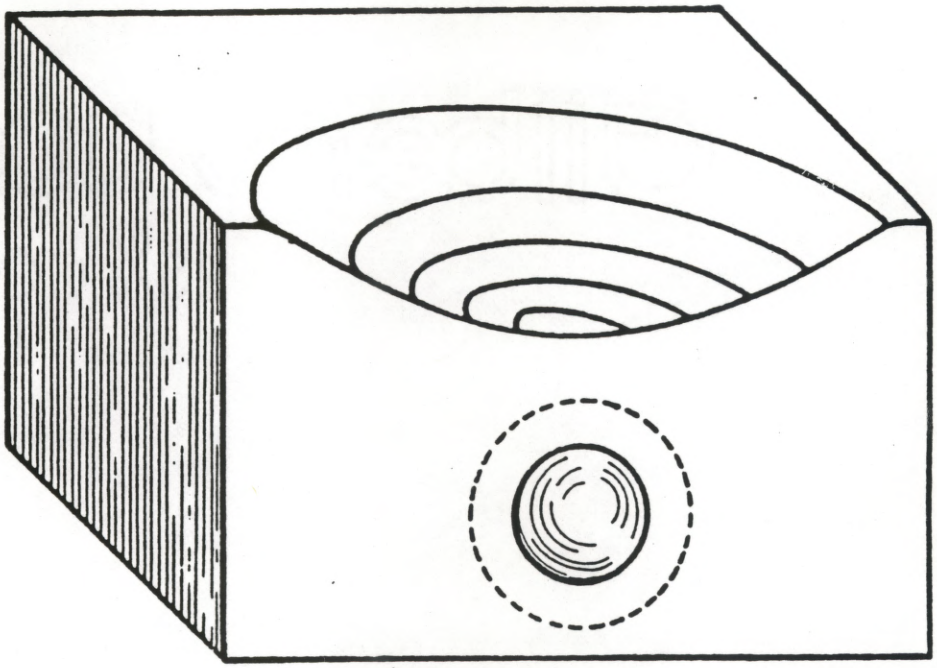

Figure 22. Surface subsidence above a contracting nucleus of strain (from Geertsma, 1973).

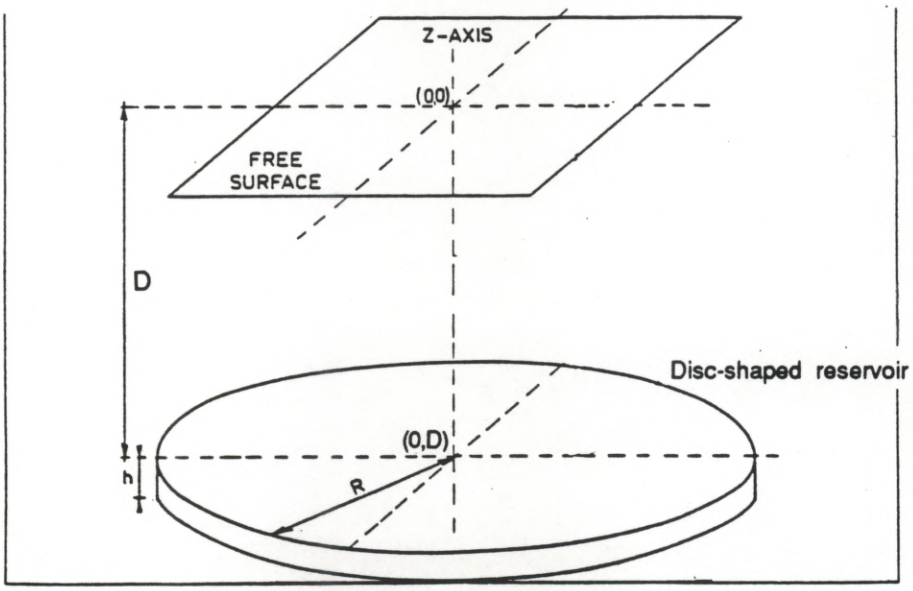

Figure 23. Idealized reservoir geometry for Geertsma's (1973) reservoir compaction model. R = radius of disc-shaped reservoir, D = depth of burial, h = reservoir thickness.

For this geometry and assumptions, the subsidence above the disc-shaped reservoir can be calculated by integrating the nucleus solution (eq. 4) over the entire reservoir volume to yield

$$u_z(r,0) = -2c_m (1 - \upsilon) \Delta P \, h \, R \int_0^\infty e^{-D\alpha} J_1 (\alpha R) J_0 (\alpha r) \, d\alpha \qquad (5)$$

where J_0 and J_1 are Bessel functions of zero and first order, respectively. Tables of numerical values for the "Hankel-Lipschitz" integral for selected values of r/R and D/R are provided in Geertsma (1973).

For the calculation, values for parameters were determined for each of the eight fields for which pressure decline data were collected. A disc-shaped geometry was applied to the major reservoir(s) within each field. Thicknesses, areal extents, and depths of the major producing interval(s) within each field were obtained from type sections and other information in the hearing files at the Texas Railroad Commission as well as from Galloway and others (1983). The data are presented in Table 7 .

The most difficult parameter to define for a reservoir is the uniaxial compaction coefficent, c_m. This parameter is not routinely determined for reservoir rock, therefore, very few data are available either in the literature or in Railroad Commission files. For this analysis, I relied on laboratory-determined ranges of values presented in Geertsma (1973) for sandstone reservoirs. The values range over two orders of magnitude, dependent on depth of burial, porosity, and degree of consolidation. Low and high estimates of c_m for this study were picked from Geertsma's ranges in order to encompass the full range of reasonable values, based

on the depth of burial and average porosity of the reservoir sandstone. Since the compaction coefficient is linearly related to surface subsidence (eq. 5), the surface subsidence also can vary over two orders of magnitude, holding all other factors constant.

Although the results from this simple model must be viewed with caution, the model does represent a method of comparing the potential for subsidence for some of the large oil-and-gas fields within the study area. Furthermore, by varying the value of c_m over a range reasonable for each field based on depth of burial and average porosity, it is possible to develop a range of possible responses for the field. Table 8 shows the model results for the eight fields for which data were available. The table shows low and high estimates of surface subsidence (based on low and high estimates of c_m) at both the center of the field ($r = 0$) and at the edge of the assumed-circular field ($r = R$).

The Goose Creek field provides the best check on the validity of the model because the surface subsidence resulting from the depressurization is documented in Pratt and Johnson (1926). Table 8 shows the low-to-high range of estimated subsidence from 25 cm to 72 cm at the center of the field and from 12 cm to 35 cm at the edge of the assumed-circular field, a radius of 1680 m (5500 feet) from the center. Fig. 24 shows the elliptical bowl of subsidence developed between 1917-1925 at Goose Creek. The maximum measured subsidence was approximately 100 cm, occurring at the center of the field. The subsidence decreased to near zero at distances of approximately 2.5 km along the major axis of the ellipse and approximately 1.7 km along the minor axis. This shows that, even using the high value for the compaction coefficient, the model underestimated the subsidence that

Field	low Uz (r=0) (cm)	low Uz (r=R) (cm)	high Uz (r=0) (cm)	high Uz (r=R) (cm)
Anahuac	5	3	16	10
Clam Lake	3	2	9	7
Fig Ridge/Seabreeze	1	0	1	1
Goose Creek	25	12	72	35
High Island	9	7	14	10
Lovells Lake	4	2	5	3
Oyster Bayou	0	0	1	1
Trinity Bay	0	0	1	0

Table 8. Simulated low and high estimates of surface subsidence (Uz) at center of reservoir (r = 0) and at edge of reservoir (r = R). R = radius of disc-shaped reservoir.

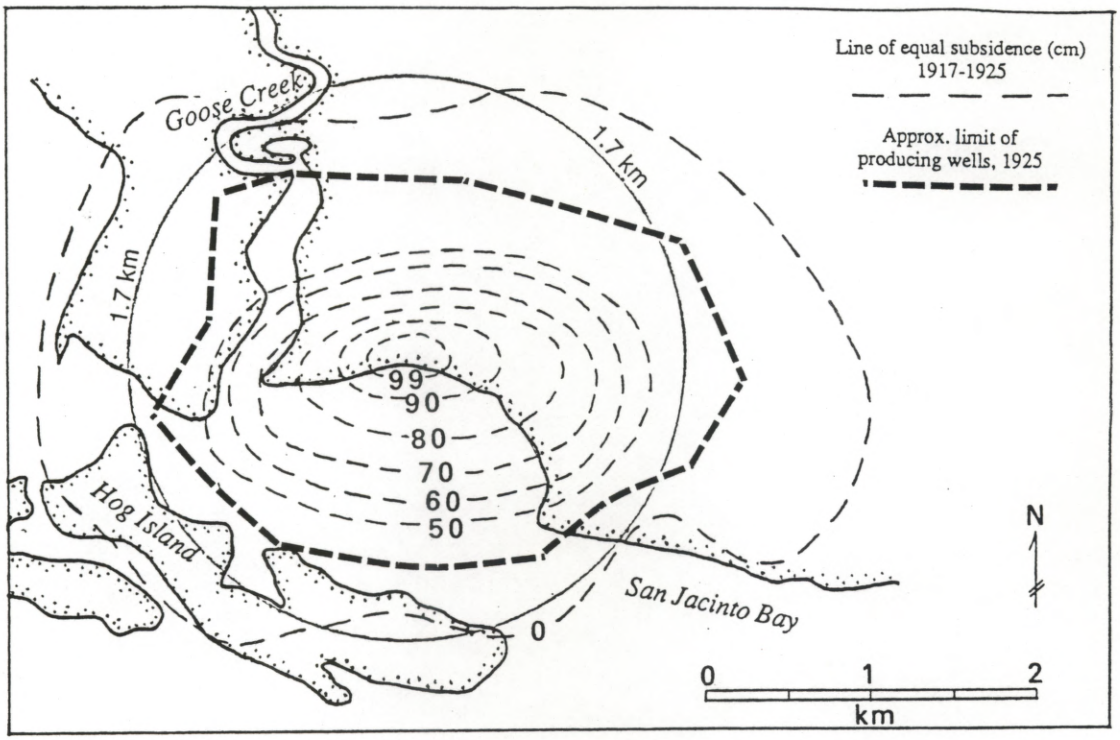

Figure 24. Contours of land-surface subsidence (cm) at the Goose Creek oil field, 1917-1925 (modified from Yerkes and Castile (1969), after Pratt and Johnson (1926)). The outline of the disc-shaped reservoir (R = 1.7 km) is included.

occurred at the center of the field by nearly 30%, whereas the model overestimated the subsidence occurring at a radius of 1700 m, even using the low value for the compaction coefficent. It should be noted that the compaction coefficient values given in Geertsma (1973) are only for the sandstone reservoir. Therefore, the model does not calculate the deformation of the clays or shales above and beneath the producing reservoirs.

These results indicate the difficulty in applying a simplified model to a highly complex physical situation. Compaction, and therefore surface subsidence, is reservoir-dependent. Although the magnitude of the subsidence values generated by the model are at best qualitative, the model suggests the potential for subsidence at the eight fields within and adjacent to the study area (Table 8). Goose Creek shows the greatest subsidence, as expected by its shallow depth of burial and large pressure decline, whereas the Oyster Bayou, Fig Ridge, and Trinity Bay fields show essentially no subsidence. The High Island, Anahuac, Lovell's Lake, and Clam Lake fields show intermediate to small amounts of subsidence.

The extensive subsurface depressurization that has occurred at the large number of oil-and-gas fields within the study area should have produced some land-surface subsidence. The lack of documentation of significant localized subsidence (similar to Goose Creek) within the study area may represent a lack of observation and study, or, perhaps, that the subsidence has occurred on a more regional scale, as speculated by Ewing (1985). The land surface within the study area is sinking at rates which are difficult to explain solely by the combined effects of groundwater withdrawal and natural consolidation of the substratum. This suggests that oil-and-gas production is a factor in the subsidence of the land surface within the study area.

3.2 Erosion:

A second major cause of coastal land loss is erosion, which causes a landward displacement of the shoreline by removal or redistribution of coastal material. Erosion has permanently removed more than 40 km^2 (10,000 acres) from the Texas Gulf Coast since the mid-to-late 1800s (Morton, 1977). In addition, both the total length of eroding coastline and the rates of erosion have increased along the Texas Coast in the last half of this century (Morton, 1979).

3.2.1 Shoreline features and sediment supply:

The shoreline between Sabine Pass and Rollover Pass is part of the erosional headland of the Pleistocene Trinity Delta. Erosion of older barrier/strandplain deposits from the inner shelf provide the primary source of sediment for the headland area (McGowen and others, 1977). However, much of the shelf between Sabine Pass and Rollover Pass is underlain by clay, therefore little sand is available for onshore transport (Morton, 1975). Sediment is transported by littoral drift from the east toward the southwest along the upper Texas Coast. Erosion of the Louisiana Coast does not contribute much sand to the area however, since the sediments are predominantly muddy. Also, much of the transported sediment is trapped by the jetties on either side of Sabine Pass (fig. 3). Morton (1979) suggested that, for the Texas Coast as a whole, jetties may trap greater than 50% of the sand supplied by updrift erosion.

Bolivar Peninsula, attached to the deltaic headland, is composed of barrier and tidal inlet sands overlying Pleistocene valley-fill sediments (Morton and Price, 1987). Bolivar Peninsula exhibits numerous abandoned beach ridges parallel to the

present shoreline (ridge-and-swale accretionary topography) that document the seaward advances of previous shorelines (LeBlanc and Hodgson, 1959; Morton, 1977). Removal and downdrift transport of small quantities of sand from the muddy shoreline stretch west of Sabine Pass provides a source of sediment for the peninsula.

Updrift rivers do not now constitute a significant source of sediment for the shoreline of the study area. Little sediment from the Mississippi River has reached the upper Texas Coast in the past 500 years since discharge has been through its eastern Plaquemines lobe (Fisher and others, 1973) and sediment discharge from the Mississippi River into the Gulf of Mexico has been reduced more than 50% since the mid-1950s by construction of upstream reservoirs (Meade and Parker, 1985). Sandy sediment transported by longshore currents within the past century has been trapped by the Sabine Pass jetties. The Sabine and Neches Rivers also contribute very little sediment to the upper Texas Coast because they carry very little bedload and most of the fine sand and silt is trapped in Sabine Lake (Fisher and others, 1973).

4.0 Historical Shoreline Movements:

4.1 Shoreline Types within the Study Area:

The shoreline of the study area was divided into four types, three natural and one man-made. The shoreline types were delineated from physical properties maps and environmental geology maps within the Environmental Geologic Atlas of the Texas Coastal Zone (Fisher and others, 1972; 1973), as well as from Morton (1975) and Paine and Morton (1986). Figure 25 shows the distribution of shoreline types. Each of the four shoreline types is described briefly below.

Sand and shell beaches: Narrow, steep beaches composed of sand and shell fragments locally grading inland to vegetated sandy slopes. Geologic units include beach, barrier/strandplain, and chenier ridge sands.

Clay bluffs: Steep bluffs of interbedded clay, silt, and sand. Bluff morphology is controlled primarily by bluff orientation in relation to wind direction and wave fetch and secondarily by sand content of the clayey deposits (Paine and Morton, 1986). Geologic unit is the Beaumont Formation, which is composed of several fluvial-deltaic deposits, including interdistributary and overbank muds, meanderbelt and distributary sands, and crevasse splay deposits.

Marshes: Coastal marshes and tidal flats. Very low relief, therefore susceptible to frequent flooding and tidal inundation. High organic content and muddy substrate. Geologic units include coastal and estuarine marshes, tidal flats.

Man-made land: Dredging spoil and miscellaneous rubble used to artificially stabilize shorelines.

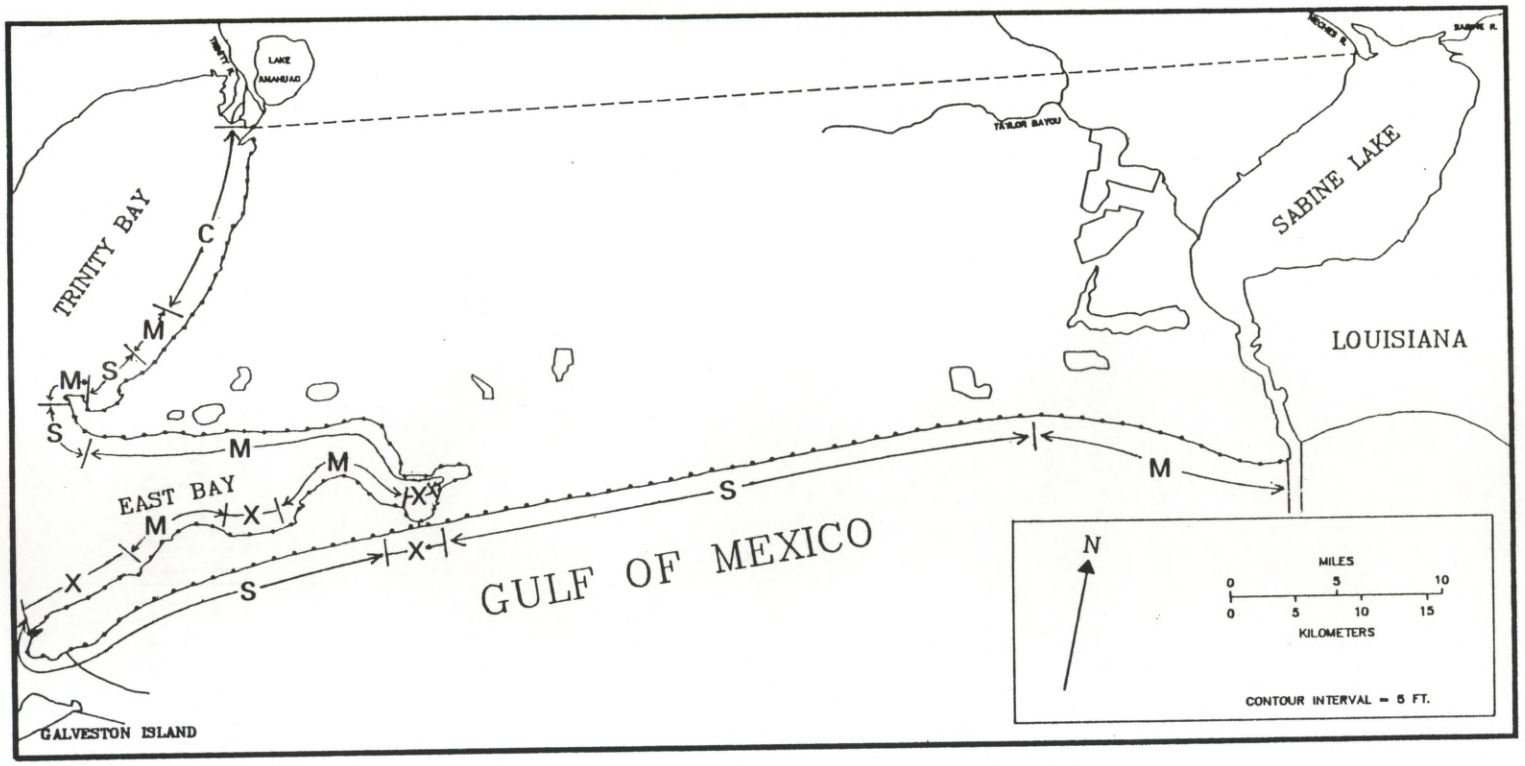

Figure 25. Distribution of shoreline types within the study area.
S = sand/shell, M = marsh, C = clay bluff, X = artificially-altered.
Dots represent points of measurement for shoreline movement.
Numbers of the points are shown in fig. 26.

4.2 Methodology:

Data for historical movements of the shoreline within the study area were obtained from Morton (1975) and Paine and Morton (1986). Morton (1975) analyzed shoreline displacement along the beach segment between Sabine Pass and Bolivar Roads, whereas Paine and Morton (1986) analyzed the shorelines of Trinity, Galveston, West, and East Bays. East Bay and the eastern shore of Trinity Bay are within the area of interest for this study. The methodology employed in both studies was essentially the same and is briefly described below.

Documentation of long-term changes in shoreline configuration was accomplished by comparison of shoreline positions from topographic maps, coastal charts, and aerial photographs from different times over the past century. The changes in position over time were determined at points spaced every 5000 feet along the shoreline. Aerial photographs provide the most accurate indication of shoreline position at the time the photograph was taken, and thus were used exclusively for times since 1930. All original sources (i.e. maps, charts, and photographs) were reproduced to maintain a uniform scale of 1:24,000. Transferral of shoreline position from the original sources of data to the 1:24,000 base map allowed quantification of changes in shoreline position with time at each point of measurement. Care was taken to avoid distortions caused by variations in scale and resolution in the original sources. Measurements of linear distances were made to 0.01 inch, equivalent to 20 feet on a map scale of 1:24,000. Because of the imprecision inherent in this methodology, Morton and Paine stress that trends and direction of change are of greater importance than actual calculated rates of change.

The trends of shoreline change determined for time periods greater than 100 years are significant and can not be ignored.

Morton (1975) used 62 points of measurement on the open-gulf shoreline between Sabine Pass and Bolivar Roads. Paine and Morton (1986) used 55 points of measurement in East Bay and 66 points in Trinity Bay, of which 25 points are along the eastern shore which is within the study area. For this study, the points have been numbered sequentially from 1 at Sabine Pass to 142 at the junction of the Trinity River with Trinity Bay immediately southwest of Anahuac (fig. 26).

Morton (1975) presents shoreline movement data for the periods 1882-3 to 1930, 1930 to 1955-7, and 1955-7 to 1974. Paine and Morton (1986) present data for the periods 1851 to 1930 and 1930 to 1982. Appendix 3a is a compilation of these data for all 142 points. For consistency with the data from East and Trinity Bays, only data for the 1880s to 1930 (first period) and 1930 to 1974 (second period) are considered for the Sabine Pass to Bolivar Roads section.

For the purpose of developing baseline relations between shoreline movement and relative sea-level rise, the difference in the time span of the second period (1930-1974 for the open Gulf shoreline between Sabine Pass and Bolivar Roads; 1930-1982 for East and Trinity Bays) necessitates calculating a separate baseline rate of RSL rise for each of the two time spans, since the baseline rates of shoreline movement are correlated with relative sea-level rise for the identical time span. The rate of rise for 1930-1974 is 6.9 mm/yr (see Table 1), which is used to develop the baseline relation for the open Gulf shoreline (points 1-62). The rate of rise for 1930-

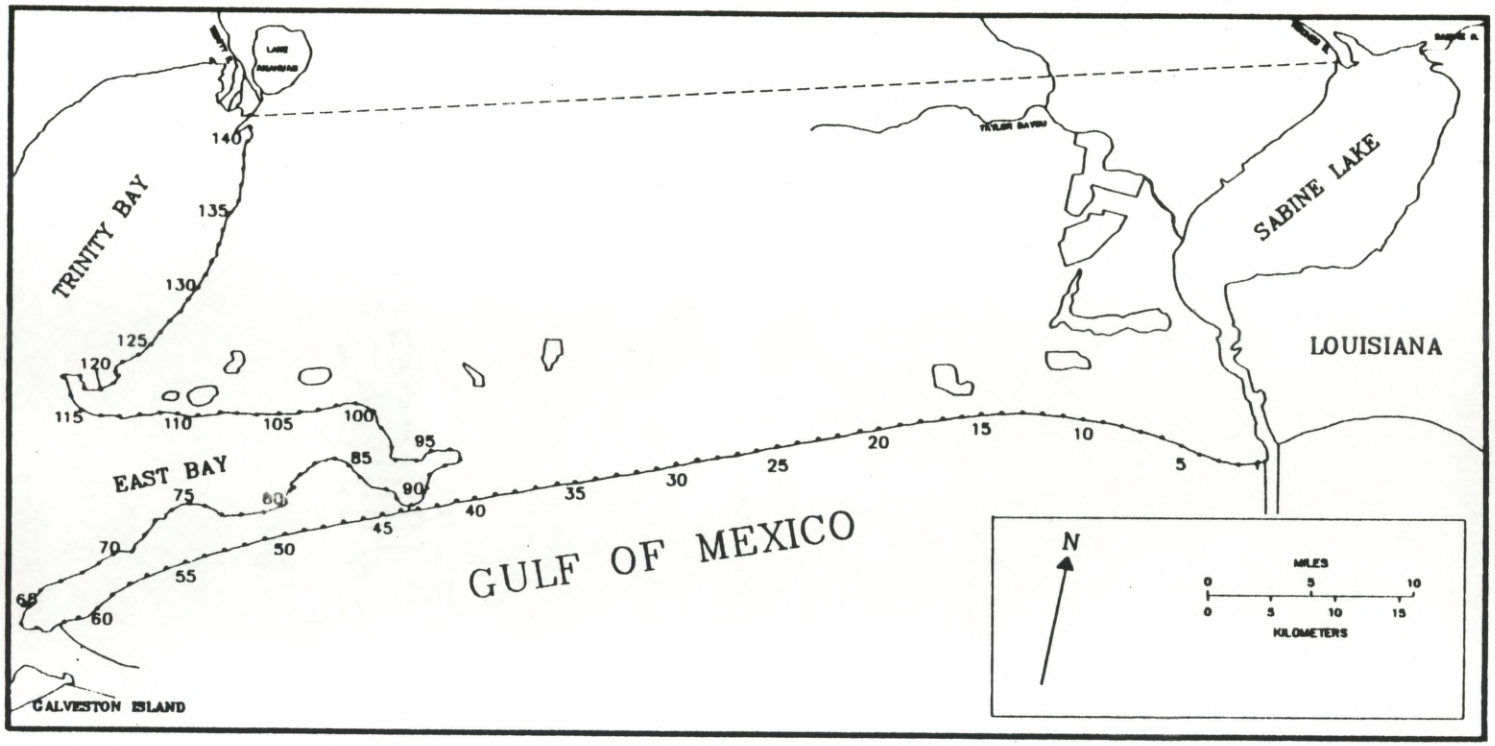

Figure 26. Points of measurement for historical shoreline movement.

1982 is 7.6 mm/yr, which is used to develop the relation for the shoreline of East Bay and Trinty Bay (points 63-142).

Figure 27 is a plot of the sea-level records (annual means) for the Pier 21 and Sabine Pass stations. Years for which shoreline-movement data are available are marked on the Pier 21 series. Although there is some scatter of the pertinent data points about the baseline regression lines, the deviations are not great enough to render the correlation between relative sea-level rise and shoreline movement invalid.

The data for the section between Sabine Pass and Bolivar Roads is somewhat problematical because of the measurements of shoreline position made in the mid-1950s. A drought occurred in the mid-1950s that was severe enough to impact coastal water levels (fig. 27). Measurements of shoreline position made during these years will show an apparent shoreline accretion caused by the lower water levels (i.e. shoreline emergence). This apparent accretion is evident in the data (Appendix 3a). The shoreline position in 1955-7 is far enough seaward to overwhelm the measurement of landward movement that occurred between 1955-7 and 1974. Subsequently, the baseline movement for this shoreline section, obtained by adding the movements for the 1930 to 1955-7 and 1955-7 to 1974 periods, shows a smaller net retreat than would be calculated had the apparent accretion in the former period not been added in. The calculated baseline rate of relative sea-level rise, however, is not affected significantly by the short-term lowering of water levels in the 1950s. Therefore, since the 1950s drought decreases the baseline shoreline retreat but not the baseline rate of relative sea-level rise, future projections based on these rates will be conservative in terms of shoreline retreat and loss of land. Without the 1950s data,

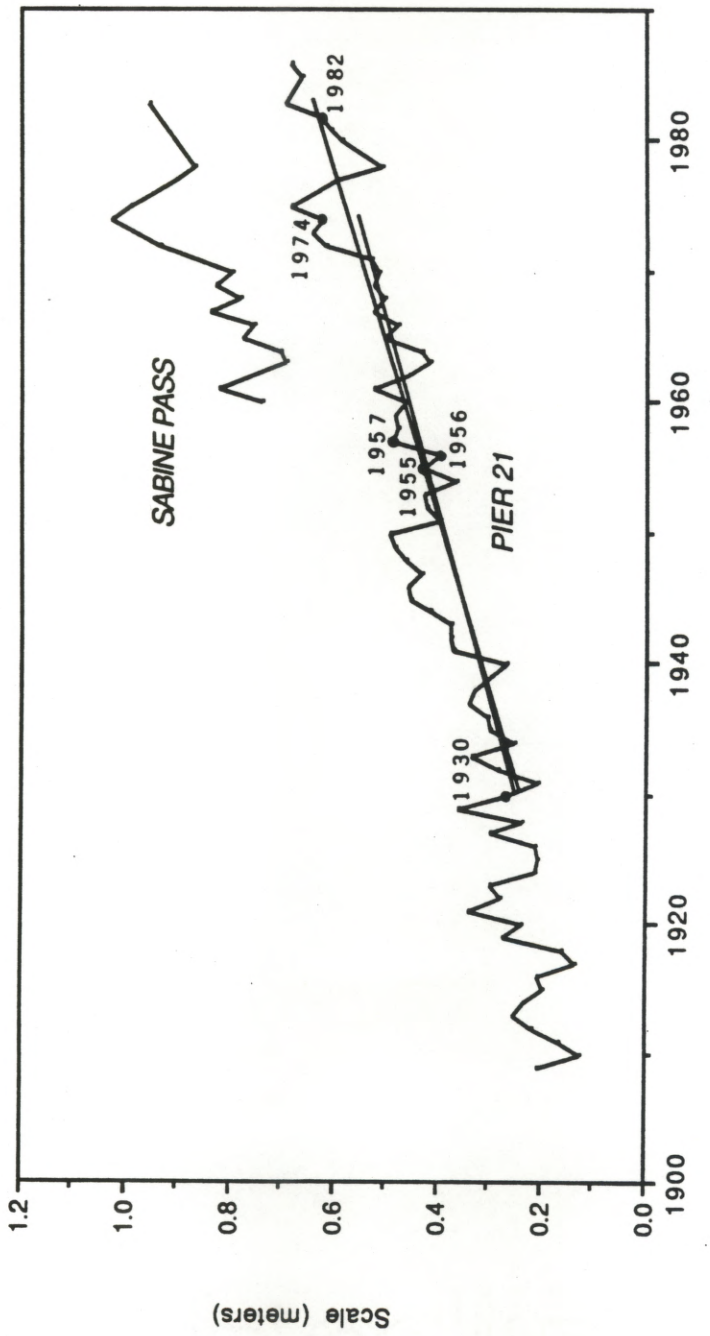

Figure 27. Tidal records at Sabine Pass and Pier 21 stations showing lines of regression for the two baseline periods. Included are years for which measurements of shoreline position are available. (Data from the National Ocean Service, NOAA).

the relation between shoreline retreat and relative sea-level rise would indicate more retreat for a given rise.

4.3 Historical Trends:

Two methods were used to synthesize the data for historical shoreline movements. The first method involves averaging small numbers of adjacent points in order to determine local variations in shoreline movement across the study area. The second method involves averaging all points within a common shoreline type for four discrete sections of the study area shoreline. The first method is advantageous for determining shoreline response as a function of location, whereas the second method allows comparison of rates of erosion based primarily on shoreline type. The final analysis involves discretizing the shoreline into ten segments, based on a combination of the two methods.

4.3.1 Averages for subjectively-chosen groups of points:

In order to provide a more representative indication of historical movement for a stretch of shoreline, I calculated an average value for groups of adjacent points for each time period. Selection of the points to be grouped was subjectively made, based on differences in shoreline type as well as general uniformity in direction (erosion or accretion) and magnitude of movement over the full period of record. An alternate method is to objectively group the points according to a set number of points (e.g. groups of three adjacent points). The method of grouping points subjectively is preferable to this latter method since it allows differentiation of erosional trends by shoreline type and location. Appendix 3b is a compilation of averaged values for the

subjectively-chosen groups of points. Appendix 3c provides graphs of the averaged cumulative shoreline movement for each group of points. Figures 28, 29, 30 and 31 are diagrams summarizing the averaged cumulative movement for the shoreline stretches encompassed by the point groups during both time periods for each of the following shoreline sections: Sabine Pass to Bolivar Roads, the south and north shores of East Bay, and the eastern shore of Trinity Bay, respectively. All displacement that occurred by 1930 and 1974 or 1982 is relative to the position of the shoreline in 1882 or 1851, depending on the shoreline section. The figures allow visualization of historical shoreline movement for an entire section of shoreline. Areas most susceptible to retreat appear as spikes on the graphs. For example, the shoreline between points 8 and 11 has retreated further than any other portion of the shoreline between Sabine Pass and Bolivar Roads (fig. 28), probably due to the change in orientation of the shoreline there (fig. 26).

4.3.2 Averages for shoreline types:

A second method of analyzing shoreline movement is to calculate historical changes for each of the three natural shoreline types. Data were not used for points on man-made land since the distances measured are inaccurate and not representative of natural conditions. For this analysis, the shoreline was divided into four major sections: Sabine Pass to Bolivar Roads, the south shore of East Bay, the north shore of East Bay, and the eastern shore of Trinity Bay (hereafter called Trinity Bay). For each section, the average change for all points within a common shoreline type was calculated for each period (Table 9). All shoreline types show increasing rates of retreat between the two periods except the long section of sandy shoreline between

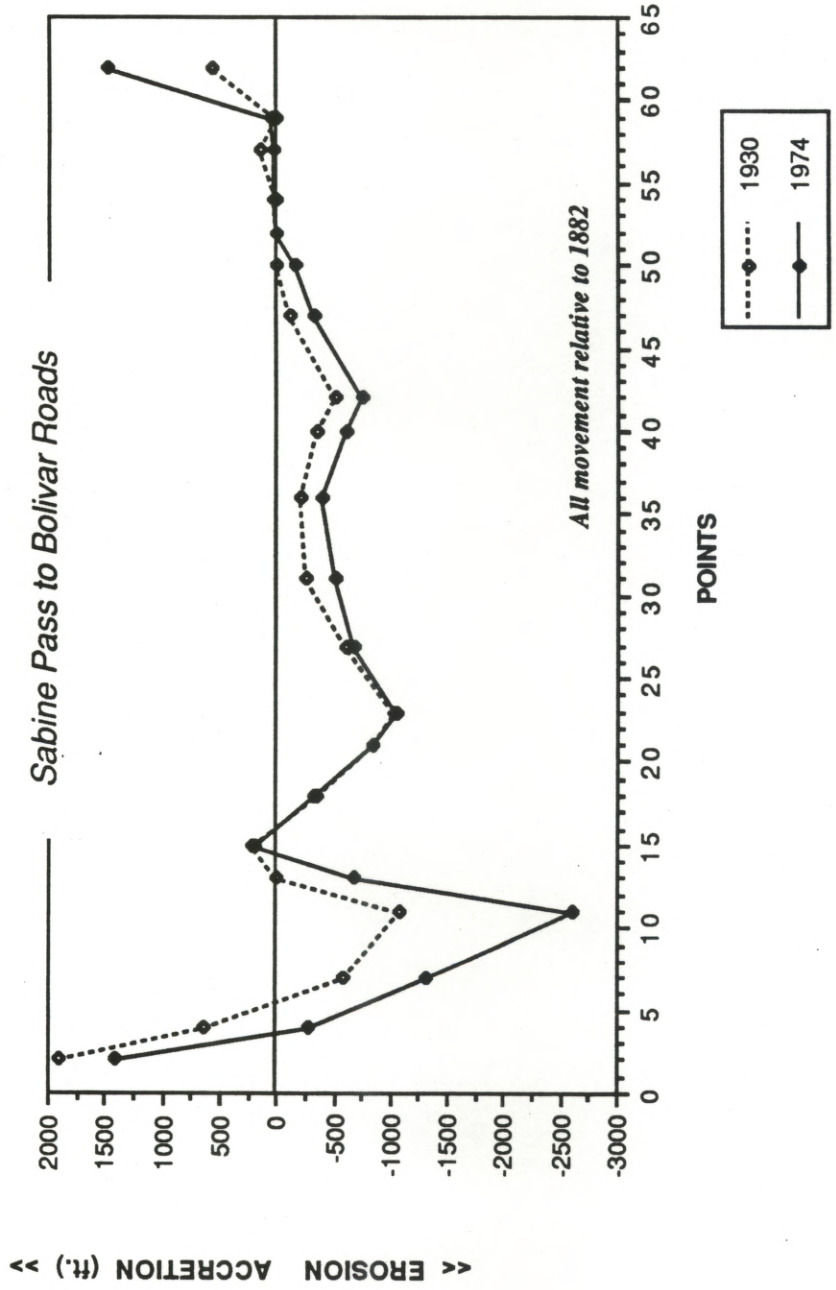

Figure 28. Average cumulative movement for subjectively-chosen groups of points between Sabine Pass and Bolivar Roads (1882-1974).

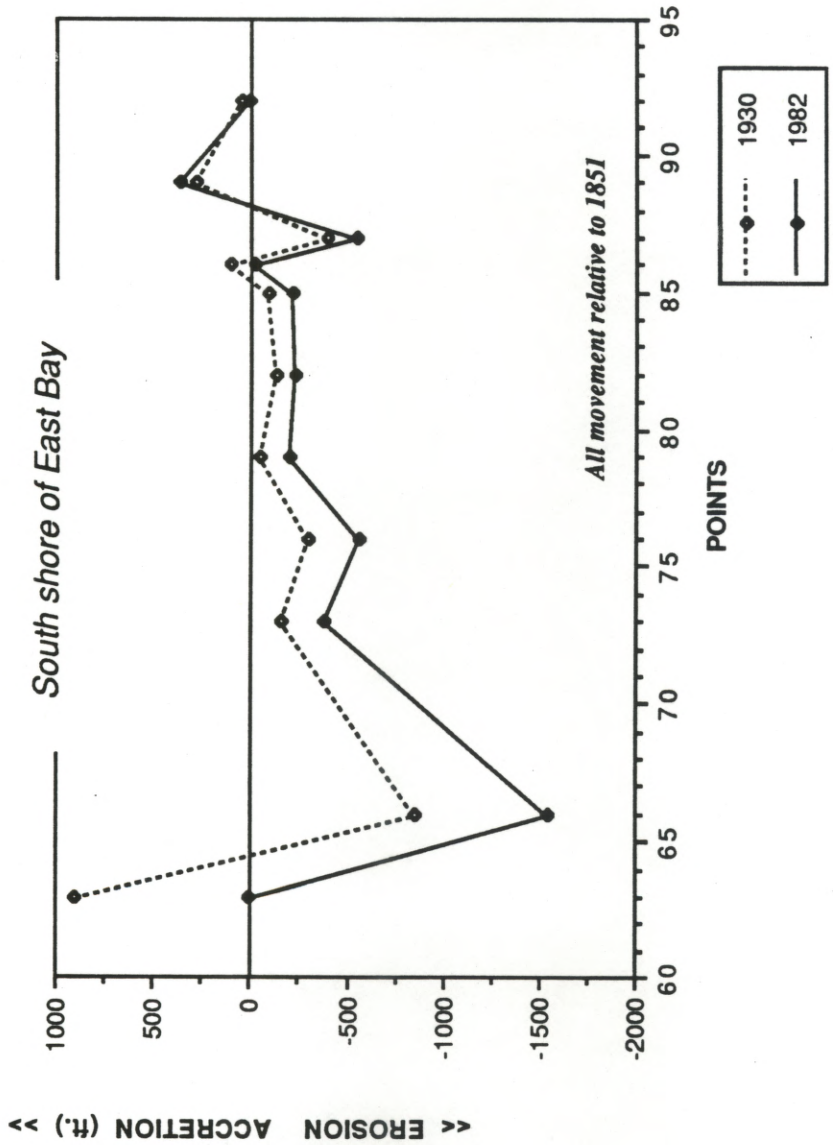

Figure 29. Average cumulative movement for subjectively-chosen groups of points along the south shore of East Bay (1851-1982).

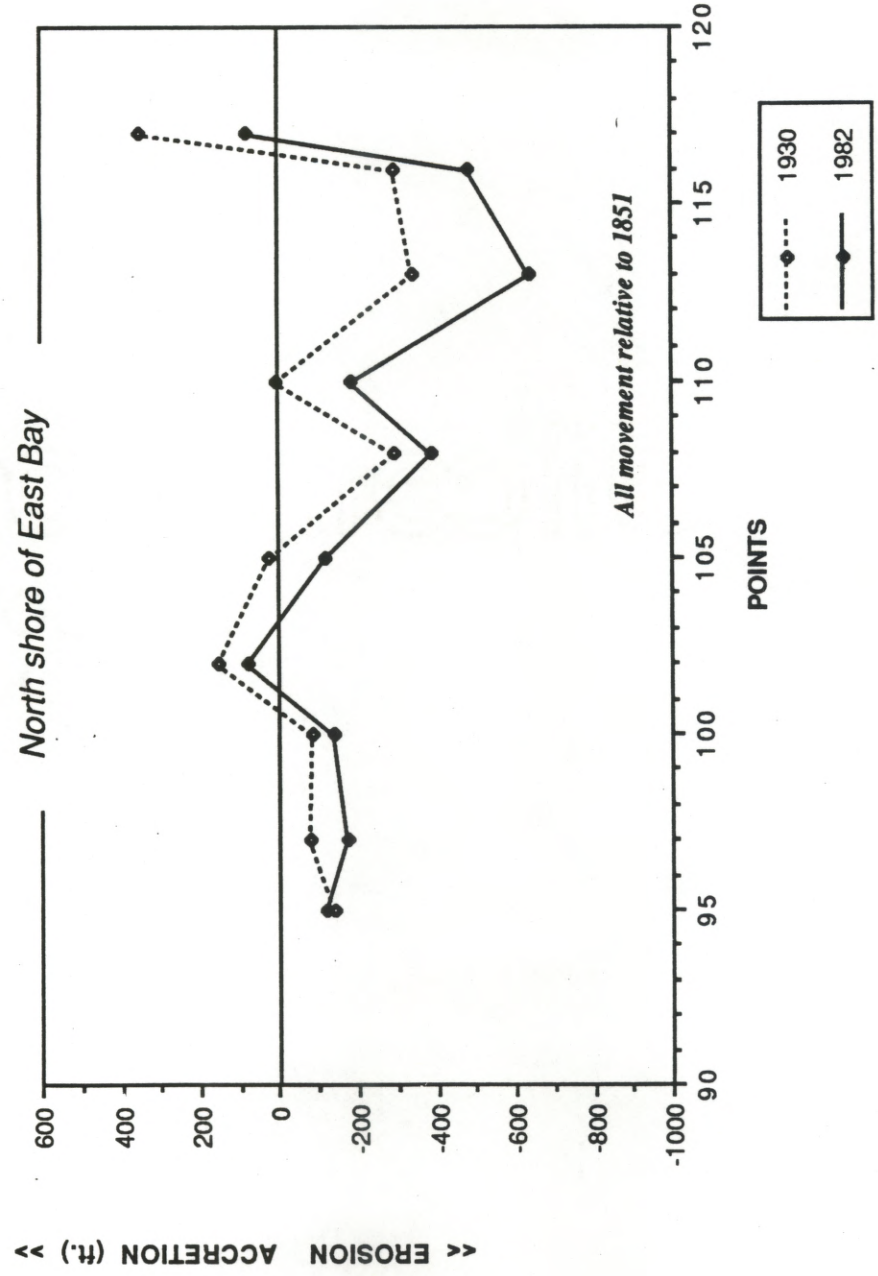

Figure 30. Average cumulative movement for subjectively-chosen groups of points along the north shore of East Bay (1851-1982).

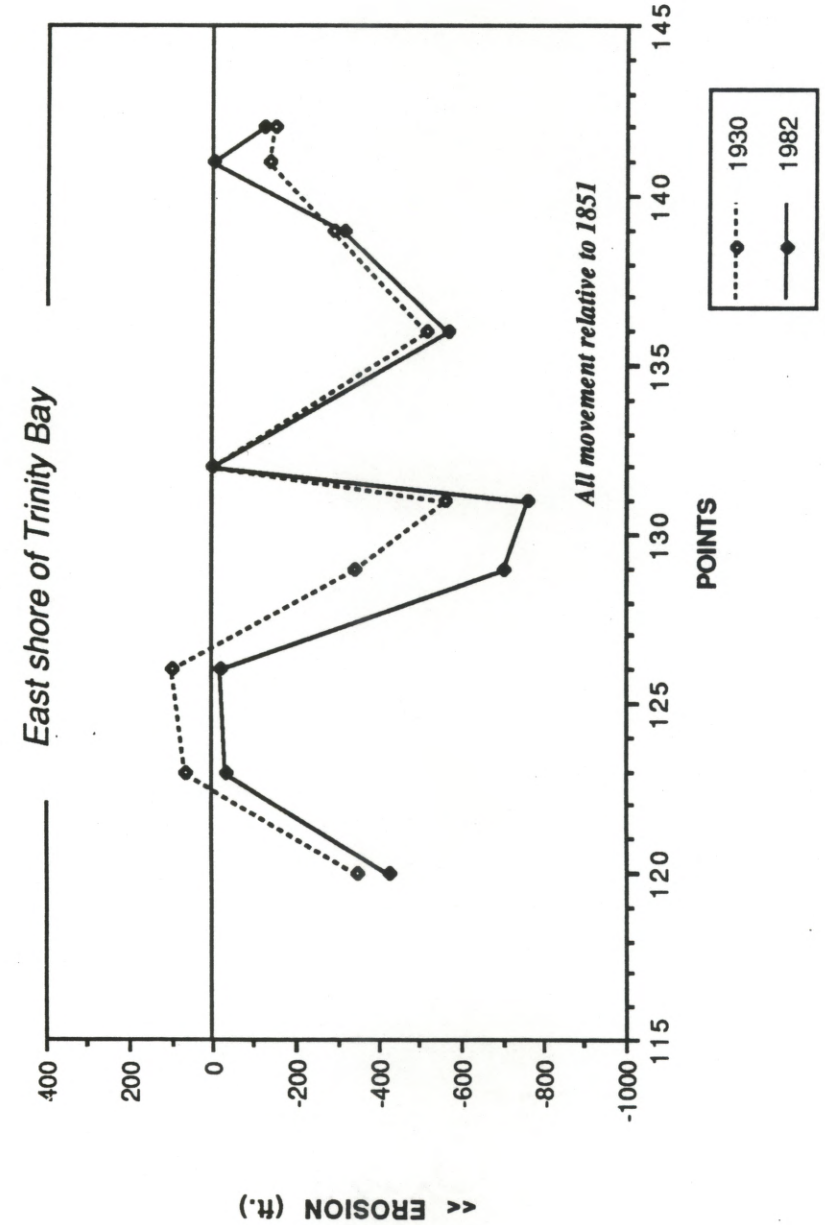

Figure 31. Average cumulative movement for subjectively-chosen groups of points along the east shore of Trinity Bay (1851-1982).

Table 9. Average rate of shoreline movement (m/yr) for different shoreline types.

Shoreline Section	Sand/Shell		Marsh		Clay Bluff	
	1800s to 1930 (m/yr)	1930 to 1974/1982 (m/yr)	1800s to 1930 (m/yr)	1930 to 1974/1982 (m/yr)	1800s to 1930 (m/yr)	1930 to 1974/1982 (m/yr)
Sabine Pass to Bolivar Roads:	-2.4	-1.2	-4.3	-7.6	NA	NA
South Shore of East Bay:	-5.5	-2.7	-0.6	-0.9	NA	NA
North Shore of East Bay:	-0.6	-1.2	-0.6	-0.9	NA	NA
East Shore of Trinity Bay:	-0.1	-0.6	-0.3	-1.5	-1.2	-0.3

Sabine Pass and Bolivar Roads (-8 to -4 ft./yr) and the clay bluff shoreline in Trinity Bay (-4 to -1 ft./yr). The latter is probably the result of the development of a spoil ridge running along the Trinity River ship channel (fig. 3). The ridge was constructed to stabilize the channel and was nearly continuous between Anahuac and Smith Point in 1956. By 1982, however, only isolated mounds persisted (Paine and Morton, 1986). The apparent deceleration occurring along the shoreline between Sabine Pass and Bolivar Roads is probably the result of misleading shoreline position measurements taken in the mid-1950s when lower water levels caused emergence of the shoreline.

It is difficult to compare the rate of retreat for different shoreline types within the study area because shoreline orientation and other variables such as wave fetch appear to be more important than shoreline type in determining historical rates of movement. Between Sabine Pass and Bolivar Roads and along the east shore of Trinity Bay, the marshes retreated at higher rates than did the sand/shell beaches, whereas the reverse is true along the south and north shores of East Bay (Table 9). Along the east shore of Trinity Bay, the unprotected clay bluffs retreated at higher rates than did either the sand/shell or marsh shorelines between 1851 and 1930. The rate of retreat of the clay bluffs between 1930 and 1982 is lower than for the other two shoreline types, for reasons discussed above.

4.4 Shoreline Discretization:

For the purpose of developing individual empirical relations between shoreline movement and relative sea-level rise, the study area shoreline was discretized into 10 segments. In performing the discretization, primary consideration

was given to general uniformity in rates of movement over the past record as well as shoreline orientation. Uniformity of shoreline type was a minor consideration. Figure 32 shows the ten shoreline segment subdivisions. A listing of the points comprising each segment is presented in Table 10.

4.5 Baseline Rates of Shoreline Movement:

Table 10 is a listing of the rate of shoreline movement (in m/yr) for each segment over the baseline period: 1930 to 1974 for segments 1 through 3; 1930 to 1982 for segments 4 through 10.

Segment 1: Segment 1 showed the highest rate of shoreline retreat (-7.0 m/yr) during the baseline period. The 13 points comprising segment 1 showed an average retreat of 291 m. Segment 1 is composed of easily-eroded tidal flat deposits and is immediately downdrift of the jetties at Sabine Pass, effectively cut off from most updrift sediment supply.

Segment 2: The longest segment of shoreline is segment 2, a relatively uniform stretch of sand and shell beach. The shoreline recession occurring within the shoreline stretch between points 20-42 is most representative of the behavior of the segment (R.A. Morton, pers. comm., 1988). Therefore, these points were used to characterize the segment. The shoreline surrounding Rollover Pass (points 43-45) has been artificially stabilized with steel sheet pilings to maintain the fishing inlet, therefore these points are not included in the analysis. During the baseline period,

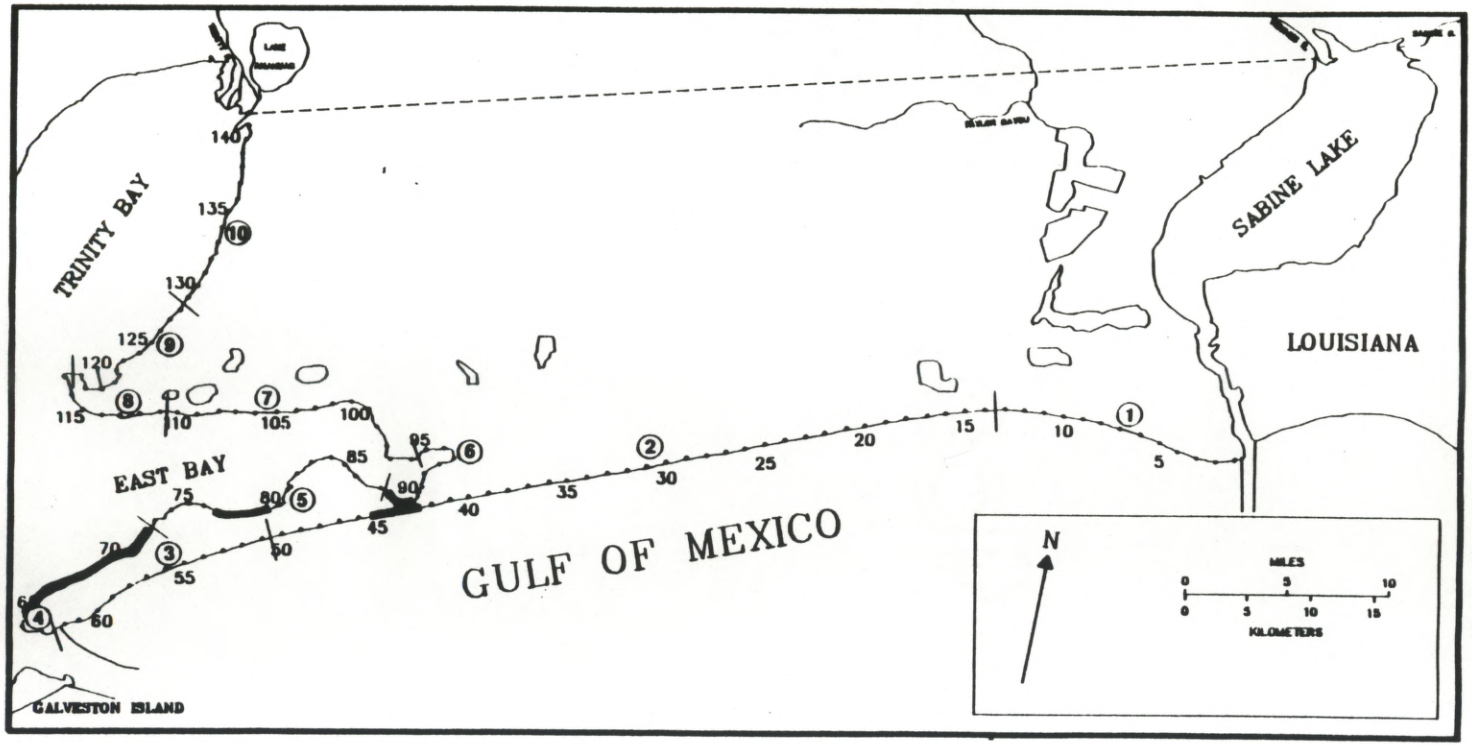

Figure 32. Location of shoreline segments. Darkened stretches indicate artificially-altered shoreline.

Segment	Points	Average baseline* movement (m)	Rate of baseline movement (m/yr)
1	1-13	-291	-7.0
2	20-42	-53	-1.2
3	51-62	67	1.6
4	63-64	-152	-2.9
5	73-76,80-87	-52	-1.0
6	90-95	-4	-0.1
7	96-110	-33	-0.6
8	111-117	-76	-1.5
9	118-128	-51	-1.0
10	129-142	-11	-0.2

* 1930 to 1974 for segments 1-3; 1930 to 1982 for segments 4-10

Table 10. Baseline rate of shoreline movement (m/yr) for each of the ten shoreline segments.

the 22 points analyzed within this segment retreated an average of 53 m, for a rate of -1.2 m/yr.

Segment 3: Segment 3 is the only segment to show net accretion during the baseline period. The accretion is the result of sediment from updrift sources being trapped by the jetty at Bolivar Roads. The 12 points show an average seaward movement of 67 m, for a rate of +1.6 m/yr. Accretion increases toward the jetty at Bolivar Roads, attesting to the jetty's ability to completely trap sand derived from updrift sources. Most of the mud eroded from updrift sources stays in suspension and is not stopped at the jetty (R.A. Morton, pers. comm., 1988).

Segment 4: Segment 4, although comprised of only two points, shows a rate of shoreline recession of -2.9 m/yr (average retreat of 152 m) over the baseline period, 1930-1982. Points 63 and 64 have been cut off from their source of sediment by the construction of the jetty at Bolivar Roads at the turn of the century. Prior to jetty construction, Bolivar Peninsula was prograding to the southwest as evidenced by the net accretion at points 63 and 64 for the epoch 1851-1930 (Appendix 3a). The tip of the Bolivar Peninsula is a focus for abundant wave energy, and will therefore, in the absence of incoming sediment, continue to erode at high rates unless artificially stabilized. The northern tip of the peninsula (points 65-72) has been armored with bulkheads and rip rap in order to maintain the utility of the intracoastal waterway.

Segment 5: Segment 5 comprises most of the southern shore of East Bay that remains unprotected. Points 73-76 and 80-87 retreated an average of 52 m (-1.0

m/yr) during the baseline period. This marshy segment is subject to erosion associated principally with northers blowing across East Bay during winter storms. The western promontory (points 73-76) is subject to longer northerly wave fetch than is the eastern one (points 80-87) and therefore shows slightly higher rates of erosion (Appendix 3a). The shoreline segment between the promontories (points 77-79) has been stabilized in an attempt to protect the intracoastal waterway. Regardless, the points have retreated at rates similar to the unprotected stretches. The shoreline at points 88 and 89 has been stabilized in an effort to maintain Rollover Pass.

Segment 6: Segment 6 (points 90-95) is the highly-protected easternmost shoreline of East Bay. Minimal wave fetch produces a low-energy environment within this segment, thereby providing a naturally-stable shoreline, although some human alteration has occurred adjacent to the intracoastal waterway. The six points within this restricted segment retreated an average of 4 m (-0.1 m/yr).

Segment 7: The low rate of retreat in segment 7 (points 96-110) indicates the importance of winter storms in shaping the shoreline. During the baseline period, the 15 points within the segment retreated an average of 33 m (-0.6 m/yr). This segment occupies much of the marshland on the north shore of East Bay. Throughout much of the year this segment is subject to southerly wave fetch resulting from predominant south-southeast winds in the area. Yet segment 7 has retreated only

about 60% as far as the southern shore (segment 5) over the same time, indicating that the majority of erosion is accomplished by winter storm waves.

Segment 8: Segment 8 (points 111-117) is predominantly marsh with a narrow sandy stretch (points 115-116) of Ingleside strandplain deposits at Smith Point. The 7 points within segment 8 retreated an average of 76 m (-1.5 m/yr) during the baseline period, more than twice as far as segment 6. This segment is well-exposed to long southerly wave fetch across East Bay, which is the primary reason for the high rate of retreat relative to the previous segment. A gradual increase in the amount of retreat between points 114-117 may also be an indication of the transition from marsh to more easily eroded sand shoreline. Point 117 retreated more than 80 m (275 ft.) due to its highly unprotected location at the tip of Smith Point.

Segment 9: Segment 9 is composed of both sandy shoreline (points 119-124) and marsh (points 117 and 125-128). The segment retreated an average of 51 m (-1.0 m/yr) within the baseline period. Higher rates of retreat occurred in the northern points (points 126-128) with an anomalously high retreat of 213 m (700 ft.) at point 128. Although this point is at the approximate transition between marsh and clay bluff shorelines, the reason for this rapid retreat is uncertain.

Segment 10: The shoreline within segment 10 is composed entirely of bluffs carved within clayey deposits of the Beaumont Formation. The bluffs increase in elevation from less than 1.5 m (5 ft.) between points 129-133 to greater than 4.5 m (15 ft.) between points 137-142. Segment 10 has been relatively stable over the baseline

period, retreating an average of 11 m (-0.2 m/yr). As mentioned above, this is probably the result of construction of a spoil ridge in the1950s for the purpose of maintaining the Trinity River channel. The segment's average rate of (natural) retreat between 1851-1930 was approximately -1.5 m/yr. The data for the two periods show drastic decreases in retreat at all points (except point 132 which has been stationary over the entire period of record), and a change from erosion to accretion at points 140-142 (Appendix 3a). This recent stability can only be explained by human alteration of the shoreline, although the accretion at the northern three points may be partially caused by growth of the Trinity River delta.

5.0 Land Loss Projections:

5.1 Methodology:

Three scenarios of future coastal land loss are developed for each of the 10 shoreline segments as follows:

(1) Determine the baseline relation between relative sea-level rise and shoreline movement. The baseline scenario is an extrapolation of the baseline shoreline movement to 2050 (i.e. multiply the baseline rate by 65 years, assuming 1985 as the starting year). The baseline rates of shoreline movement are displayed in fig. 33. This scenario represents the most conservative estimate of coastal land loss because it assumes no acceleration in the rate of relative sea-level rise by the year 2050.

For the low- and high-rise scenarios:

(2) Obtain low and high estimates of eustatic sea-level rise at 2050 from a statistical synthesis of nine recently-published projections of accelerated eustatic rise caused by global warming. The published projections and statistical methods are described in the following section.

(3) Calculate the component of subsidence at 2050 by extrapolation of the baseline subsidence rate (baseline rate of relative sea-level rise minus baseline rate of eustatic rise) as determined from the Pier 21 data.

(4) Add the subsidence and eustatic (low and high) components to obtain the projected low and high relative sea-level rise at 2050. The rise in relative sea level is due to increasing eustatic rise since the subsidence component is assumed constant (section 1.2.1).

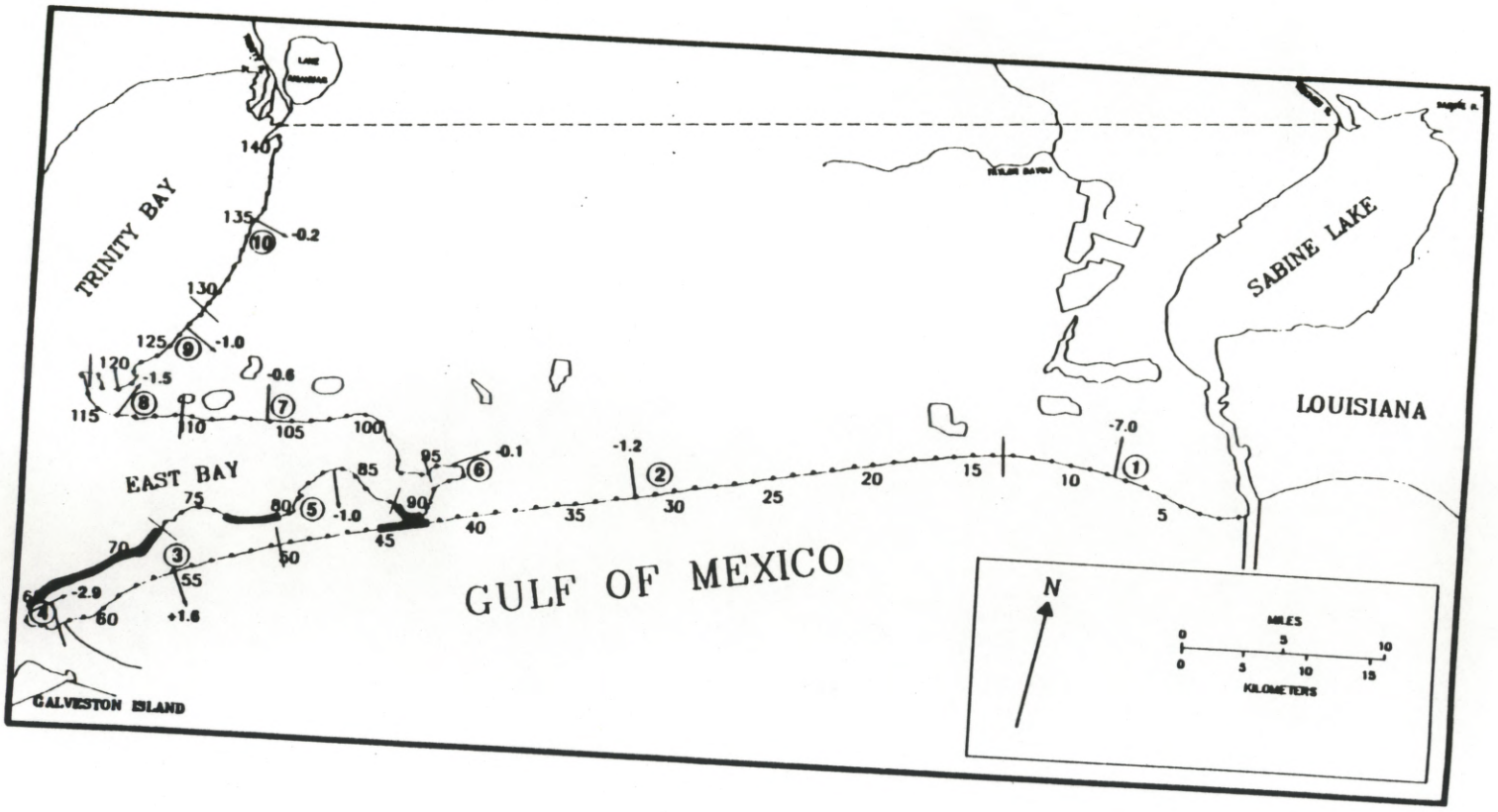

Figure 33. Baseline rates of shoreline movement (m/yr) for each of the ten shoreline segments.

(5) Calculate low and high multiplicative factors for relative sea-level rise equal to the ratio of accelerated low and high relative sea-level rise to baseline relative sea-level rise at 2050.

(6) Calculate low and high rates of shoreline movement by applying the multiplicative factors to baseline rates of shoreline movement. Multiply these rates by 65 years to determine the projected shoreline movement by 2050.

7) For all scenarios, areal land loss (or gain) within a shoreline segment is calculated by multiplying the shoreline movement by the segment length.

5.2 Estimates of eustatic rise at 2050:

Nine projections of eustatic sea-level rise in response to climatic warming in the next century were taken from the recent literature (since 1983). The projections include high and low projections from the combined efforts of the Carbon Dioxide Assessment Committee and Polar Research Board of the National Research Council (1983, 1985), the Environmental Protection Agency (EPA, 1986), and the Scientific Committee on Problems of the Environment (SCOPE, 1986), in addition to high, mid, and low projections from the Marine Board (MB, 1987) of the National Research Council (fig. 34). Appendix 1 is a detailed summary of the methods employed by each organization to develop their projections. The shape of the NRC (1983, 1985) and SCOPE (1986) curves in fig. 34 represent some artistic license since predicted values of eustatic rise were provided only at 2100. The curves were drawn to mimic the general shape those developed by the Marine Board (1987).

Values for eustatic rise at 10-year intervals between 2000 and 2100 were determined for each curve. At each 10-year increment, the mean and standard

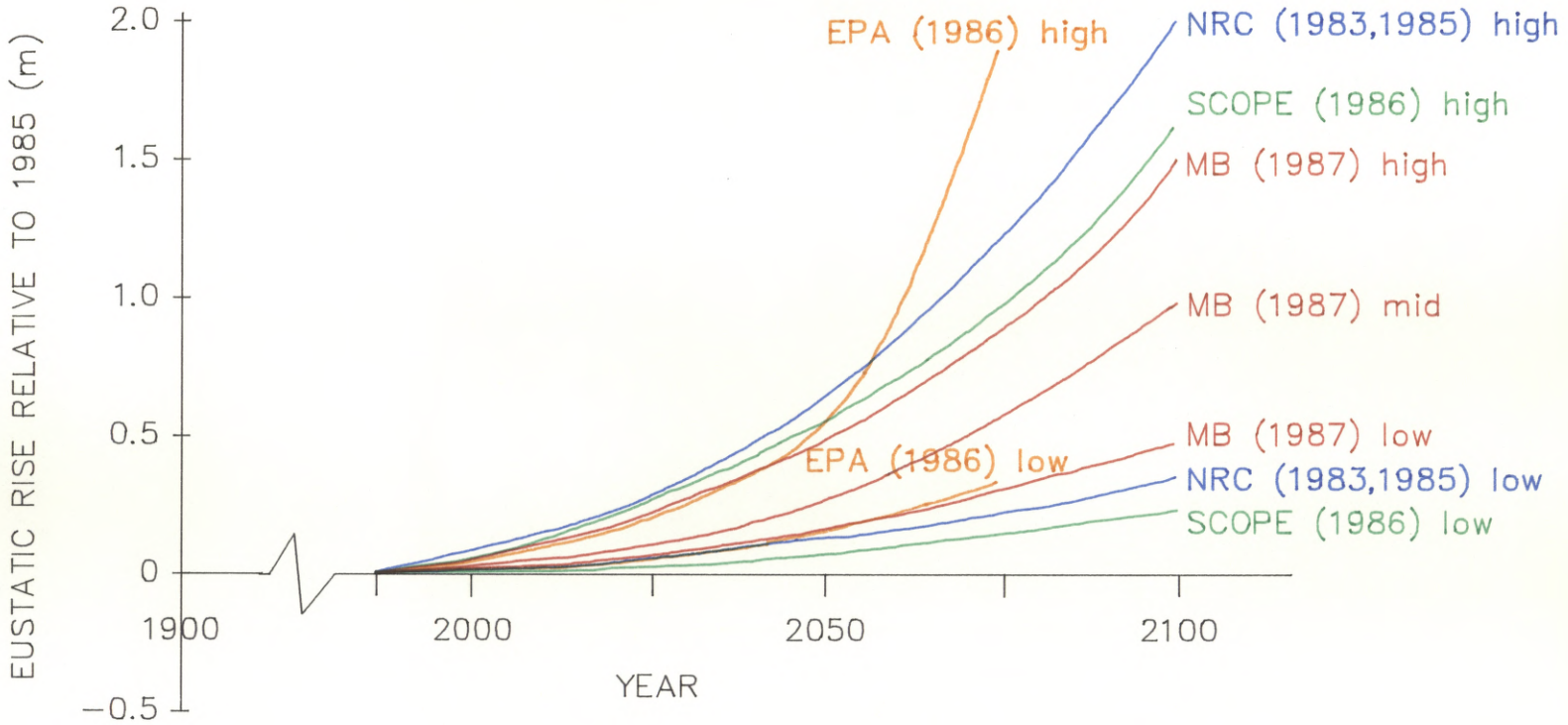

Figure 34. Projections of eustatic sea-level rise in the next century.
NRC: National Research Council CO2 Assessment Committee (1983) and Polar Research Board (1985)
SCOPE: Scientific Committee on Problems of the Environment (1986)
EPA: Environmental Protection Agency (1986)
MB: Marine Board of the National Research Council (1987)

deviation (σ) of the nine values were calculated. The mean plus and minus one standard deviation was calculated as a measure of the variance in the data. The mean of the four high projections and the mean of the four low projections were also calculated (Table 11). These data, along with the extrapolated baseline eustatic rise of 2.2 mm/yr, are graphically displayed in fig. 35. There is very close agreement between the mean - 1 σ and the mean of the four low projections (low-rise estimate), as well as between the mean + 1 σ and the mean of the four high projections (high-rise estimate) (fig. 35). Although there is no apparent statistical reason for this agreement, it implies that the envelope created by the curves represents a reasonable range of estimates for future eustatic rise, based on the best available projections. Although the synthesized low-rise and high-rise curves are nonlinear, they are nearly linear to the year 2050. Therefore, a linear rise to 2050 is a valid extrapolation.

For this study, the mean of the nine projections is taken to be eustatic rise in the low-rise scenario (0.35 meter at 2050); the mean plus one standard deviation (equal to the mean of the four high projections) represents eustatic rise in the high-rise scenario (0.57 meter at 2050).

5.3 Calculation of multiplicative factors:

Segments 1-3: For segments 1-3, the baseline period is 1930 to 1974, in accord with the shoreline movement data from Morton (1975). The baseline rate of relative sea-level rise for 1930 to 1974 is 6.9 mm/yr (Table 12). Subtracting the baseline eustatic rise of 2.2 mm/yr leaves a baseline rate of subsidence of 4.7 mm/yr. Extrapolation of these rates gives a baseline rise of relative sea-level of 0.45 m at 2050, of which 0.14 m is eustasy and 0.31 m is subsidence.

	2000	2010	2020	2030	2040	2050	2060	2070	2080	2090	2100
NRC, high	0.09	0.16	0.25	0.36	0.49	0.65	0.85	1.04	1.35	1.66	2.00
SCOPE, high	0.08	0.15	0.23	0.34	0.45	0.57	0.71	0.88	1.08	1.42	1.63
MB, high	0.07	0.13	0.21	0.30	0.40	0.51	0.64	0.80	0.98	1.20	1.50
EPA, high	0.06	0.11	0.17	0.26	0.38	0.56	0.92	1.52			
MB, mid	0.04	0.07	0.11	0.15	0.21	0.29	0.39	0.51	0.66	0.82	1.00
EPA, low	0.03	0.05	0.07	0.10	0.14	0.19	0.23	0.31			
MB, low	0.02	0.04	0.06	0.09	0.12	0.17	0.23	0.30	0.36	0.42	0.50
NRC, low	0.02	0.04	0.05	0.08	0.12	0.15	0.18	0.22	0.26	0.31	0.37
SCOPE, low	0.01	0.02	0.03	0.05	0.07	0.10	0.12	0.15	0.18	0.22	0.25
Mean of all	0.04	0.08	0.13	0.19	0.26	0.35	0.47	0.64	0.70	0.86	1.04
St. Dev. of all	0.03	0.05	0.08	0.12	0.16	0.22	0.31	0.46	0.45	0.57	0.69
Mean + St. Dev	0.08	0.13	0.21	0.31	0.43	0.57	0.78	1.09	1.15	1.44	1.72
Mean - St. Dev	0.01	0.03	0.05	0.07	0.10	0.14	0.17	0.18	0.24	0.29	0.35
Mean of 4 highs	0.07	0.13	0.21	0.31	0.43	0.57	0.78	1.06	1.14	1.43	1.71
Mean of 4 lows	0.02	0.03	0.05	0.08	0.11	0.15	0.19	0.25	0.27	0.32	0.37
Baseline*	0.033	0.055	0.077	0.099	0.121	0.143	0.165	0.187	0.209	0.231	0.253

* Baseline = 2.2 mm/yr

NRC: National Research Council Carbon Dioxide Assessment Committee (1983) and Polar Research Board (1985)
SCOPE: Scientific Committee on Problems of the Environment, International Council of Scientific Unions (1986)
EPA: Environmental Protection Agency (1986)
MB: Marine Board of the National Research Council (1987)

Table 11. Ten-year incremental values and statistics for nine eustatic sea-level rise projections (see fig. 34).

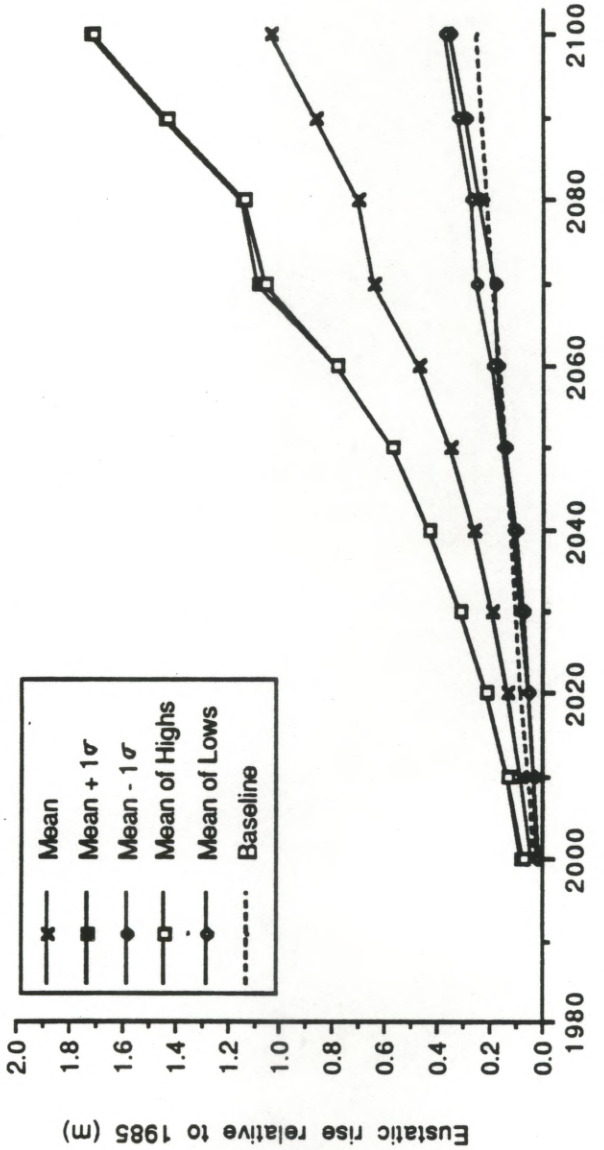

Figure 35. Statistical synthesis of nine eustatic sea-level rise projections (see fig. 34). See text for nomenclature.

In the low-rise scenario, eustatic sea level will rise 0.35 m. Adding the constant 0.31 m of subsidence gives a rise of relative sea level of 0.66 m by 2050. The ratio 0.66 m/0.45 m equals a low-rise multiplicative factor of 1.5.

In the high-rise scenario, eustatic sea level will rise 0.57 m by 2050, therefore relative sea-level rise will be 0.88 m. The high rise multiplicative factor is 2.0 (0.88 m/0.45 m).

Segments 4-10: The rate of relative sea-level rise for the baseline period 1930-1982 is 7.6 mm/yr, equal to 0.49 m by 2050. The baseline subsidence rate is 5.4 mm/yr, equal to 0.35 m at 2050. Addition of the 0.35 m low estimate of eustatic rise and the 0.35 m of subsidence equals a 0.70 m rise in relative sea level at 2050 in the low scenario. The high scenario combines 0.57 m of eustatic rise with 0.35 m of subsidence for a relative sea-level rise of 0.92 m by 2050. The low- and high-rise multiplicative factors are 1.4 (0.70/0.49) and 1.9 (0.92/0.49), respectively. This indicates that there is little difference in using the two different baseline periods for the two sets of shoreline segments (1-3 and 4-10). The values for eustatic rise, subsidence, and relative sea-level rise at 2050 for each of the three scenarios are summarized in Table 12.

5.4 Shoreline displacement and land loss scenarios:

Table 13 is a compilation of the rates of shoreline movement, the total shoreline displacement, and resulting areal land loss (or gain) predicted to occur by 2050 within each of the 10 shoreline segments for the three scenarios.

	Segments 1-3	Segments 4-10
Baseline Period:	1930 to 1974	1930 to 1982
Rate of relative sea-level rise (m/yr)	0.0069	0.0076
Rate of eustatic rise (m/yr)	0.0022	0.0022
Rate of land-surface subsidence (m/yr)	0.0047	0.0054
Baseline scenario at 2050		
Eustatic rise (m)	0.14	0.14
Land-surface subsidence (m)	0.31	0.35
Relative sea-level rise (m)	0.45	0.49
Low-rise scenario at 2050		
Eustatic rise (m)	0.35	0.35
Land-surface subsidence (m)	0.31	0.35
Relative sea-level rise (m)	0.66	0.70
High-rise scenario at 2050		
Eustatic rise (m)	0.57	0.57
Land-surface subsidence (m)	0.31	0.35
Relative sea-level rise (m)	0.88	0.92

Table 12. Rates of eustatic rise, land-surface subsidence, and relative sea-level rise for the two baseline periods, and the estimated magnitude of each at 2050 in each of the three scenarios.

Shoreline segment:	1	2	3	4	5	6	7	8	9	10	NET
Length (km)*	21	55	18	4	18	9	24	10	16	18	
Rate of movement (m/yr)											
Baseline	-7.0	-1.2	1.6	-2.9	-1.0	-0.1	-0.6	-1.5	-1.0	-0.2	
Low-rise	-10.5	-1.8	2.4	-4.1	-1.4	-0.1	-0.8	-2.1	-1.4	-0.3	
High-rise	-14.0	-2.4	3.2	-5.5	-1.9	-0.2	-1.1	-2.9	-1.9	-0.4	
Displacement by 2050 (m)											
Baseline	-455	-78	104	-189	-65	-7	-39	-98	-65	-13	
Low-rise	-683	-117	156	-264	-91	-9	-55	-137	-91	-18	
High-rise	-910	-156	208	-358	-124	-12	-74	-185	-124	-25	
Areal change (km2)											
Baseline	-9.6	-4.3	1.9	-0.8	-1.2	-0.1	-0.9	-1.0	-1.0	-0.2	**-17.2**
Low-rise	-14.3	-6.4	2.8	-1.1	-1.6	-0.1	-1.3	-1.4	-1.5	-0.3	**-25.2**
High-rise	-19.1	-8.6	3.7	-1.4	-2.2	-0.1	-1.8	-1.9	-2.0	-0.5	**-33.8**

* All segment lengths exclude the length of artificially-altered shoreline stretches.

Table 13. Rates of shoreline movement, total shoreline displacement, areal land loss within each segment and net areal change for each of the three scenarios. 1 km2 = 247 acres.

Segment 1: Segment 1 shows the highest baseline rate of shoreline retreat (-7.0 m/yr). Consequently, an erosion rate of -14.0 m/yr is predicted in the high-rise scenario. The respective shoreline displacements at 2050 are 455 and 910 m, resulting in losses of land over the 21-km-long segment of 9.6 km^2 (2371 acres) and 19.1 km^2 (4718 acres). Shoreline recession of even 0.5 km in the baseline scenario will inundate Highway 87 near points 11-14 (fig. 26). The more-probable shoreline retreats occurring in the low- and high-rise scenarios (683 and 910 m, respectively) will require relocation of the highway at least a kilometer inland, and even further to protect it from washing out during large storms.

Segment 2: It is estimated that the sandy shoreline of segment 2 will retreat 65 and 130 m in the baseline and high-rise scenarios, respectively. The high-rise displacement will also inundate Highway 87, primarily between points 20 and 40 where it runs immediately adjacent to the coast. The highway washed out during Hurricane Alicia in 1983 and was subsequently relocated. The accelerated rates of retreat predicted in the low- and high-rise scenarios will necessitate reconstruction or abandonment of the highway. Small coastal communities, such as Gilchrist and Caplen near Rollover Pass, should anticipate relocating houses as valuable beach-front property is lost. Furthermore, in the stretch east of High Island, accelerated erosion may remove the thin sand veneer that overlies marsh and clayey sediments, leaving a muddy shoreline (similar to segment 1) that could be subject to even higher rates of retreat. The sands on Bolivar Peninsula are thicker (up to 10 m) so that rates of retreat are expected to remain fairly constant for a given scenario.

Segment 3: Continued impoundment of sand at the Bolivar Roads jetty is predicted to cause an average seaward migration of 104 m in the baseline scenario, thereby adding 1.9 km^2 (469 acres) of new land updrift of the jetty. 3.7 km^2 (914 acres) are added in the high-rise scenario.

To examine the possibility of continued accretion of segment 3 in the face of accelerated sea-level rise, areal changes between Sabine Pass and Bolivar Roads during the period 1930-1974 were analyzed. Unpublished planimeter data, originally developed for a study by Morton (1977) of shoreline changes for the Texas Gulf Coast, were used for the analysis. The data consist of areal land changes for the periods 1930-1955/7 and 1955/7-1974 within 61 shoreline sections between successive pairs of points (1-62) (Appendix 4). To obtain more accurate numbers, a 62nd section covering the stretch between point 62 and the jetty was included since the greatest volume of sediment is deposited immediately adjacent to the jetty itself. Although planimeter data for the section were not available, examination of historical shoreline postions labeled on USGS topographic maps indicates that the shoreline moved approximately uniformly next to the jetty (between point 61 and the jetty). Therefore, in lieu of more quantitative data, the values of areal change for the previous section (between points 61-62) were applied to the section between point 62 and the jetty (see Appendix 4).

Changes for the two periods were added to obtain the areal change for the period 1930-1974 (baseline period). Since the data were from aerial photographs taken in the mid-1950s, the familiar problem of apparent accretion caused by shoreline emergence occurs within the data for the period 1930-1955/7 (see section 4.2).

A net erosion of 2.1 km^2 (509 acres) in segment 2 was calculated for the baseline period by adding the component areal changes within points 20-42. Similarly, a net accretion of 1.6 km^2 (400 acres) was calculated for segment 3, using the sections within points 58-jetty. The net loss of 0.5 km^2 (124 acres) represents mud transported to deeper water. Applying the low-rise and high-rise multiplicative factors (1.5 and 2.0) directly to the baseline areal changes produces erosion of 3.2 km^2 (764 acres) and accretion of 2.4 km^2 (600 acres) in the low-rise scenario, and erosion of 4.2 km^2 (1018 acres), accretion of 3.2 km^2 (800 acres) in the high-rise scenario.

Sediment volumes could be derived from these land areas if the depth of erosion, sand percent in the eroding segment, and depth of aggradation in the accreting segment were known. It could then be determined if the depth of aggradation in segment 3 would be sufficient to match sea-level rise by 2050 in each of the scenarios. Aggradation greater than sea-level rise would suggest continued accretion, and vice versa where the aggraded sediment would be submerged. Both sand percent and depth of erosion could be estimated with sufficent accuracy for performing rough calculations. The depth of aggradation, however, is an unknown because the bathymetry and areal extent of subaqueous deposition near the jetty are uncertain. It is intuitively probable that the rate of sea-level rise will eventually surpass the rate of sediment aggradation so that, although sand will continue to be deposited near the jetty, it will occur subaqueously. In this case, the segment will gradually reverse from land gain to land loss by submergence.

Segment 4: At a baseline rate of -2.9 m/yr, the two points within segment 4 will retreat 189 m by 2050 (Table 13). In the high-rise scenario the retreat will be 358 m. The tip of Bolivar Peninsula is exposed to considerable erosive energy. The northern shore of the peninsula (points 65-72) has been stabilized with dredging spoil in an effort to slow the rapid erosion that occurred between 1851-1930, threatening the intracoastal waterway (Appendix 3a). However, the spoil mounds have been eroding at greater than 1 m/yr since their deposition (Paine and Morton, 1986). This vital stretch of shoreline, including segment 4 (points 63-64) will need to be continually restabilized if rapid loss of land is to be prevented.

Segment 5: Segment 5 is composed of two marshy promontories (points 73-76, 80-87) separated by a recessed stretch of artificially-stabilized shoreline (points 77-79). The shoreline between points 77 and 79 was protected in order to maintain the intracoastal waterway, which runs immediately adjacent to the shoreline. The stabilization has not been successful, however, since the three points have retreated distances comparable to the surrounding shoreline during the baseline period (Appendix 3a). The segment will retreat 65 and 124 m, equivalent to a loss of 1.2 km^2 (296 acres) and 2.2 km^2 (543 acres) of land, in the baseline and high-rise scenarios, respectively.

The promontories are low-elevation, essentially-flat marshes (fig. 4). This suggests that the primary cause of land loss should be submergence, as opposed to erosion. If an accurate estimate of the topographic slope of the marsh can be made, a check of the reliability of the multiplicative factors can be made since shoreline displacement for a rise of sea level can be calculated. Using the baseline values of a

53 m average retreat for a 0.40 m rise in relative sea level (0.0076 m/yr x 52 yrs) gives a slope of 7.5×10^{-3}.

An alternate approach is to accurately measure the map distance between the coast (0 elevation) and the 5-foot contour and calculate the slope, assuming it is linear. For each of the 12 points within the segment, distances were measured perpendicular to the contour line on the original 1:250,000 topographic map to the nearest 400 foot (122 m), and then averaged. The average distance is 3100 m (10,200 ft.). By this method, the estimated slope is equal to 5.0×10^{-4} (5 ft./10,200 ft.). It should be noted that spoil ridges along the intracoastal waterway rise above 5 feet elevation, and therefore provide the 5 foot-contour line closest to the segment 5 shoreline. This contour line (not included on Plate 1) was avoided in the measurements because it does not represent the natural slope of the marsh surface. A baseline rise in sea level of 0.40 m transgresses 800 m on a slope of 5.0×10^{-4}, suggesting that the slope calculation was errant. This poor agreement may be the result of the inability to accurately define the land-water interface, as well as the incorrect assumption of a linear topographic slope. In marshy areas, there is an extensive wetland area, which is transitional between upland and open water. The position of the coastline is ambiguous because it is difficult to differentiate the wetland from open water. Furthermore, as the sea transgresses, much of the upland is converted to wetland and the relatively steep storm berm between the upland and wetland retreats but is not removed (R.A. Morton, pers. comm., 1988). Therefore, the submergence predicted by assuming a linear slope (i.e. no break in slope) will not be realized since the transgression must still overcome the higher slope separating the wetland from the higher ground inland.

Segment 6: Segment 6 is protected from the erosive energy that characterizes the previous segments. It is, however, a low-lying marsh area subject to submergence by rising relative sea level. The shoreline in segment 6 has the lowest baseline rate of retreat (-0.1 m/yr), therefore it will have the lowest estimates of future retreat: 7 m in the baseline scenario and 12 m in the high-rise scenario. Since segment 6 is only 9 km long, each of these retreats amounts to a loss of only 0.1 km^2 (25 acres) of land. Submergence is, and will continue to be, the principal cause of shoreline displacement in segment 6.

Segment 7: The marshy northern shore of East Bay will retreat at a moderate rate of 0.6 m/yr in the baseline scenario, causing a landward displacement of 39 m by 2050. A displacement of 74 m will occur in the high-rise scenario. The area behind this shoreline segment is flat Holocene marshland extending inland between 3-8 km to the contact with the Beaumont Formation. Land loss within this segment is principally the result of permanent inundation of wetland, although erosion by predominant southeasterly winds may also be a factor. Within segment 7, 0.9 km2 (222 acres) and 1.8 km^2 (445 acres) of marshland will be lost in the baseline and high-rise scenarios, respectively. This loss will represent loss of ecologically-important wetlands such as in the Anahuac National Wildlife Refuge (fig. 3).

Segment 8: Segment 8 (points 111-117) will retreat 98 m by 2050 in the baseline scenario, and 185 m in the high-rise scenario, representing land losses of 1.0 and 1.9 km^2 (247 and 469 acres, repectively). The area inland of segment 8 is not as

susceptible to submergence as segment 7 because of the northeast-trending Ingleside sand ridge (fig. 4) that exceeds 10 ft. elevation along most of its length (Plate 1). However, the marshes adjacent to the ridge (points 111-114, 117) are likely to be slowly lost to submergence.

Segment 9: The 16-km-long segment 9 shoreline is composed of both Ingleside sands (points 119-124) and marsh (points 118, 125-128). The shoreline segment will retreat an average of 65 and 124 m in the baseline and high-rise scenarios, respectively. Erosion is probably the dominant process of land loss within this segment since the concave shape of Smith Point peninsula focuses storm wave energy from the north, causing erosion of the sandy shoreline. Also, slopes are higher due to the presence of the sand ridge (Plate 1). Erosion will continue to be the principal process of land loss in the future.

The losses occurring along the northern shore of the Smith Point peninsula (segment 9), combined with the losses along the southern shore (segment 8) will significantly alter the peninsula configuration. The marshy tip of the peninsula (points 117-118) will likely be submerged. Continued erosion will remove large volumes of Ingleside sand as the promontory is slowly removed.

Segment 10: The shoreline within segment 10 is composed of clay and fine sand deposits of the Beaumont Formation. As discussed in section 4.5, human alteration of the shoreline in this segment has reduced rates of retreat between the early period (1851-1930) and the later period (1930-1982). Therefore, projecting the baseline rate to 2050 results in a nearly-insignificant displacement of 13 m (25 m in the high-

rise scenario). However, these values may be representative of the future situation since it is probable that the artificial stabilization here will continue in an effort to preserve the economically-important Trinity River ship channel.

Adding the estimates of areal land change for the ten segments (Table 13) produces a net change of land area for the entire study area coastline of -17.2 km^2 (4248 acres) in the baseline scenario, -25.2 km^2 (6224 acres) in the low-rise scenario, and -33.8 km^2 (8349 acres) in the high-rise scenario.

6.0 Conclusions:

Coastal land loss will proceed at different rates for the ten shoreline segments within the study area. The rate of land loss is dependent upon both natural factors (shoreline type and slope, and segment location and orientation), and human alteration.

Data from nonsubsiding tidal gages along the Florida Gulf Coast are used to define a 2.2 mm/yr baseline rate of eustatic sea-level rise for the Gulf of Mexico. Baseline rates of relative sea-level rise measured at the Pier 21 tidal gage at Galveston are 6.9 mm/yr for the period 1930-1974, and 7.6 mm/yr for the period 1930-1982. The residual 4.7 and 5.4 mm/yr are attributed to land-surface subsidence. The three contributory causes of land-surface subsidence within the study area, natural consolidation, groundwater withdrawal, and oil-and-gas production, can not be differentiated, except qualitatively.

Natural consolidation of thick clay-rich Holocene sedimentary sequences probably accounts for a large percentage of the subsidence measured at the Pier 21 and Sabine Pass tidal gages. Subsidence rates measured by releveling of several bench marks near Smith Point are in general agreement with rates determined at the gages. The rates of movement are less inland.

Groundwater pumpage within the study area is minor because of poor groundwater quality in the underlying Chicot aquifer. As a result, maximum water level declines have not exceeded 11 m during the past 40 years. Such small potentiometric declines are incapable of producing significant surface subsidence,

although groundwater pumpage in the metropolitan Houston area has probably caused some subsidence along the eastern shore of Trinity Bay.

Production of oil and gas in the area causes depressurization of hydrocarbon reservoirs and, perhaps, regionally-continuous deep aquifers. The depressurization is possibly associated with regional subsidence, as well as localized faulting (Ewing, 1985). There is little documentation of localized subsidence in the study area resulting from hydrocarbon production. An attempt to model surface subsidence above producing reservoirs was unsuccessful in reproducing observed subsidence at the Goose Creek oil field, west of the study area. High and low estimates of subsidence were generated because of poorly-constrained limits on the reservoir sandstones' uniaxial compaction coefficient (c_m). Simulated subsidence at the center of the producing reservoirs of eight fields within and adjacent to the study area ranged between 0 and 25 cm for low c_m estimates, and between 1 and 72 cm for high c_m estimates. The model results are of use for qualitatively comparing the potential for subsidence at the eight fields.

Land loss projections for the year 2050 are developed by integrating future projections of relative sea-level rise with empirical relations between relative sea-level rise and shoreline movement. A range of relative sea-level rise of 0.45-0.49 m by 2050 is obtained by projecting the baseline rates of relative sea-level rise. A synthesis of nine recently-published projections produces a range of eustatic rise of 0.35-0.57 m by 2050. Assuming these values represent low-rise and high-rise estimates, and assuming a constant rate of land subsidence, relative sea level is estimated to rise between 0.66-0.70 m by 2050 in the low-rise scenario, and between 0.88-0.92 m in the high-rise scenario.

An empirical relation between baseline rates of relative sea-level rise and shoreline movement is developed for each of the ten shoreline segments. Multiplicative factors of approximately 1.5 for the low- and 2.0 for the high-rise scenarios are calculated from the ratios of projected relative sea-level rise to baseline relative sea-level rise at 2050. Applying the low-rise factor to the baseline relation results in estimates of a minimum retreat of 9 m in segment 6 and a maximum retreat of 683 m in segment 1. The losses of land associated with these retreats are 0.1 km^2 (25 acres) and 14.3 km^2 (3532 acres), respectively. Applying the high-rise factor results in shoreline recession of 12 m and 910 m, equal to losses of 0.1 km^2 (25 acres) and 19.1 km^2 (4718 acres) of land, in these respective segments. Since segment 3 was accretionary during the baseline period, continued accretion to 2050 is calculated for segment 3, resulting in formation of 1.9 km^2 (469 acres) in the baseline and 3.7 km^2 (914 acres) in the high-rise scenario. However, it is probable that the rate of sea-level rise will surpass the rate of sediment aggradation near the jetty, resulting in a gradual reversal from land gain to land loss by submergence in this segment. The net change of land area for the entire study area coastline is -17.2 km^2 (4248 acres) in the baseline scenario, -25.2 km^2 (6224 acres) in the low-rise scenario, and -33.8 km^2 (8349 acres) in the high-rise scenario.

The moderate shoreline retreats and losses of land calculated in this study probably represent conservative estimates. Recent rates of relative sea-level rise (between 1958 and the mid-1980s) at Sabine Pass and Pier 21 are greater than 11 mm/yr, 50-60% higher than the calculated rates of 6.9-7.6 mm/yr that were used as the baseline for this analysis. Since the entire analysis is developed from these baseline rates, low values will produce low estimates of land loss. Furthermore,

rates of retreat calculated for the shoreline section between Sabine Pass and Bolivar Roads (segments 1-3) are probably too low due to anomalously low sea level when the aerial photographs were taken in the mid-1950s. The lower level produces temporary emergence of the shoreline which appears as accretion relative to the 1930 photographs. Finally, future shoreline displacement within marshy segments may be greater than estimated in this study since sea-level rise beyond a certain limit could cause inundation of huge areas if small steep berms are overtopped, allowing transgression across a gently-sloping surface.

7.1 Appendix 1: Future Eustatic Sea-Level Rise Projections

During the past decade several private research groups and government agencies have attempted to estimate the rise in eustatic sea level that could result from projections of global warming. In general, these studies have concentrated on three major factors: (1) thermal expansion of the world's ocean water, (2) melting of alpine glaciers, and (3) melting of large continental glaciers in Antarctica and Greenland. Each of these factors will be considered in more detail as they relate to the individual sea-level rise projections. Changes in bathymetry of the ocean floors have likely been a factor in sea-level fluctuations on a geologic time scale, but can be considered insignificant for the 100-125 -year time period these projections cover.

For this project, I have chosen nine different sea-level rise projections developed and published within the past five years by four different scientific organizations, The National Research Council (NRC), utilizing the 1983 work of the Carbon Dioxide Assessment Committee (CDAC) and the 1985 work of the Polar Research Board's (PRB) Committee on Glaciology, the Environmental Protection Agency (EPA), the Scientific Committee on Problems of the Environment (SCOPE) of the International Council of Scientific Unions (ICSU), and the Committee on Engineering Implications of Changes in Relative Mean Sea Level, part of the Marine Board (MB) of the National Research Council (fig. 34). With the exception of the Marine Board's, these various projections rely on the results of state-of-the-art atmospheric models, the best available data on the role of the oceans and the atmosphere in climate change, as well as the most reasonable forecasts for future population, energy demand, fossil fuel availability and consumption, and the resulting emissions of carbon dioxide and other greenhouse gasses. These

projections can therefore be considered the best-available estimates of future eustatic sea-level rise.

This chapter presents a summary of the methods and assumptions employed by each of the four organizations in developing their sea-level rise projections.

Carbon Dioxide Assessment Committee (1983) and Polar Research Board (1985), National Research Council:

The Carbon Dioxide Assessment Committee (CDAC) of the National Research Council (NRC) was created in 1980 to develop and implement a comprehensive assessment of CO_2 release and its possible impacts. The CDAC studied a vast range of scientific concerns including detection of carbon dioxide-induced changes, projections of future CO_2 emissions, and a number of possible effects of a CO_2-enriched atmosphere. These effects include climate change, agricultural impacts, impacts on hydrology, and changes in sea level. In addition, the CDAC defined possible responses to the problems of increasing carbon dioxide as well as making recommendations for further research.

The CDAC's sea-level rise scenarios due to increased anthropogenic CO_2 and other greenhouse gasses were initially published in Changing Climate (NRC, 1983). This document discussed estimated atmospheric alteration, the resulting climate change, and sea level rise.

Atmospheric alteration: Nordhaus and Yohe (1983) employed recent developments in total energy and economic modeling to construct a relatively simple model of an idealized global economy and resultant CO_2 emissions. Their analysis of

probabilistic scenarios for future CO_2 emissions integrated energy and production sectors of the economy, and also considered the cost and availability of fossil fuels.

In addition, this probabilistic scenario analysis attempted to recognize the inherent uncertainties in future economic, energy, and carbon cycle developments by identifying the most important parameters containing the uncertainty, examining current agreement and disagreement about these parameters, and then specifying a reasonable range of scenarios for each of these parameters. The result of the entire process is then the generation of a range of values, or "pathways", and associated uncertainties for major economic, energy, and carbon dioxide parameters.

The model had 10 key parameters with significant associated uncertainty. These were: (1) ease of substitution between fossil fuels; (2) general productivity growth; (3) extraction costs for fossil fuels; (4) trends in real costs for producing energy; (5) airborne fraction for carbon dioxide emission; (6) fuel mix among fossil fuels; (7) population growth; (8) trends in relative costs of fossil and nonfossil fuels; and (10) total resources of fossil fuels. Each of the 10 parameters has a set of estimates gathered from various researchers. Assuming a normal distribution of these estimates, the authors constructed what they termed a "judgemental probability distribution" for each parameter. Each judgemental probability distribution was then discretized into high, medium, and low values, corresponding to 25, 50, and 75% percentiles, respectively. There were thus 3^{10} (= 59,049) different probabilistic scenarios possible.

The data input to the model were gathered from diverse sources with differing levels of precision. In general, commonly agreed-upon values for parameters such as population growth or productivity growth were obtained from recent literature on

energy and economic modeling. Values for other more difficult-to-identify parameters were obtained from results of various studies or by examining recent trends.

Using the model and data as stated, the authors randomly sampled 1000 of the more than 59,000 possible combinations. The 1000 outcomes represent a very wide range of projections for carbon dioxide emmissions to the year 2100. The central conclusion of the study is that there is a 95% chance that atmospheric CO_2 concentrations will eventually double (defined as being a concentration of 600 ppmv), but not before the year 2100, there is a 75% chance of the doubling occurring by 2100, a 50% chance by 2065, a 25% chance by 2050, and a 5% chance by the year 2035. These figures are listed below. Furthermore, the study estimated an increase in global precipitation of 7-11% for a doubled-CO_2 environment. The CDAC has yet to update the estimates generated by Nordhaus and Yohe (1983).

% chance	Year of doubled concentrations
95	After 2100
75	2100
50	2065
25	2050
5	2035

Although the CDAC was primarily concerned with the future concentrations of carbon dioxide, a brief article was devoted to the prospect of increasing concentrations of the other chief greenhouse gasses, chlorofluorocarbons, methane, and nitrous oxide (Machta, 1983). No projections were developed by the CDAC for these non-CO_2 greenhouse gasses. The committee reviewed present trends of increased concentrations along with published projections for future trends and

subsequently concluded that non-CO_2 greenhouse gasses would enhance climate changes expected from rising atmospheric CO_2 and confuse expected CO_2-induced changes.

Climate change: The NRC also presented scenarios for a changed global climate resulting from a carbon dioxide-enriched atmosphere. Global warming projections were originally developed by the Climate Research Board and published in Carbon Dioxide and Climate: A Scientific Assessment (NRC,1979). In response to new research results, a second report, entitled Carbon Dioxide and Climate: A Second Assessment, was written by the CO_2/Climate Review Panel and published in 1982 (NRC, 1982). The CDAC's 1983 report, Changing Climate, found no reason to update the projections for CO_2-induced global warming that were originally generated in the 1979 NRC report, and were not revised in the 1982 NRC report.

The only accurate method for predicting future climate is the construction of numerical models based on the full set of of fundamental physical principles that control the climatic system. Although the basic physical laws governing the behavior of the myriad components of the climatic system are relatively well known, the various interactive processes and mechanisms remain uncertain. Important interactive processes include the quantity of atmospheric water vapor, albedo (determined primarily by land and sea ice), the capacity of the oceans to absorb heat, and cloudiness. All four of these are considered to be crucial, yet very poorly understood, feedback processes that regulate the response of the climatic system to pertubations, such as increased concentrations of atmospheric greenhouse gasses. It is these feedback processes that provide the most uncertainty in climatic projections,

and are therefore the primary cause of divergence in different researchers' model results.

The most sophisticated climate models are three-dimensional general circulation models (GCMs), which represent the atmosphere, land surface and the oceans. A succinct review of GCMs, as well as other types of climate models, is given by Schlesinger (1983). General circulation models determine surface pressure and the vertical distribution of velocity, temperature, density, and water vapor as a function of time from the mass conservation and hydrostatic laws, Newton's second law of motion, the laws of thermodynamics, the equation of state, and the conservation law for water vapor (Smagorinsky, 1974 ; Schlesinger, 1983).

The Climate Research Board's 1979 report (NRC, 1979) assessed and compared results from a variety of climate models including energy balance models (EBMs), radiative-convective models (RCMs), as well as general circulation models (GCMs). The central conclusion of the report was that the estimated equilibrium global surface warming resulting from a doubling of atmospheric CO_2 (taken to be 600 ppmv) would be "near 3°C with a probable error of $\pm$ 1.5°C". The report Carbon Dioxide and Climate: A Second Assessment (NRC, 1982) reviewed the results of eight GCMs developed between 1975 - 1982 and found a range of results between 2 - 4 °C, all within the range of uncertainty of the earlier report. The latest NRC report, Changing Climate (NRC, 1983) defined areas of necessary additional research in the field of climate prediction, but found no reason to change the original projection. Consequently, this earliest projection (3 $\pm$ 1.5°C) has not been changed by either of the subsequent NRC reports on the subject. The NRC contends that temperature increases might be amplified in the polar latitudes due to a lower albedo

resulting from decreased snow and ice cover. However, an increase in cloudiness coupled to increased precipitation may at least partly offset this decrease in albedo. Although much uncertainty exists, the NRC estimated that temperature increases of 4-6°C in the polar regions are likely. This same 4-6°C increase has been generated by Hansen and others (1984) at the Goddard Institute for Space Studies (GISS) using a sophisticated three dimensional GCM.

Sea-level rise: The most up-to-date NRC projections of sea-level rise due to a warmer global climate are a combination of results generated in 1983 and in 1985. Revelle (1983), assuming a global warming of 3-4°C, used a simplified two layer model for the oceans. The upper layer is a 70-meter-thick mixed surface layer in which the temperature change is uniform and equal to the change in surface temperature. The lower layer represents the rest of the ocean in which heat is transported by advection and turbulent diffusion. A one-dimensional mixing model was used for the sake of its simplicity. Average increases in water temperature at various depth intervals to 1000 m were calculated for 10° latitude bands. These increases were added to existing average values for the same intervals. Using available coefficients of thermal expansion for sea water, Revelle calculated the increase in specific volume of sea water. The total change in specific volume (and thus in sea level) between 0-1000 m for each 10° latitude band was multiplied by the percentage of ocean area within that band to determine the projected rise in global sea level due to thermal expansion . By this method, Revelle arrived at a rise of 30 cm for a 3-4°C rise in global surface temperature, conservatively estimated to occur by the year 2100.

Revelle's (1983) estimate of sea-level rise due to thermal expansion has not been revised by the NRC, and is thus a component of the current NRC sea-level rise scenario. Revelle also estimated the contributions to sea-level rise from alpine glaciers and the melting of the Greenland Ice Sheet. These estimates, however, were revised in 1985 by the Polar Research Board of the NRC.

The Polar Research Board (1985) published the results of a Workshop on the Interactions between Land Ice and the Oceans conducted by its Committee on Glaciology. The goals of the workshop were to define the current knowledge concerning the exchange of water between glacial ice and the oceans during the past century, what the situation is at present, and what can reasonably be expected during the next century, given existing climate modeling predictions. The findings of the workshop provided the first in-depth look at the possible contribution of melting glacial ice to sea-level rise.

For the purpose of analysis, the Polar Research Board made three subdivisions of the world's ice masses: (1) alpine glaciers and small ice caps (which include all glacial ice exclusive of Greenland and Antarctica), (2) the Greenland Ice Sheet, and (3) the Antarctic Ice Sheet. The PRB's analysis and prediction for each is described below.

Alpine glaciers and small ice caps:

Meier (1984) initially made an estimate of the contribution of small glaciers to sea-level rise since the beginning of the century. He compiled glacier-balance and volume-change data from various international sources for 25 glaciers in 13 regions, all between 38° and 69° N latitude. The average period of record for the glaciers was

from 1900-1961. Using this sparse, geographically-biased volume-change data, together with extended mass-balance histories generated by hydrometeorological (HM) models, Meier estimated a 61-year average change in glacier mass for the 25 glaciers and scaled this result to a global estimate by considering the intensity of the seasonal mass balance fluxes (accumulation and ablation) for 68 glaciers in 31 regions with a worldwide geographic distribution. To do this, Meier defined the annual mass balance, b, and the balance amplitude, a, as follows:

$$b = b_w + b_s \qquad \text{(A 1.1)}$$

$$a = (b_w - b_s) / 2 \qquad \text{(A 1.2)}$$

where b_w is the winter mass balance and b_s (usually negative) is the summer mass balance.

The 1900-1961 data for 25 glaciers was averaged by region and then scaled to a global average in terms of sea level change by

$$h(1961) - h(1900) = -(1/J) \left[\sum_{j=1}^{J} (b^*_j / a_j) \right] \left[\sum_{k=1}^{K} (a_k G^*_k) \right] \qquad \text{(A1.3)}$$

where h is the sea-level equivalent of global glacier balance, b^*_j is the average balance change in the jth region for the 61-year period (J = 13), a_j is the annual amplitude associated with the b^*_j, G^*_k is the average area of glacial ice in the kth region of the world (K = 31), a_k is the average annual amplitude associated with each G^*_k, and A is the area of the world's oceans.

The scaled results suggest that the melting of the world's alpine glaciers and small ice caps contributed 0.46 ± 0.26 mm/yr between 1960-1961. Although Meier's analysis represents a rough approximation, it suggests that the wastage of small glaciers may account for between one-fourth and one-half of the eustatic rise observed over that time period.

Meier further concluded that more than a third of the calculated glacier contribution to sea level comes from the mountains bordering the Gulf of Alaska, with the high mountains of Central Asia and the Patagonian Andes also making appreciable contributions. These areas combine large areas of ice with high rates of accumulation and ablation, and therefore, possible high rates of wastage. In contrast, areas with large annual amplitude and small ice area (e.g. Washington State and New Zealand), and areas with small annual amplitude and large ice area (e.g. Canadian Arctic) are much less important in terms of sea-level rise contribution. A preliminary study of the mass balance in the Canadian Arctic Islands supports this contention. Koerner (1985) indicates that the larger ice caps in this region have likely been close to steady state for a long period of time due to the apparent great stability of the Islands' ice edges.

Existing hydrometeorological (HM) models provide a means of estimating changes in the rate of glacial melting in response to long-term changes in atmospheric conditions. These HM models generally relate glacial accumulation to winter precipitation, ablation to summer air temperature, and the net balance to the difference in accumulation and ablation. Coefficients relating melt rate to summer air temperature show a significant range, from 0.57-0.98 m/yr per degree Celsius (Meier, 1984). Applying the average of the HM coefficients to the probable average

air temperature rise of 1.5-4.5°C, Meier calculated a possible rate of glacier melting equivalent of 1.7-5.2 mm/yr of sea-level rise. Assuming the temperature rise occurs in 100 years and the rise in annual meltwater contribution were linear, this rate corresponds to a total rise of 10 to 30 cm in the next century. These figures, then, represent the PRB's current best estimate of the future contribution of alpine glaciers and small ice caps to sea-level rise.

Greenland Ice Sheet:

The mass balance of the Greenland Ice Sheet can be estimated by use of a hydrological budget method. This method calculates the time rate of change of ice-sheet volume as the sum of the volume of accumulation (input) and the volume of melting and iceberg calving (output) for a year. All volumes are calculated in terms of water equivalents. However, the size of Greenland, the corresponding lack of data coverage (primarily in north and east portions of the ice sheet), and the error limits (20-40% for each of the three terms) associated with this method make it highly speculative at present.

An alternative method is to measure rates of thinning or thickening (derived from surface elevations) in specific areas and extrapolate these rates over the entire ice sheet (Reeh, 1985). As of 1985, the available data on surface elevation changes are restricted to the margins of western Greenland, where thinning has been documented since the turn of the century and is continuing at present, and to the central portion of the ice sheet (between 70-72° N latitude) where the ice sheet is generally thickening on the west-facing slopes and thinning on the east-facing slopes. Lack of data make it uncertain as to which of these rates is larger.

Reeh (1985) admits that an accurate estimate of the current contribution to sea-level rise from the Greenland Ice Sheet is not currently possible, by any method. In fact, even the sign of the contribution is unknown. Reeh does, however, submit a few illustrative values that probably represent the best available estimates. Extrapolation of the observed average thinning rate of about 0.3 m/yr for the west Greenland ablation area to the total ablation area results in a mass loss corresponding to a sea-level rise of 0.2-0.3 mm/yr. In contrast, extrapolation of the observed average thickening rate of 0.1 m/yr for the interior regions in south and central Greenland to the total accumulation area of the ice sheet, results in a mass gain corresponding to a sea-level lowering of about 0.4 mm/yr.

The Greenland Ice Sheet has a strong potential for contributing to climate-induced sea level rise due to its large ablation area. Current rough estimates of future sea level rise due to the accelerated melting of the Greenland Ice Sheet are based on calculations of the change in altitude of the equilibrium line - the line where accumulation equals ablation (Ambach and Kuhn, 1985; Binschandler, 1985). A small increase in the altitude of the equilibrium line can significantly increase the area of ablation on typical low-gradient glacier surfaces.

In order to estimate the shift of the equilibrium line in response to a warmer climate, Bindschandler (1985) of the Polar Research Board constructed a simple steady-state, two-dimensional model to represent a single flowline within the ice cap. The accumulation rate was considered constant (at 10% higher than present, in accord with projections of increased global precipitation) and the rate of ablation decreased linearly with altitude. To complete the model, a term for calving rate, based on published data, was assumed constant. The rise of the equilibrium line was

calculated using measured values of the surface temperature gradient versus altitude. Two scenarios were thus developed: an increase in equilibrium line altitude of (1) 500 m and (2) 1000m, corresponding approximately to increases in surface temperature of 3 and 6°C respectively.

The model results indicate that the mass balance becomes strongly negative in both scenarios. As the equilibrium line shifts upward, the decrease in accumulation area outweighs the increase in accumulation rate, while the average rate of ablation and the area of ablation increase. The net mass balances for the 3 and 6°C scenarios are -461 km^3/yr and -1259 km^3/yr, respectively, compared with a mass balance near zero at present. The respective rates of sea-level rise are 1.3 mm/yr and 3.5 mm/yr. These figures require that the ice cap be in equilibrium with the atmospheric temperature, a process which realistically might take on the order of 1000 years. Therefore, to make a best estimate of the sea-level rise expected by the year 2100, Bindschandler (1985) assumed a scenario in which atmospheric warming increased from the year 2000 until 2050 to the assumed values of 3 and 6°C, where it remained until 2100. The resulting change in sea level due to the partial melting of the Greenland Ice Sheet would be 0.10 m (equilibrium line shift of 500 m) for the 3°C case, and 0.25 m (equilibrium line shift of 1000 m) for the 6°C case.

Antarctic Ice Sheet:

The behavior of the Antarctic Ice Sheet represents the largest uncertainty in estimating the present and future interactions between glacial ice and the oceans. Accumulation data is not yet available for greater than one third of the continent, and there are no measurements on outflow for more than half of the Antarctic coast. In

addition, there is confusion about the contribution to overall mass balance from basal melting beneath floating ice shelves. The rate of data acquisition, as well as the quality of the data, has been increasing steadily in the past decade, primarily because of the implementation of satellite altimetry. As more data have become available, estimates of net mass balance for the Antarctic Ice Sheet have, in general, become closer to zero, ranging between -20% to +50% from a state of balance.

Budd and Smith (1985) assessed the present Antarctic mass balance by comparison of computed and observed balance velocities. The balance velocity represents the average velocity through a vertical column of the ice sheet as required to keep the mass of ice in steady-state balance with a given accumulation rate. Extensive amounts of new data on ice thickness and accumulation rates were obtained for their computations from traverses of previously-little-studied East Antarctica by Australian in 1983, and the Soviet Union in 1984. Balance ice-volume flux and balance velocity were computed for every point on a 20-km-resolution square grid covering the entire Antarctic surface. In general, the pattern of balance velocities was found to correspond well to the recognized major glacier outflow areas.

The results of the computations suggest that the Antarctic Ice Sheet net mass balance is slightly positive with a range of uncertainty of 0 to +20%, i.e. it should be removing water from the oceans. This conclusion is qualitatively supported by other recent research results compiled in the 1985 Polar Research Board report. Bentley (1985) concludes that although both melting rates and thickening rates vary widely across the Ross Ice Shelf, this southern section of West Antarctica is probably gaining mass at present. Doake (1985) finds no definitive evidence of significant

changes in mass balance for the Antarctic Peninsula or the Weddell Sea areas of West Antarctica, although the data that do exist suggest a small net loss. Orheim (1985) concludes that internationally-collected statistics on icebergs suggest that the rate of iceberg calving is probably 3 to 4 times higher than commonly accepted values and, as a result, the present mass balance of Antarctica may actually be negative. This contention may be supported by the fact that, in late October of 1987, the largest piece of floating ice on record (over 2700 km^3) detached from the Ross Ice Shelf (EOS, Dec. 1, 1987, p. 1625). In general, however, Budd and Smith (1985) conclude that in terms of sea level, the present apparent net gain in Antarctic mass represents a net decrease contribution to sea level of about 0 to -1.2 mm/yr.

Most of the large Antarctic glaciers and ice streams drain directly into large ice shelves, in contrast to those in Greenland, which flow directly into the ocean. These large Antarctic ice shelves are grounded both above and below sea level, with large portions floating. The ice shelves impose a backpressure on ice flowing into them. The largest ice shelves impose very large backpressures due to grounded ice rises that make it difficult to push the shelves seaward. Climatic warming might cause the shelf ice to thin and also accelerate calving. This causes the ice-shelf thickness in contact with the ice rises and shelf margin to be reduced, thereby reducing backpressure, and subsequently, increasing ice disharge into the shelves.

Increased ice drainage due to accelerated basal melting of floating ice shelves in West Antarctica is generally considered the most probable cause for a major sea-level rise due to global warming. Basal melting rates are controlled principally by the temperature of ocean currents beneath the ice shelves. There is great uncertainty concerning the behavior of these polar ocean currents.

Thomas (1985) assessed the possible responses of the Antarctic Ice Sheet to a doubled-CO_2 climate by the year 2050 by formulating two models. The first model (A) assumes that increased ice discharge exactly equals ice lost from the ice shelves by increased melting from the total area of Antarctic ice shelves. This model represents a great oversimplification and is included for comparison with the results of the second model. The second model (B) is far more elaborate. Model B simulates the initial response of Ice Stream B flowing from West Antarctica into the Ross Ice Shelf, and assumes that ice discharge from the entire ice sheet will respond in the same way. The resulting estimates probably represent upper limits for total ice discharge for Antarctica. The model assumes that basal melting rates increase linearly, beginning in the year 2000 and reaching a maximum value in 2050. Thereafter, they remain constant. Four cases were considered, based on the combination of two scenarios for calving and two scenarios for maximum values (M_{max}) for basal melting rate. The four cases are:

Case 1: $M_{max} = 0$ in 2000, $M_{max} = 1$ m/yr in 2050.
Calving rate exactly balances increased forward motion to keep seaward ice fronts in their present position.
Case 2: $M_{max} = 0$ in 2000, $M_{max} = 1$ m/yr in 2050.
Major calving after 2050 that cause seaward ice fronts to retreat to a line linking adjacent areas of grounded ice.
Case 3: Same as Case 1, but with $M_{max} = 3$ m/yr in 2050.
Case 4: Same as Case 2, but with $M_{max} = 3$ m/yr in 2050.

For Cases 1 through 4, Thomas' resultant estimates for sea-level rise by the year 2100 range between 0.20 and 2.25 m. Thomas further states that the current glaciological and oceanographic consensus is that a M_{max} of approximately 1 m/yr probably represents the maximum enhanced melting rate during the next century. Therefore, cases 3 and 4 appear highly unlikely. Thomas' model, representing the

best available estimates, indicates that sea-level rise caused by increased Antarctic ice discharge will be in the range of 0.2-1.0 m by the year 2100. Thomas states that a value of approximately 0.25 m is "most likely", and the higher estimates will be realized only if ocean circulation patterns also change due to the changing climate.

Environmental Protection Agency (1986):

The NRC's estimate of the earth's response to a significantly altered atmospheric chemistry represents an estimate of equilibrium conditions based on a hypothetical "instantaneous" doubling of carbon dioxide. Hoffman and others (1986) of the EPA presented a somewhat more realistic analysis of greenhouse-induced global warming based on projections of time-dependent changes in emissions and concentrations of CO_2 and a variety of other greenhouse gasses. In an effort to avoid extremes, Hoffman and others adopted a slightly narrower range for low and high estimates of global warming at equilibrium in a doubled-CO_2 environment than did the NRC. The low estimate of 2°C was derived from the GCM results of Manabe and Wetherald (1975) of the Princeton Geophysical Fluid Dynamics Laboratory. The high estimate of 4°C was obtained from the GCM results of both Washington and others (1977) and Hansen and others (1983).

Hoffman and others modified a one-dimensional radiative-convective model developed by Lacis and others (1981) to determine the radiative forcing effect of greenhouse gas increases at any time. This model uses a time-marching procedure to compute the vertical atmospheric temperature profile from calculated net radiative and convective energy fluxes. The modified model accounts for the effects of carbon

dioxide, methane, nitrous oxide, sulfur dioxide, and nine specific chlorofluorocarbons. High and low projections for increasing abundances of the constituent greenhouse gasses were synthesized from a variety of reliable estimates generated during the 1980s. The equilibrium values of 2-4°C for doubled concentrations were used to set the temperature sensitivity of the model. At any time, the realized warming will be a fraction of the equilibrium warming that could occur for the given atmospheric composition at that time. The proportion of the equilibrium warming expected is dependent on the effective heat capacity of the oceans. In Lacis and others' model, diffusion is used as a surrogate for heat transport into the oceans, thereby delaying the required warming for an incremental increase in greenhouse gasses. The model uses a simple two-layer oceanic system, with different diffusion coefficients for each layer. For an increment of greenhouse gas increase, the difference between the model-calculated warming and the equilibrium warming is termed the unrealized warming - the warming that would occur even if concentrations remained constant, but which has not yet occurred due to the time lag caused by oceanic heat absorption.

Hoffman and others divided their future projections into three periods. The years 1985-2000, termed the forescast period, is period of relative certainty due to the reliability of extending current trends for population growth, economic activity, and subsequent greenhouse gas emissions. The years 2000-2030, termed the bounding period, is a period of declining certainty where reasonable bounds can still be placed on the trends. The period of 2030-2060, termed the contingency period, is characterized by loss of confidence in the bounds placed on population and economic growth. In this period, various contingencies for emissions projections are tested.

Low and high scenarios for transient global temperature changes were generated by the model based on low and high emissions estimates in combination with the low and high equilibrium temperature estimates. Estimates of global sea-level rise in response to global warming were generated by examining the contributions of thermal expansion of ocean water, melting of alpine glaciers, increased meltwater runoff from Greenland, and enhanced ice discharge from the Antarctic Ice Sheet. For the analysis of the latter two, it was assumed, in agreement with current knowledge, that the temperature rise in the high latitudes would be 1.5 times the global average. Neither increased meltwater runoff from Antarctica nor enhanced ice discharge from Greenland were included in Hoffman and others' assessment due to lack of confidence in current estimates for these sources.

The contribution from thermal expansion was calculated by applying coefficients of thermal expansion for sea water to the estimated annual increments of heat added to the oceans. The addition of heat to the oceans and the subsequent temperature rise was calculated within the one-dimensional model for a simplified two-layer ocean. Thermal expansion was estimated to raise sea level by 15 to 34 cm by 2060.

The contribution from alpine glaciers was estimated using the relationship between temperature increase and increased discharge of alpine meltwater developed by Meier (1984). By this method, low and high estimates of 7 to 18 cm rise in sea level by the year 2060 were developed.

An estimate of the contribution from increased runoff from the Greenland Ice Sheet was generated by use of a single empirical equation that approximates the results of Bindschandler's (1985) two-dimensional flowline model. The equation is:

$$\text{Annual Sea Level Rise (cm)} = 0.0248 * (\text{Greenland temp. rise } °C)^{1.49} \quad \text{(A1.4)}$$

This method gives estimates for Greenland's contribution to sea level rise as 2 to 7 cm by 2060, suggesting that increased meltwater from Greenland is a relatively minor factor. However, increased ice discharge from Greenland was not considered in this analysis.

Hoffman and others' assessment of accelerated ice discharge from Antarctica relied on Thomas' (1985) projections. Since Thomas' study indicates that most of the effects of Antarctic ice discharge would not likely be felt before 2040, the sea level contribution is not considered to be large by 2060. Due to the huge uncertainties in predicting the behavior of Antarctica, Hoffman and others attempted to cover what they considered a reasonable range in estimates by arbitrarily choosing low and high values of approximately 6 cm and 45 cm by 2060. Increased meltwater runoff from the Antarctic Ice Sheet was not included in this assessment.

Scientific Committee on Problems of the Environment (SCOPE) (1986):

The approach of Robin (1986) to determining the rise of sea level in response to global warming is to interpret observational data and to emphasize correlations and simple model that involve the minimum number of assumptions. As more assumptions become involved, models can more easily be adjusted to fit existing data, but this does not, in Robin's opinion, improve the model's ability to make accurate forecasts.

Robin made an in-depth review of the various components and exchange rates within the global hydrological cycle, as well as the current knowledge on the possible effects on each caused by changes in global temperature. From this review, he determined that there are so many deficiencies in present knowledge that a full evaluation of sea-level rise involving the contributions of all relevant physical processes is impossible. Therefore, he made use of a simple linear correlation between changes in global mean temperature and global mean sea level.

Use of a linear correlation was justified by examining several processes that show an approximately linear response to temperature. These processes include thermal expansion of sea water within the temperature range of interest, the shift in altitude of glacier equilibrium lines, and the change in saturation water vapor pressure over small ranges of temperature change. Although there are numerous other relevant physical processes, such as those involving oceanic and atmospheric dynamics, which are unlikely to show this linear response, they are considered to be so poorly understood at present that a linear approximation is reasonable.

Robin obtained scenarios for global mean temperature-changes in response to a doubling of CO_2 from Dickinson (1986), another SCOPE researcher. Dickinson synthesized the results of numerous researchers concerning the two major sources of uncertainty in modelling future climate change, the feedback effects of ice albedo and cloud radiative properties. For each of these independent variables, a normal distribution of the various estimates is assumed. From these distributions, the expected value and standard deviation is determined for each parameter. These expected values were compared with values used in the GCMs of Washington and Meehl (1983), Washington and Meehl (1984), and Hansen and others (1984). These

three GCMs generated a range of temperature increase of 1.3-4.8°C for a doubled-CO_2 environment. On the basis of the comparison, along with limits imposed by his own judgement, Dickinson estimated the temperature change for steady-state CO_2 doubling to be 3.5 ± 2°C, with a 68% chance that the change would be between 2.5-4.5°C.

Robin's linear correlation between global mean temperature and global mean sea level was based on Gornitz and others' (1982) linear relation between their sea-level curve for the past century and Hansen and others' (1981) global temperature curve for the same period. This relation is:

$$\Delta SL(t) = a\Delta T(t-t_o) + b \qquad \text{(A 1.5)}$$

where ΔSL and ΔT are five-year means of global sea level and temperature respectively, t is time, and t_o is the time lag in sea-level response to temperature change. The time lag was chosen to minimize the variance between the sea level curve and temperature. The coefficients a and b were obtained by least squares linear regression. The results were A = 16 cm/°C, B = 0.3 cm, and t_o = 18 years. Two alternate methods for determining the value of the coefficient A were also tested. First, equating the average global rise in sea level from 1880-1980 of 10.5 cm (Gornitz and others, 1982) to the mean rise in global air temperature of 0.4°C from the same data, gives the coefficient A = 26 cm/°C. Second, coupling Barnett's (1984) value of 14.3 cm for sea level rise between 1881-1980 and SCOPE's value of 0.5°C global temperature rise in the past century (Wigley and others, 1986) gives the coefficient A = 29 cm/°C. Robin therefore chose limits for the coefficient A of 16

and 30 cm/century. Applying the linear relation above to a global temperature rise of 1.5°C to 5.5°C over the next century, gives a sea level rise of 24-88 cm for A = 16 cm/°C, and 45-165 cm for A = 30 cm/°C. Robin therefore gives 25 cm as the low scenario and 165 cm as the high scenario for sea level rise in response to a doubling of atmospheric CO_2, which SCOPE expects to have occurred by the year 2100 (Keepin and others, 1986).

Marine Board, National Research Council (1987):

The Marine Board's Committee on Engineering Implications of Changes in Relative Sea Level adopted three eustatic sea level rise scenarios without doing any form of analysis of the contributing physical processes (Marine Board, 1987). In an effort to cover what was determined to be a reasonable range of uncertainty from previous studies (such as the three previously described), rises of 0.5 m, 1.0 m, and 1.5 m by the year 2100 were chosen as low, middle, and high scenarios, respectively. The Marine Board's equation describing the eustatic rise at any time is

$$E(t) = 0.0012t + Bt^2 \qquad \text{(A1.6)}$$

where E(t) is the eustatic rise in meters above present, and t is the time in years from present (taken to be 1985). The value of the coefficient B is 2.8×10^{-5} m/yr^2, 6.6×10^{-5} m/yr^2, and 1.05×10^{-4} m/yr^2 in the low, medium, and high scenarios, respectively. The nonlinear form of the equation appears generally consistent with future-rise estimates determined by other researchers. These scenarios cover a

somewhat smaller range of uncertainty by the year 2100 than do the estimates from the other three organizations.

7.2 Appendix 2. Water well hydrographs for nine selected wells within the study area (Data from the Texas Water Commission).

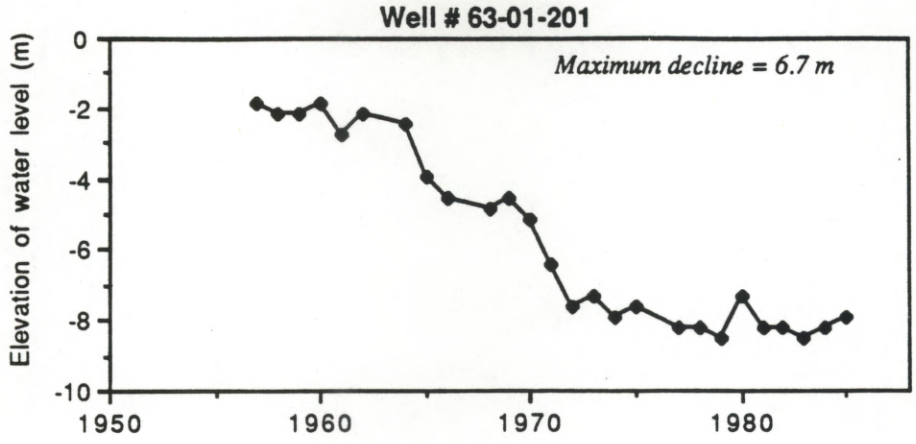

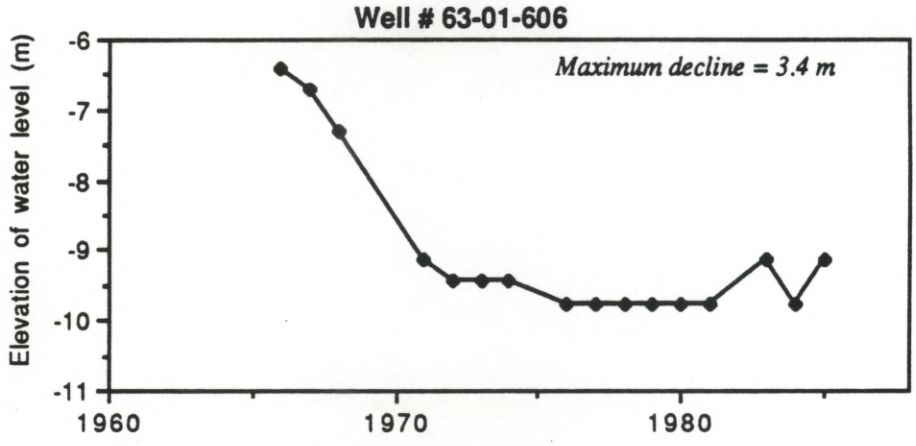

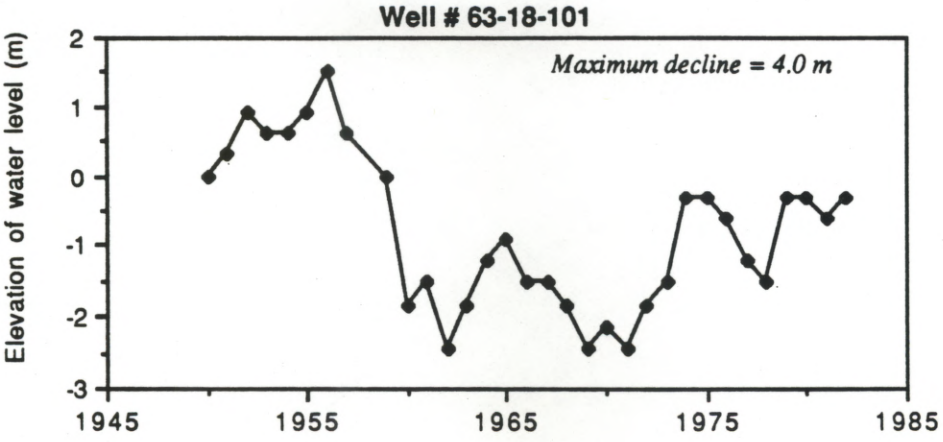

Appendix 2 (cont.)

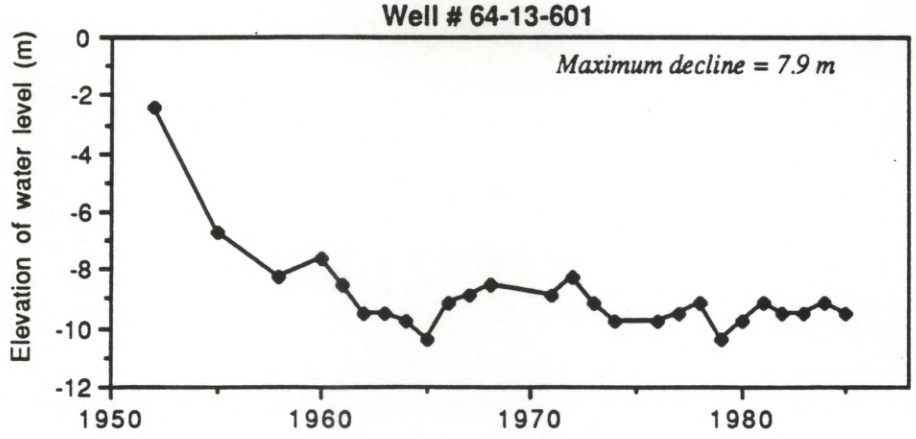

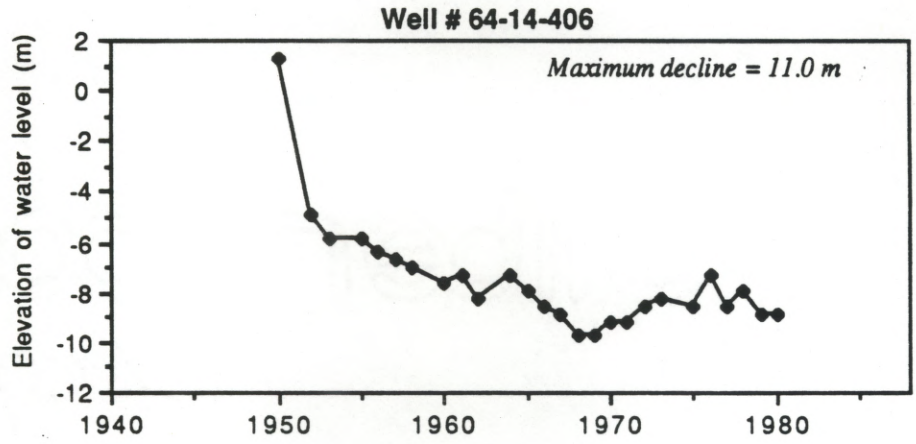

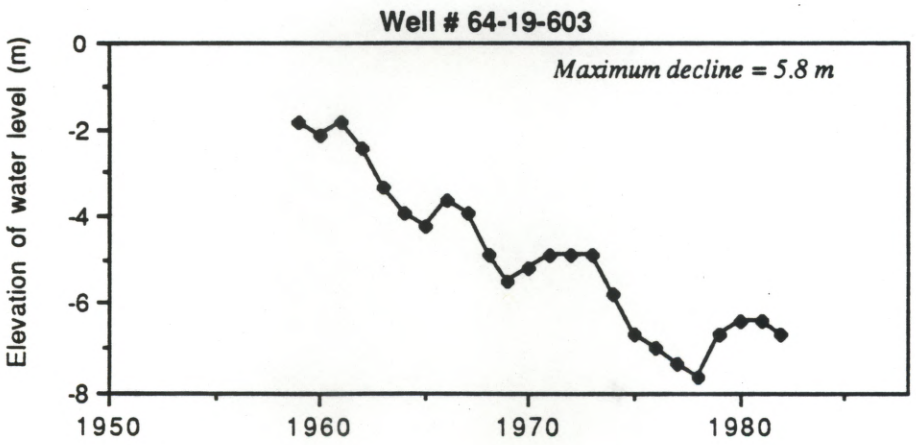

Appendix 2 (cont.)

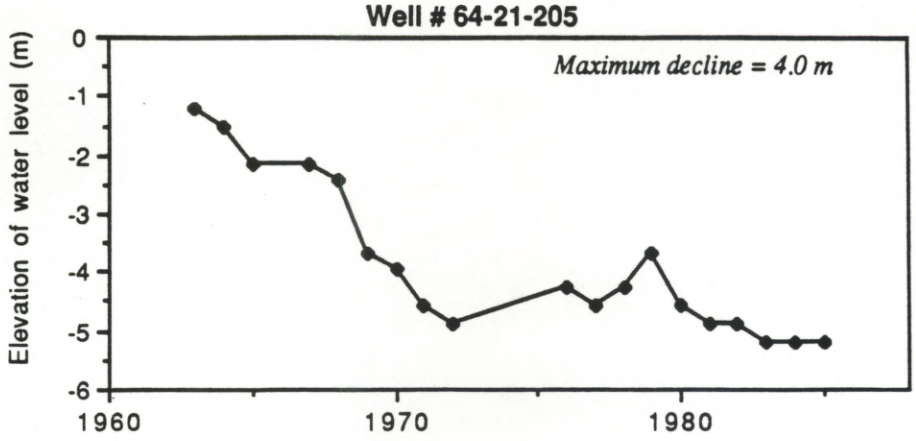

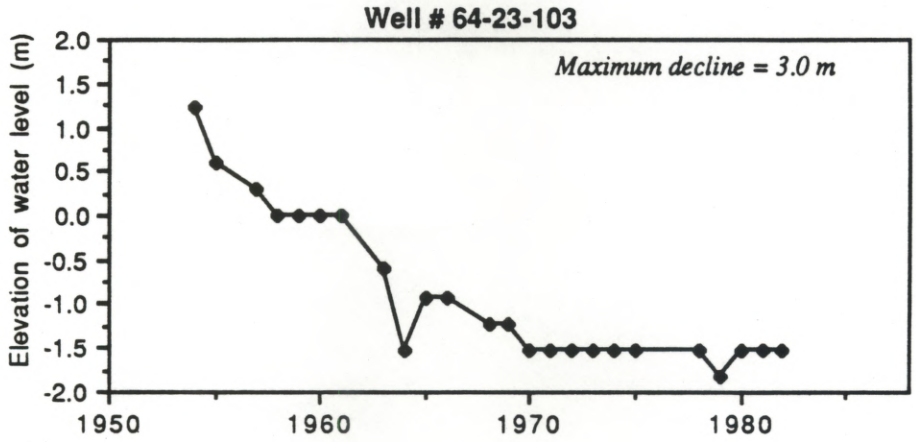

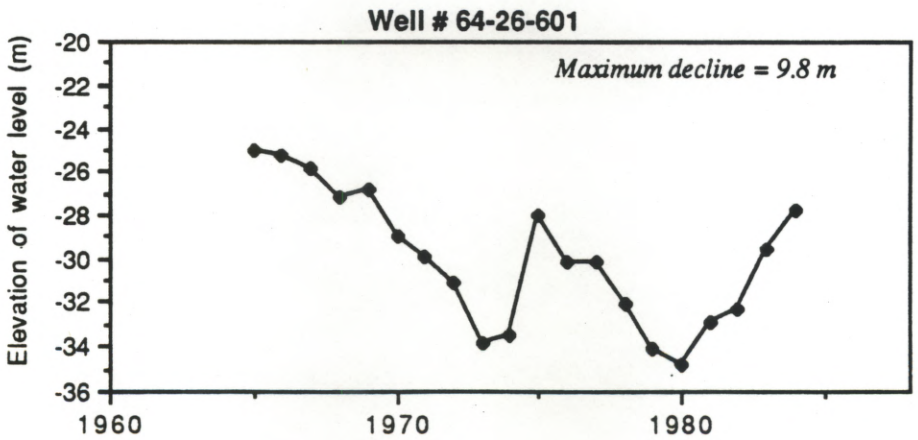

7.3.1 Appendix 3a. Data for historical shoreline movement (ft.) at each of the 142 points of measurement. Data from Morton (1975) and Paine and Morton (1986).

Point	1800s to 1930	1930 to 1955/7	1955/7 to 1974	1930 to 1974/1982	1800s to 1974/1982
1	2075	150	0	150	2225
2	1750	-550	-600	-1150	600
3	1025	-375	-775	-1150	-125
4	250	0	-675	-675	-425
5	-675	-50	-400	-450	-1125
6	-400	-400	-375	-775	-1175
7	-700	-500	-400	-900	-1600
8	-975	-850	-600	-1450	-2425
9	-1050	-975	-500	-1475	-2525
10	-975	-1225	-350	-1575	-2550
11	-1325	-1200	-375	-1575	-2900
12	25	-775	-200	-975	-950
13	0	-275	-125	-400	-400
14	250	100	-175	-75	175
15	175	225	-175	50	225
16	-100	100	-100	0	-100
17	-325	0	0	0	-325
18	-625	100	0	100	-525
19	-775	150	-75	75	-700
20	-825	150	-200	-50	-875
21	-925	150	-150	0	-925
22	-1050	125	-125	0	-1050
23	-1000	100	-150	-50	-1050
24	-775	125	-125	0	-775
25	-650	125	-200	-75	-725
26	-500	25	-125	-100	-600
27	-475	-50	-100	-150	-625
28	-250	-175	-50	-225	-475
29	-200	-200	-75	-275	-475
30	-250	-200	-50	-250	-500
31	-325	-125	-100	-225	-550
32	-350	50	-100	-50	-400
33	-275	50	-150	-100	-375
34	-200	100	-250	-150	-350
35	-75	-75	-200	-275	-350
36	-150	50	-350	-300	-450
37	-350	50	-350	-300	-650
38	-250	100	-425	-325	-575
39	-350	75	-275	-200	-550
40	-400	75	-300	-225	-625
41	-450	25	-300	-275	-725
42	-575	0	-175	-175	-750
43	-	0	-275	-275	-
44	-	100	-250	-150	-
45	-	0	-300	-300	-
46	-200	50	-250	-200	-400

Appendix 3a (cont.). Data for historical shoreline movement (ft.) at each of the 142 points of measurement. Data from Morton (1975) and Paine and Morton (1986).

Point	1800s to 1930	1930 to 1955/7	1955/7 to 1974	1930 to 1974/1982	1800s to 1974/1982
47	-25	0	-200	-200	-225
48	0	0	-175	-175	-175
49	0	0	-150	-150	-150
50	0	0	-175	-175	-175
51	0	100	-100	0	0
52	0	125	-125	0	0
53	0	150	-100	50	50
54	0	150	-125	25	25
55	100	150	-225	-75	25
56	175	150	-300	-150	25
57	175	100	-250	-150	25
58	0	300	-325	-25	-25
59	0	275	-125	150	150
60	125	400	50	450	575
61	450	600	275	875	1325
62	1100	1075	400	1475	2575
63	900	-	-	-900	0
64	1950	-	-	-100	1850
65	-725	-	-	100	-625
66	-850	-	-	-700	-1550
67	-775	-	-	75	-700
68	-550	-	-	225	-325
69	-550	-	-	375	-175
70	-350	-	-	-25	-375
71	-150	-	-	-125	-275
72	-275	-	-	-300	-575
73	-50	-	-	-250	-300
74	-350	-	-	-325	-675
75	-400	-	-	-200	-600
76	-150	-	-	-250	-400
77	150	-	-	-100	50
78	-125	-	-	-125	-250
79	-175	-	-	-250	-425
80	-250	-	-	-125	-375
81	-50	-	-	-125	-175
82	-100	-	-	-50	-150
83	-150	-	-	-125	-275
84	-75	-	-	-150	-225
85	-50	-	-	-100	-150
86	100	-	-	-125	-25
87	-400	-	-	-150	-550
88	500	-	-	75	575
89	50	-	-	100	150
90	25	-	-	-75	-50
91	25	-	-	-75	-50
92	100	-	-	0	100

Appendix 3a (cont.). Data for historical shoreline movement (ft.) at each of the 142 points of measurement. Data from Morton (1975) and Paine and Morton (1986).

Point	1800s to 1930	1930 to 1955/7	1955/7 to 1974	1930 to 1974/1982	1800s to 1974/1982
93	-225	-	-	125	-100
94	-75	-	-	-50	-125
95	-125	-	-	0	-125
96	-25	-	-	-50	-75
97	-125	-	-	-150	-275
98	0	-	-	0	0
99	-300	-	-	-50	-350
100	50	-	-	-125	-75
101	150	-	-	-75	75
102	150	-	-	-75	75
103	100	-	-	-150	-50
104	25	-	-	-175	-150
105	-50	-	-	-100	-150
106	-250	-	-	-100	-350
107	-375	-	-	-25	-400
108	-250	-	-	-175	-425
109	-50	-	-	-175	-225
110	50	-	-	-200	-150
111	-375	-	-	-425	-800
112	-400	-	-	-125	-525
113	-250	-	-	-350	-600
114	-525	-	-	-150	-675
115	-250	-	-	-175	-425
116	-100	-	-	-250	-350
117	350	-	-	-275	75
118	-750	-	-	-100	-850
119	-150	-	-	-125	-275
120	-150	-	-	0	-150
121	225	-	-	-100	125
122	125	-	-	-125	0
123	-150	-	-	-75	-225
124	150	-	-	-175	-25
125	0	-	-	-25	-25
126	150	-	-	-150	0
127	-250	-	-	-250	-500
128	-300	-	-	-700	-1000
129	-475	-	-	-125	-600
130	-525	-	-	-175	-700
131	-600	-	-	-225	-825
132	0	-	-	0	0
133	-500	-	-	0	-500
134	-725	-	-	-50	-775
135	-450	-	-	-50	-500
136	-400	-	-	-100	-500
137	-375	-	-	0	-375
138	-325	-	-	-50	-375

Appendix 3a (cont.). Data for historical shoreline movement (ft.) at each of the 142 points of measurement. Data from Morton (1975) and Paine and Morton (1986).

Point	1800s to 1930	1930 to 1955/7	1955/7 to 1974	1930 to 1974/1982	1800s to 1974/1982
139	-175	-	-	-25	-200
140	-225	-	-	225	0
141	-50	-	-	50	0
142	-150	-	-	25	-125

7.3.2 Appendix 3b. Average historical shoreline movement (ft.) for subjectively-chosen groups of points.

Points	1800s to 1930	1930 to 1974/1982	1800s to 1974/1982	Period 1 Rate (ft./yr)	Period 2 Rate (ft./yr)
1-2	1913	-500	1413	40	-14
3-4	638	-913	-275	13	-21
5-7	-592	-708	-1300	-12	-16
8-11	-1081	-1519	-2600	-23	-35
12-13	13	-688	-675	0	-16
14-15	213	-13	200	4	0
16-18	-350	33	-317	-7	1
19-21	-842	8	-833	-18	0
22-23	-1025	-25	-1050	-21	-1
24-27	-600	-81	-681	-13	-2
28-31	-256	-244	-500	-5	-6
32-36	-210	-175	-385	-4	-4
37-40	-338	-263	-600	-7	-6
41-42	-513	-225	-738	-11	-5
46-47	-113	-200	-313	-2	-5
48-50	0	-167	-167	0	-4
51-52	0	0	0	0	0
53-54	0	38	38	0	1
55-57	150	-125	25	3	-3
58-59	0	63	63	0	1
60-62	558	933	1492	12	21
63	900	-900	0	11	-17
66	-850	-700	-1550	-11	-13
71-73	-158	-225	-383	-2	-4
74-76	-300	-258	-558	-4	-5
77-79	-50	-158	-208	-1	-3
80-82	-133	-100	-233	-2	-2
83-85	-92	-125	-217	-1	-2
86	100	-125	-25	1	-2
87	-400	-150	-550	-5	-3
88-89	275	88	363	3	2
90-92	50	-50	0	1	-1
93-95	-142	25	-117	-2	0
96-97	-75	-100	-175	-1	-2
98-100	-83	-58	-142	-1	-1
101-102	150	-75	75	2	-1
103-105	25	-142	-117	0	-3

Appendix 3b (cont.). Average historical shoreline movement (ft.) for subjectively-chosen groups of points.

Points	1800s to 1930	1930 to 1974/1982	1800s to 1974/1982	Period 1 Rate (ft./yr)	Period 2 Rate (ft./yr)
106-108	-292	-100	-392	-4	-2
109-110	0	-188	-188	0	-4
111-113	-342	-300	-642	-4	-6
114-116	-292	-192	-483	-4	-4
117	350	-275	75	4	-5
118-120	-350	-75	-425	-4	-1
121-123	67	-100	-33	1	-2
124-126	100	-117	-17	1	-2
127-129	-342	-358	-700	-4	-7
130-131	-563	-200	-763	-7	-4
132	0	0	0	0	0
133-136	-519	-50	-569	-7	-1
137-139	-292	-25	-317	-4	0
140-141	-138	138	0	-2	3
142	-150	25	-125	-2	0

7.3.3 Appendix 3c. Graphs of average historical shoreline movement for subjectively-chosen groups of points.

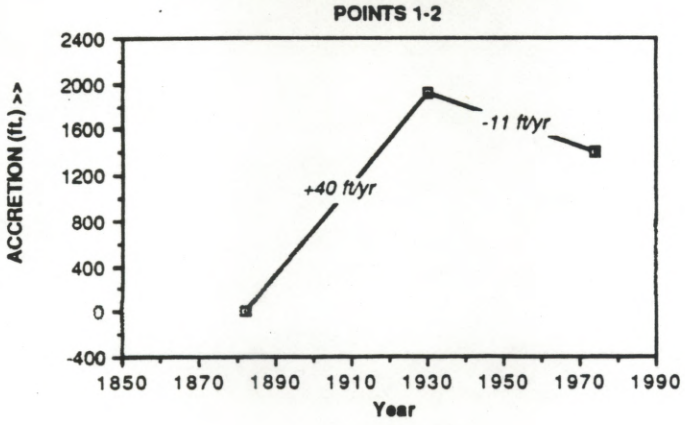

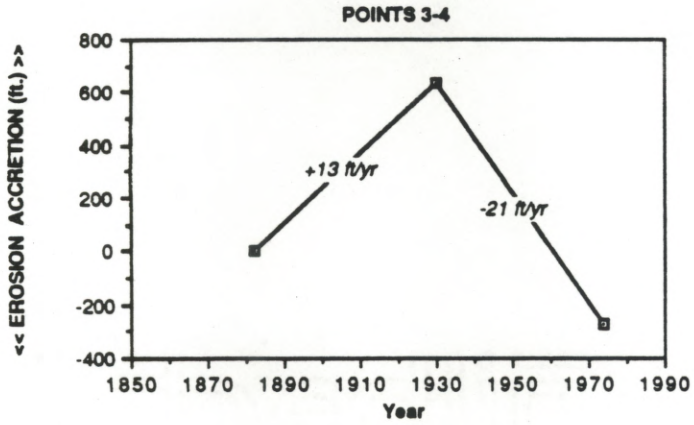

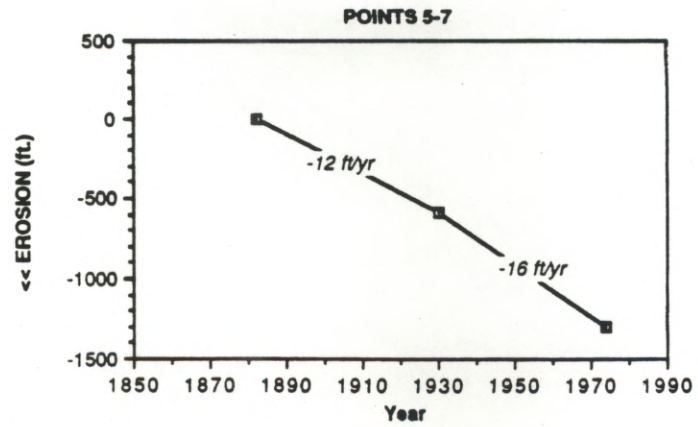

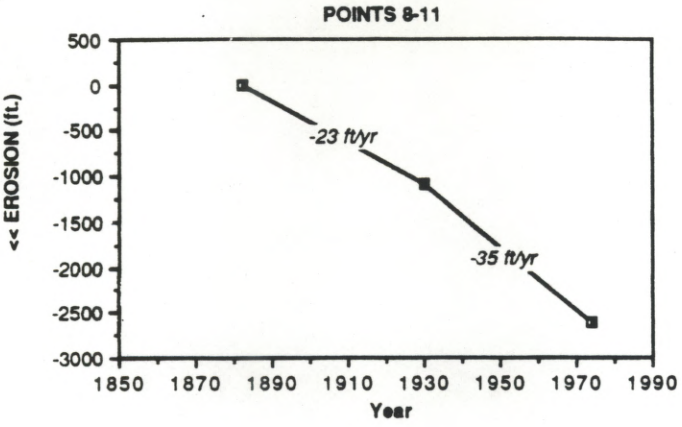
POINTS 8-11
<< EROSION (ft.)
500
0
-500
-1000
-1500
-2000
-2500
-3000
-23 ft/yr
-35 ft/yr
1850 1870 1890 1910 1930 1950 1970 1990
Year

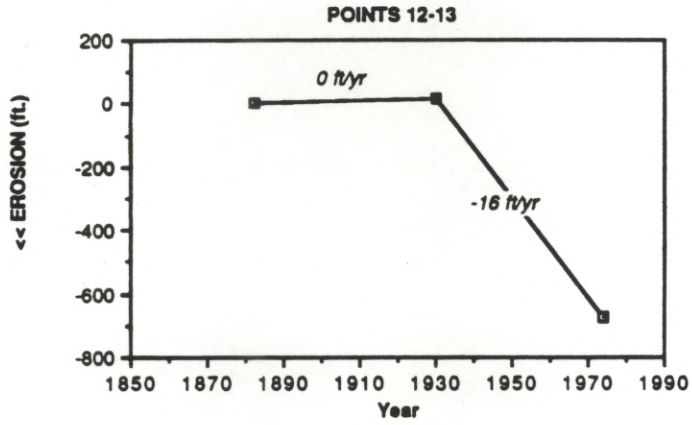
POINTS 12-13
<< EROSION (ft.)
200
0
-200
-400
-600
-800
0 ft/yr
-16 ft/yr
1850 1870 1890 1910 1930 1950 1970 1990
Year

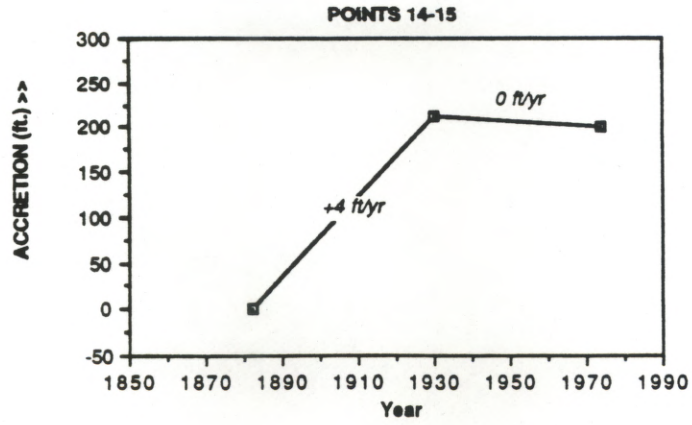
POINTS 14-15
ACCRETION (ft.) >>
300
250
200
150
100
50
0
-50
0 ft/yr
+4 ft/yr
1850 1870 1890 1910 1930 1950 1970 1990
Year

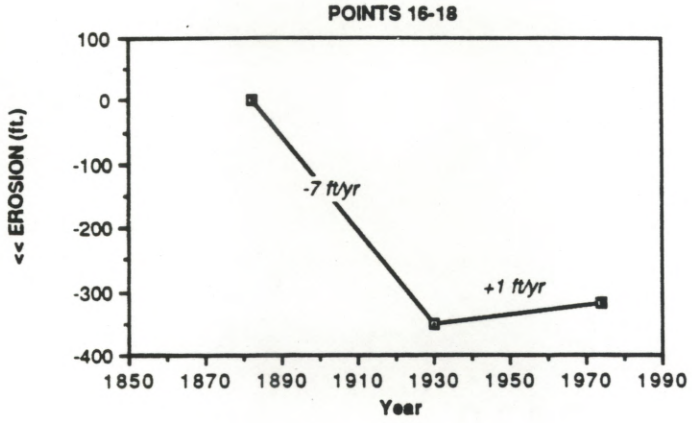
POINTS 16-18
<< EROSION (ft.)
100
0
-100
-200
-300
-400
-7 ft/yr
+1 ft/yr
1850 1870 1890 1910 1930 1950 1970 1990
Year

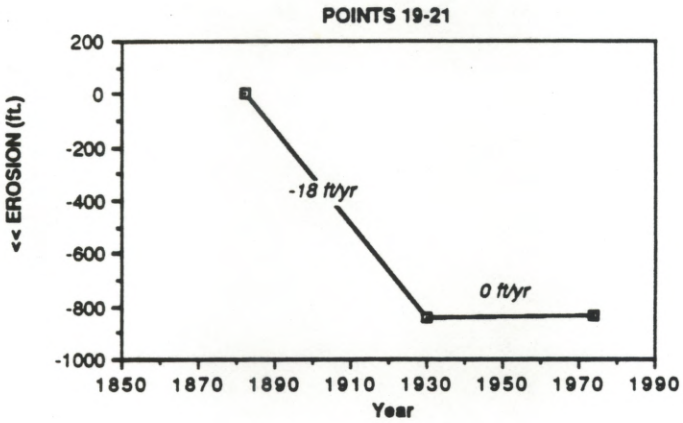
POINTS 19-21
<< EROSION (ft.)
200
0
-200
-400
-600
-800
-1000
-18 ft/yr
0 ft/yr
1850 1870 1890 1910 1930 1950 1970 1990
Year

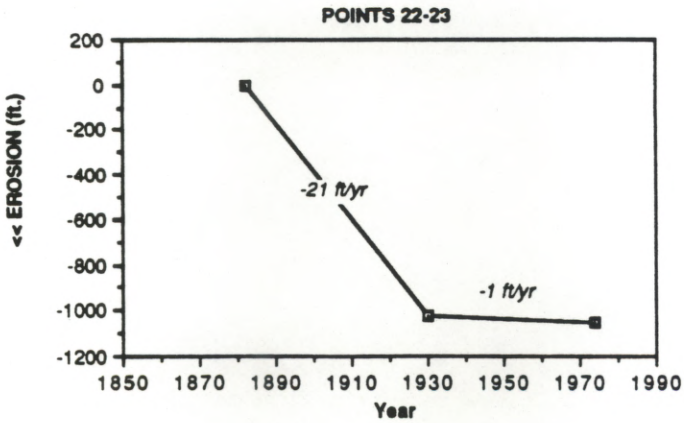
POINTS 22-23
<< EROSION (ft.)
200
0
-200
-400
-600
-800
-1000
-1200
-21 ft/yr
-1 ft/yr
1850 1870 1890 1910 1930 1950 1970 1990
Year

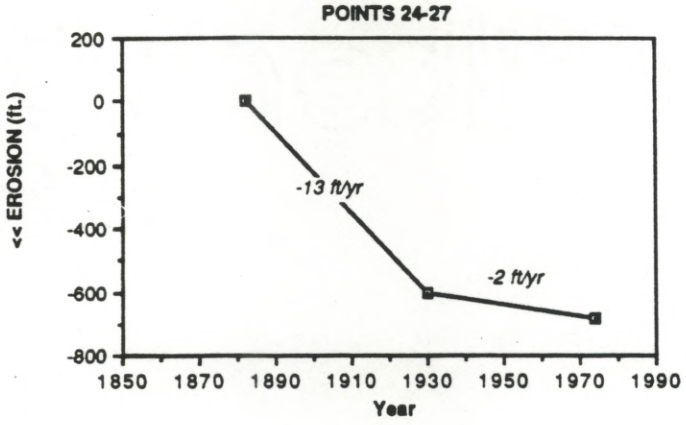
POINTS 24-27
<< EROSION (ft.)
200
0
-200
-400
-600
-800
-13 ft/yr
-2 ft/yr
1850 1870 1890 1910 1930 1950 1970 1990
Year

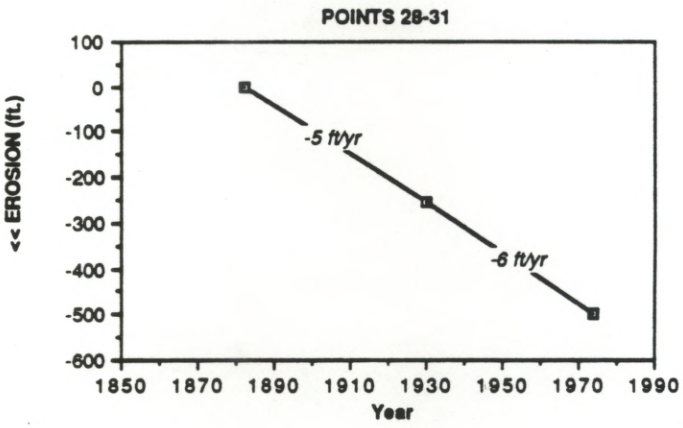
POINTS 28-31
<< EROSION (ft.)
100
0
-100
-200
-300
-400
-500
-600
-5 ft/yr
-6 ft/yr
1850 1870 1890 1910 1930 1950 1970 1990
Year

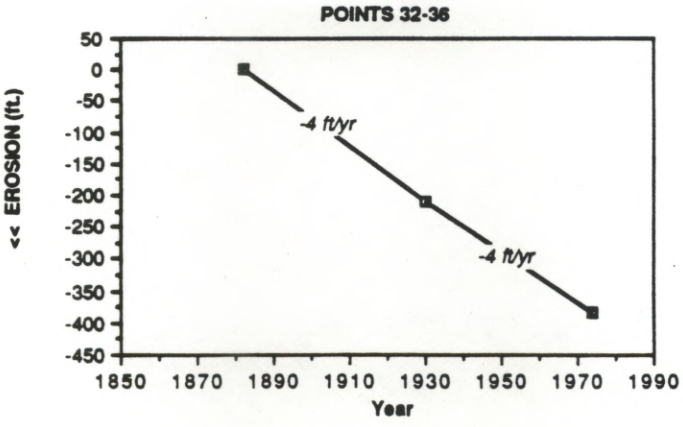
POINTS 32-36
<< EROSION (ft.)
50
0
-50
-100
-150
-200
-250
-300
-350
-400
-450
-4 ft/yr
-4 ft/yr
1850 1870 1890 1910 1930 1950 1970 1990
Year

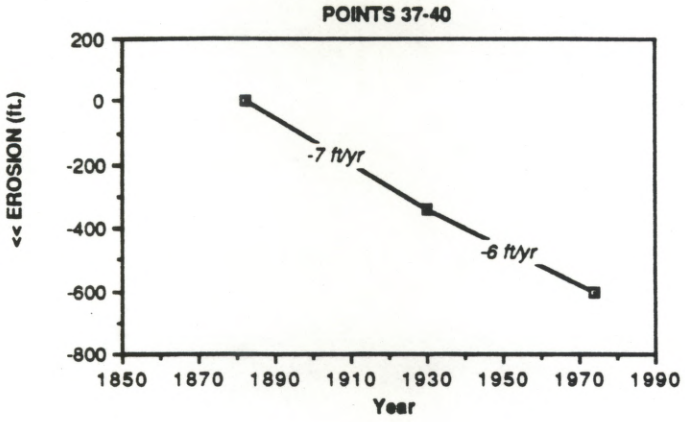
POINTS 37-40
<< EROSION (ft.)
200
0
-200
-400
-600
-800
-7 ft/yr
-6 ft/yr
1850 1870 1890 1910 1930 1950 1970 1990
Year

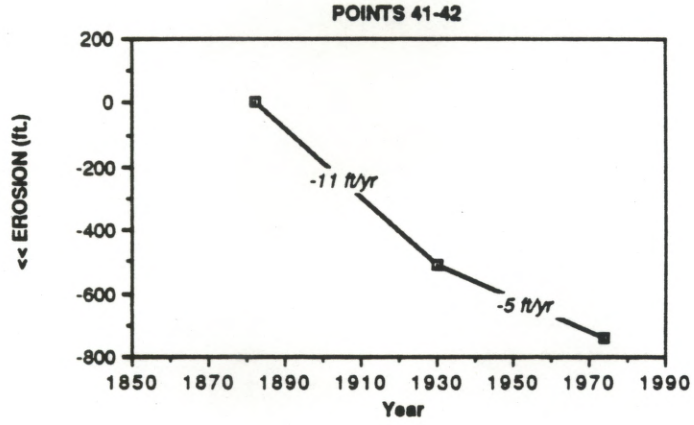
POINTS 41-42
<< EROSION (ft.)
200
0
-200
-400
-600
-800
-11 ft/yr
-5 ft/yr
1850 1870 1890 1910 1930 1950 1970 1990
Year

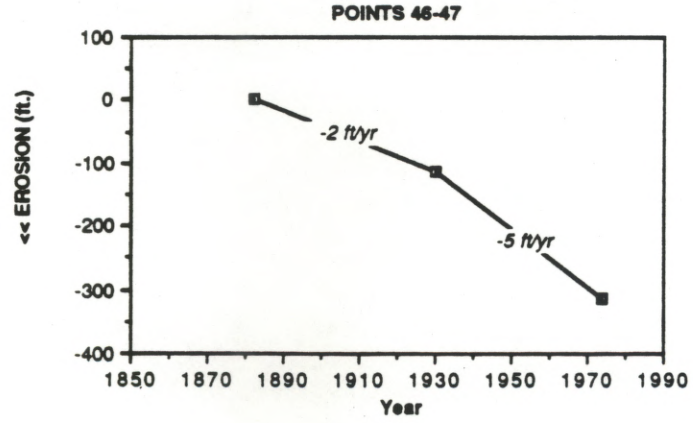
POINTS 46-47
<< EROSION (ft.)
100
0
-100
-200
-300
-400
-2 ft/yr
-5 ft/yr
1850 1870 1890 1910 1930 1950 1970 1990
Year

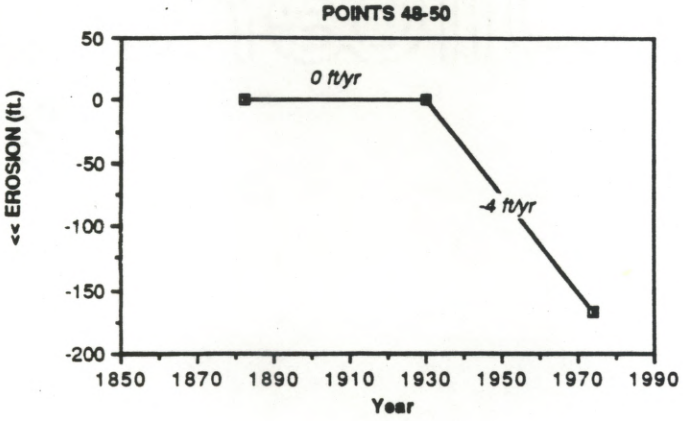
POINTS 48-50
<< EROSION (ft.)
50
0
-50
-100
-150
-200
0 ft/yr
-4 ft/yr
1850 1870 1890 1910 1930 1950 1970 1990
Year

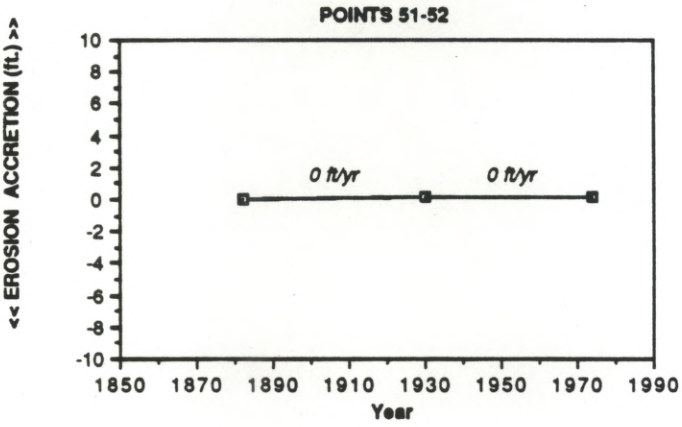
POINTS 51-52
<< EROSION ACCRETION (ft.) >>
10
8
6
4
2
0
-2
-4
-6
-8
-10
0 ft/yr
0 ft/yr
1850 1870 1890 1910 1930 1950 1970 1990
Year

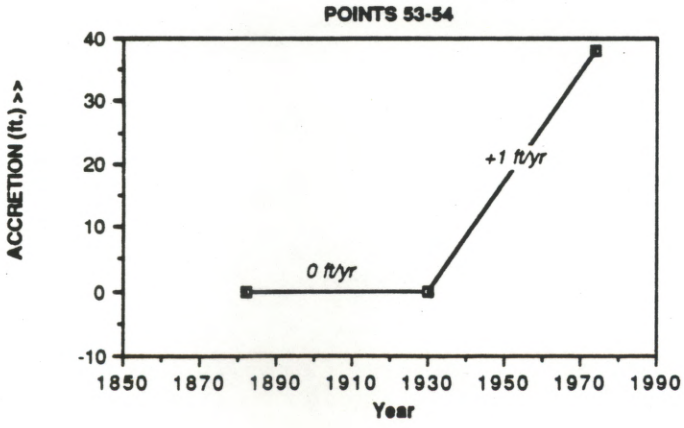
POINTS 53-54
ACCRETION (ft.) >>
40
30
20
10
0
-10
+1 ft/yr
0 ft/yr
1850 1870 1890 1910 1930 1950 1970 1990
Year

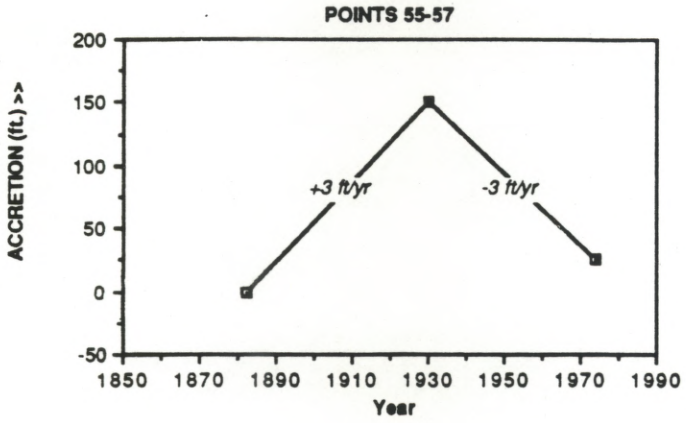
POINTS 55-57
ACCRETION (ft.) >>
200
150
100
50
0
-50
+3 ft/yr
-3 ft/yr
1850 1870 1890 1910 1930 1950 1970 1990
Year

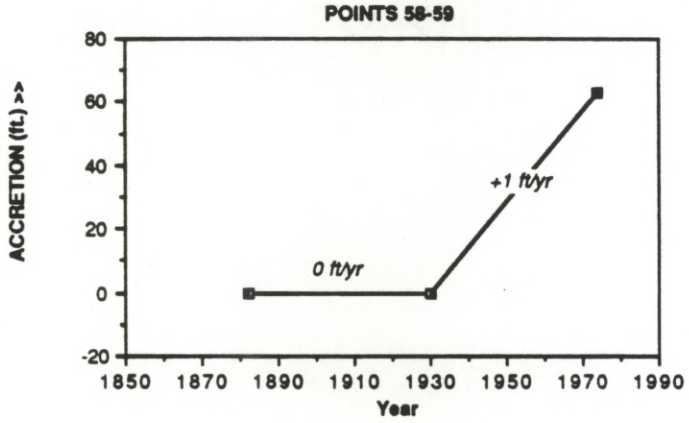
POINTS 58-59
ACCRETION (ft.) >>
80
60
40
20
0
-20
+1 ft/yr
0 ft/yr
1850 1870 1890 1910 1930 1950 1970 1990
Year

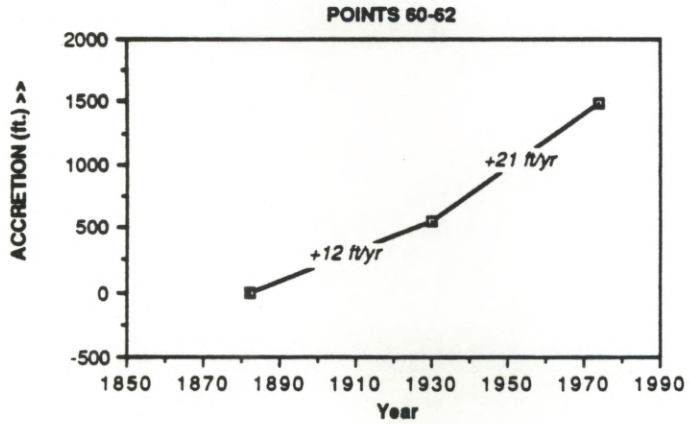
POINTS 60-62
ACCRETION (ft.) >>
2000
1500
1000
500
0
-500
+21 ft/yr
+12 ft/yr
1850 1870 1890 1910 1930 1950 1970 1990
Year

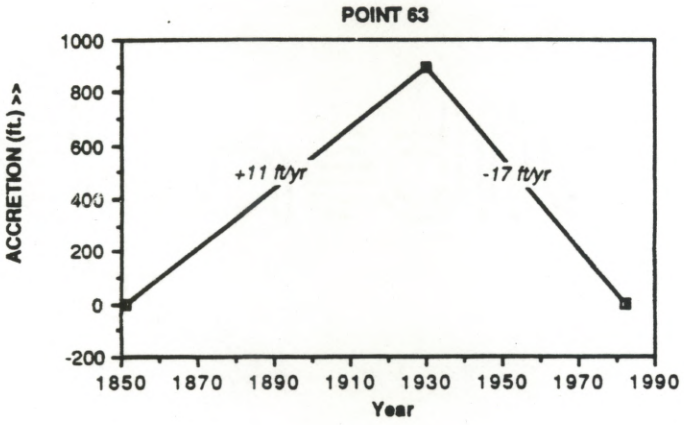
POINT 63
ACCRETION (ft.) >>
1000
800
600
400
200
0
-200
+11 ft/yr
-17 ft/yr
1850 1870 1890 1910 1930 1950 1970 1990
Year

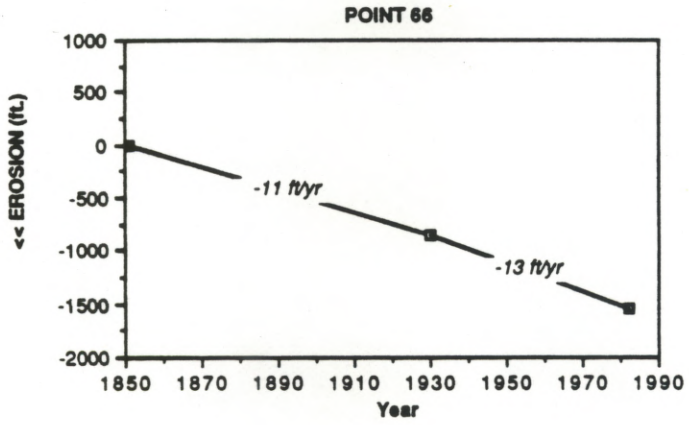
POINT 66
<< EROSION (ft.)
1000
500
0
-500
-1000
-1500
-2000
-11 ft/yr
-13 ft/yr
1850 1870 1890 1910 1930 1950 1970 1990
Year

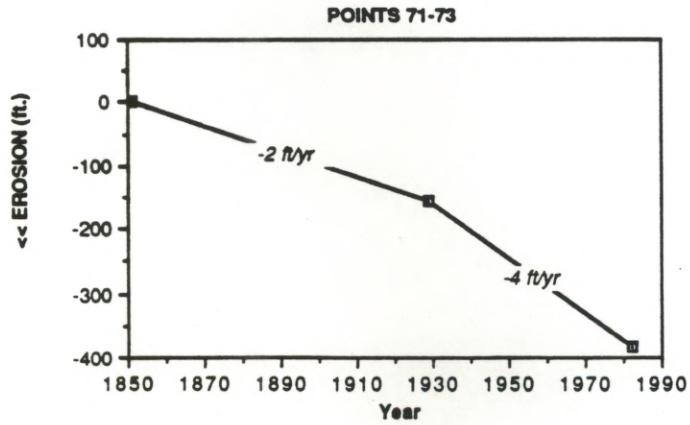
POINTS 71-73
<< EROSION (ft.)
100
0
-100
-200
-300
-400
-2 ft/yr
-4 ft/yr
1850 1870 1890 1910 1930 1950 1970 1990
Year

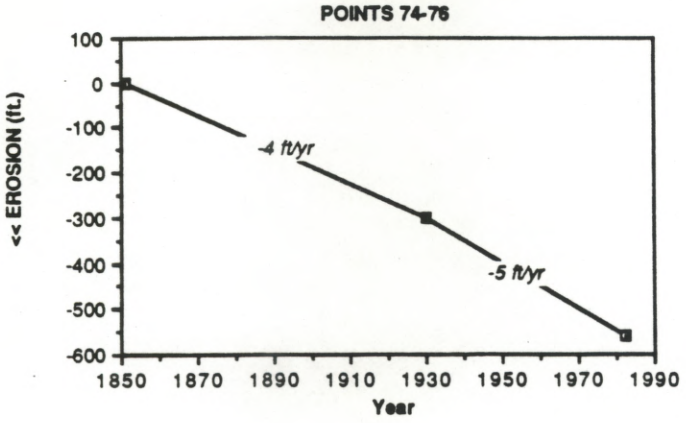
POINTS 74-76
<< EROSION (ft.)
100
0
-100
-200
-300
-400
-500
-600
-4 ft/yr
-5 ft/yr
1850 1870 1890 1910 1930 1950 1970 1990
Year

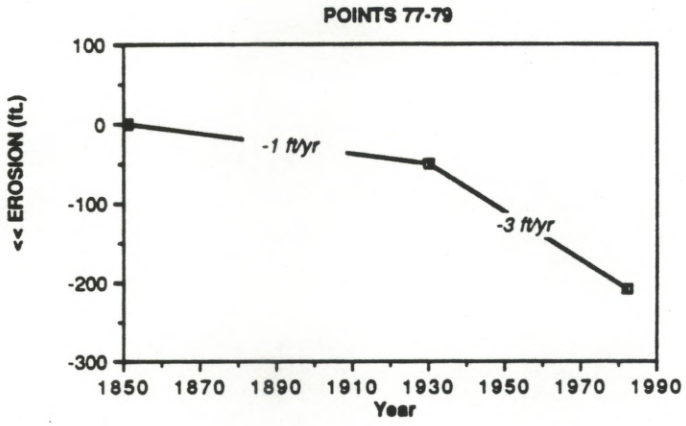
POINTS 77-79
<< EROSION (ft.)
100
0
-100
-200
-300
-1 ft/yr
-3 ft/yr
1850 1870 1890 1910 1930 1950 1970 1990
Year

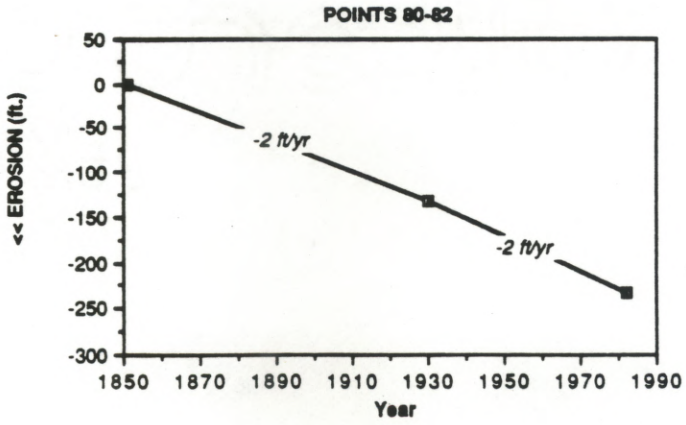
POINTS 80-82
<< EROSION (ft.)
50
0
-50
-100
-150
-200
-250
-300
-2 ft/yr
-2 ft/yr
1850 1870 1890 1910 1930 1950 1970 1990
Year

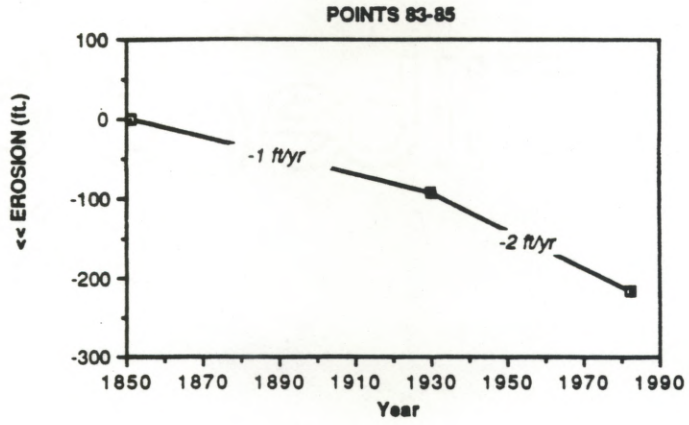
POINTS 83-85
<< EROSION (ft.)
100
0
-100
-200
-300
-1 ft/yr
-2 ft/yr
1850 1870 1890 1910 1930 1950 1970 1990
Year

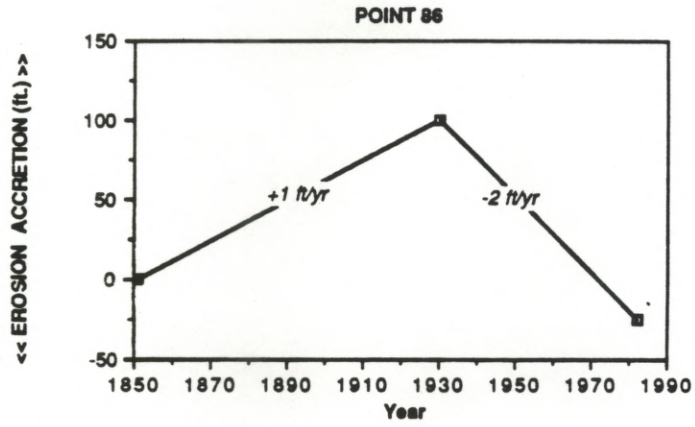
POINT 86
<< EROSION ACCRETION (ft.) >>
150
100
50
0
-50
+1 ft/yr
-2 ft/yr
1850 1870 1890 1910 1930 1950 1970 1990
Year

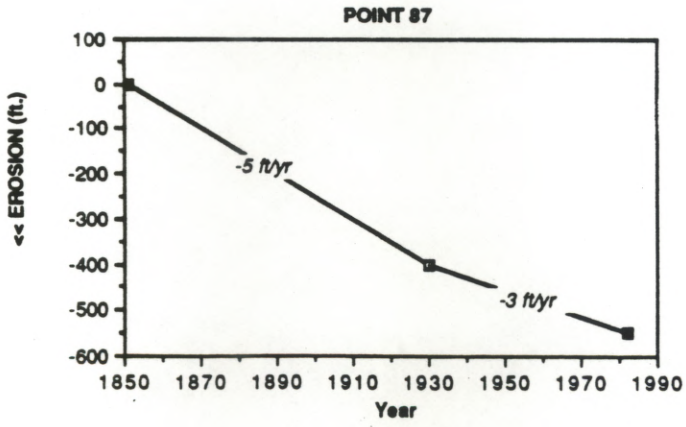
POINT 87
<< EROSION (ft.)
100
0
-100
-200
-300
-400
-500
-600
-5 ft/yr
-3 ft/yr
1850 1870 1890 1910 1930 1950 1970 1990
Year

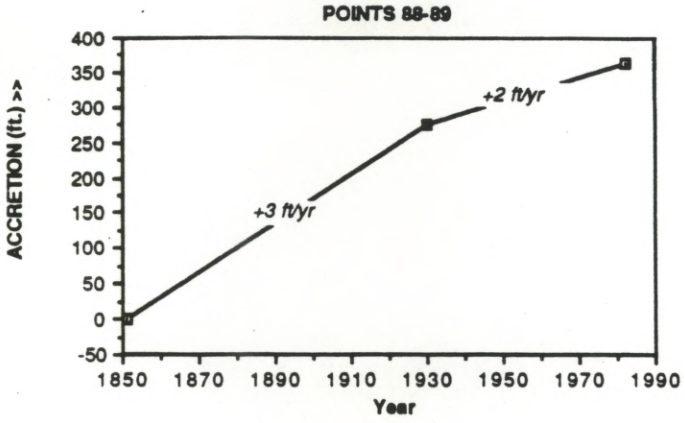
POINTS 88-89
ACCRETION (ft.) >>
400
350
300
250
200
150
100
50
0
-50
+2 ft/yr
+3 ft/yr
1850 1870 1890 1910 1930 1950 1970 1990
Year

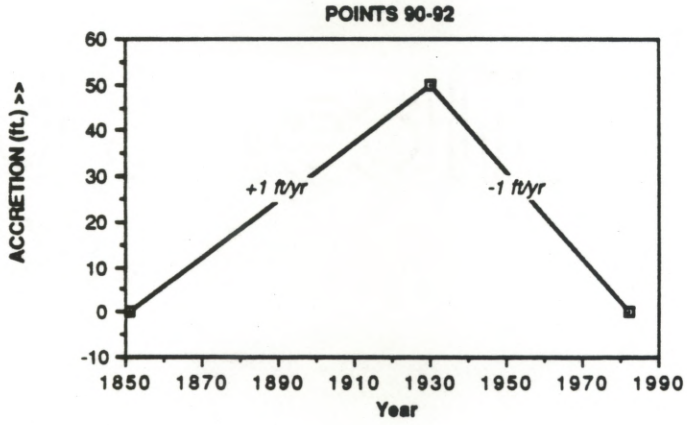
POINTS 90-92
ACCRETION (ft.) >>
60
50
40
30
20
10
0
-10
+1 ft/yr
-1 ft/yr
1850 1870 1890 1910 1930 1950 1970 1990
Year

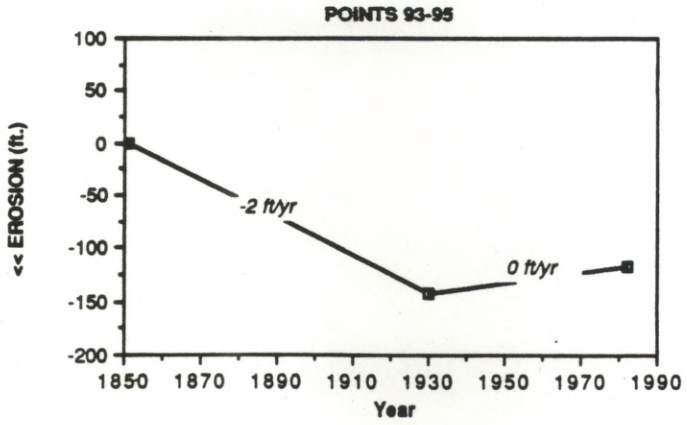
POINTS 93-95
<< EROSION (ft.)
100
50
0
-50
-100
-150
-200
-2 ft/yr
0 ft/yr
1850 1870 1890 1910 1930 1950 1970 1990
Year

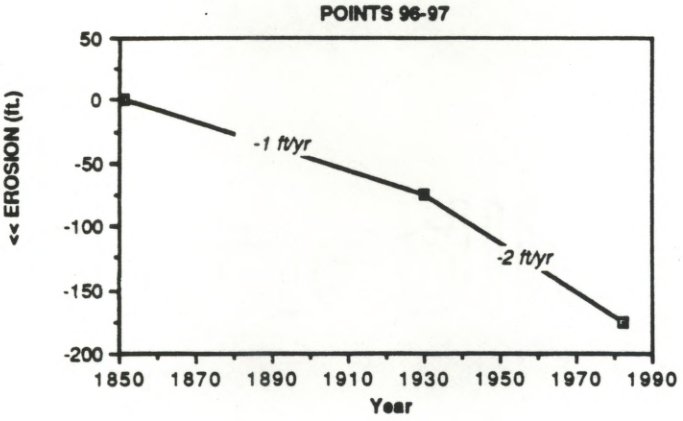
POINTS 96-97
<< EROSION (ft.)
50
0
-50
-100
-150
-200
-1 ft/yr
-2 ft/yr
1850 1870 1890 1910 1930 1950 1970 1990
Year

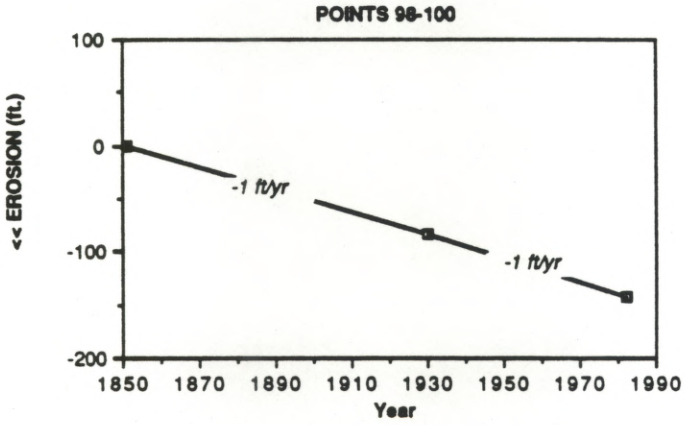
POINTS 98-100
<< EROSION (ft.)
100
0
-100
-200
-1 ft/yr
-1 ft/yr
1850 1870 1890 1910 1930 1950 1970 1990
Year

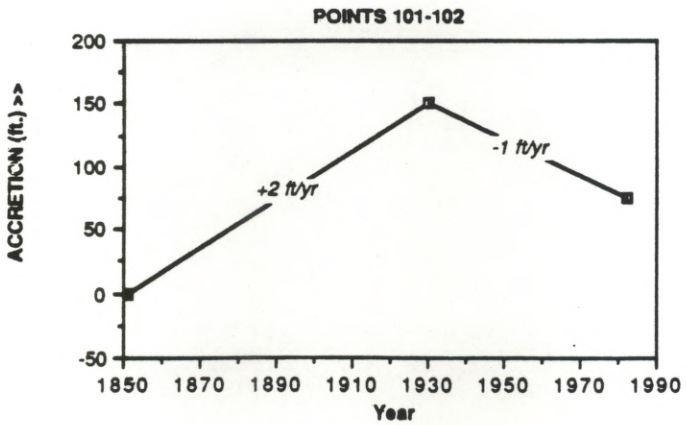
POINTS 101-102
ACCRETION (ft.) >>
200
150
100
50
0
-50
+2 ft/yr
-1 ft/yr
1850 1870 1890 1910 1930 1950 1970 1990
Year

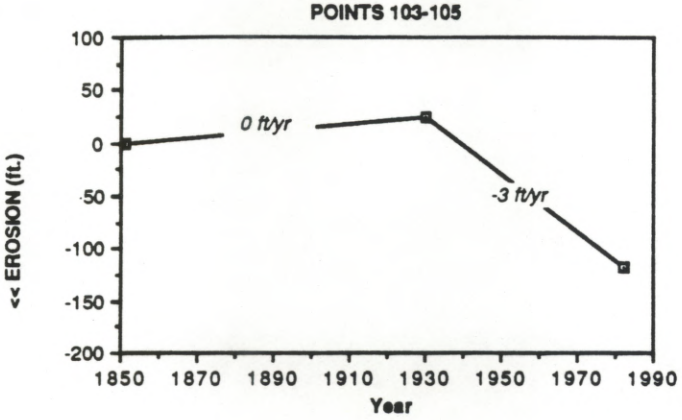
POINTS 103-105
100
50
0
-50
-100
-150
-200
<< EROSION (ft.)
0 ft/yr
-3 ft/yr
1850 1870 1890 1910 1930 1950 1970 1990
Year

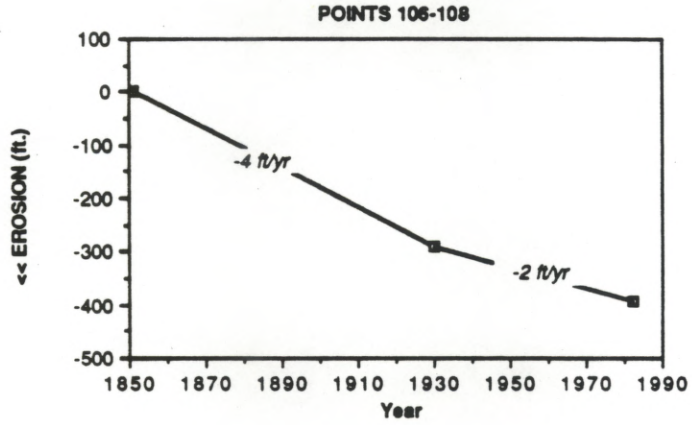
POINTS 106-108
100
0
-100
-200
-300
-400
-500
<< EROSION (ft.)
-4 ft/yr
-2 ft/yr
1850 1870 1890 1910 1930 1950 1970 1990
Year

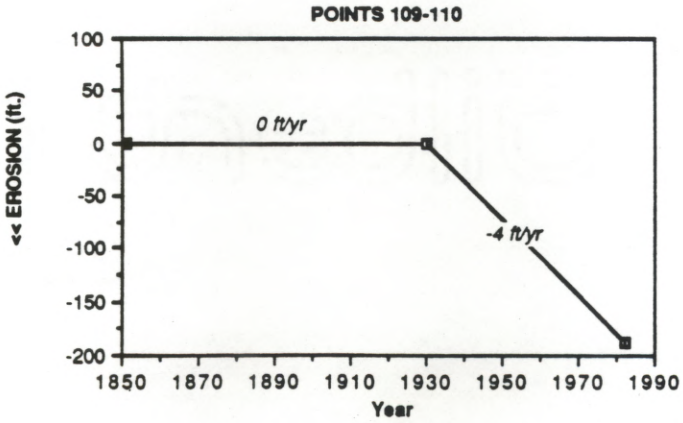
POINTS 109-110
100
50
0
-50
-100
-150
-200
<< EROSION (ft.)
0 ft/yr
-4 ft/yr
1850 1870 1890 1910 1930 1950 1970 1990
Year

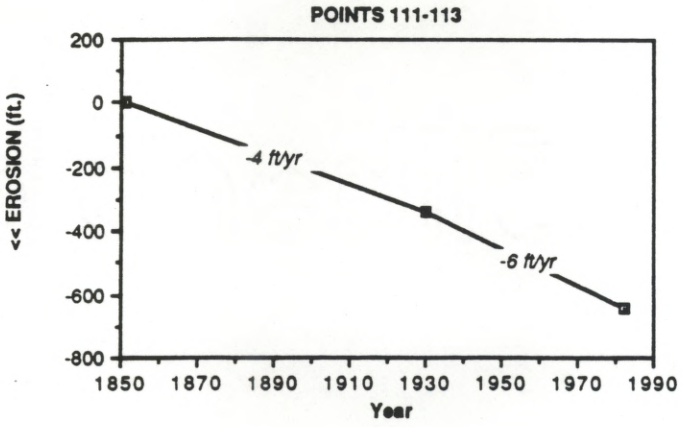
POINTS 111-113
<< EROSION (ft.)
200
0
-200
-400
-600
-800
-4 ft/yr
-6 ft/yr
1850 1870 1890 1910 1930 1950 1970 1990
Year

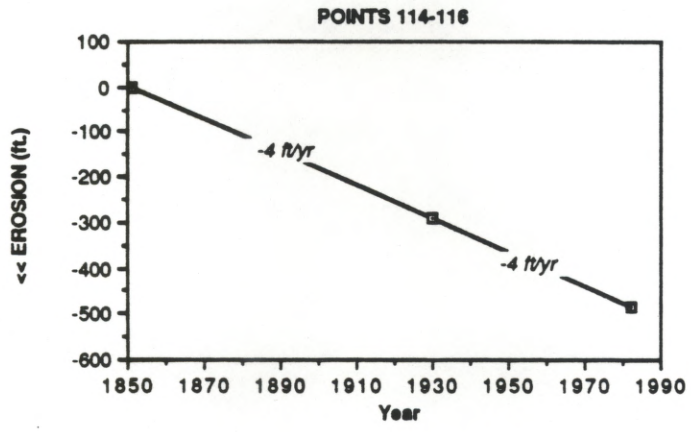
POINTS 114-116
<< EROSION (ft.)
100
0
-100
-200
-300
-400
-500
-600
-4 ft/yr
-4 ft/yr
1850 1870 1890 1910 1930 1950 1970 1990
Year

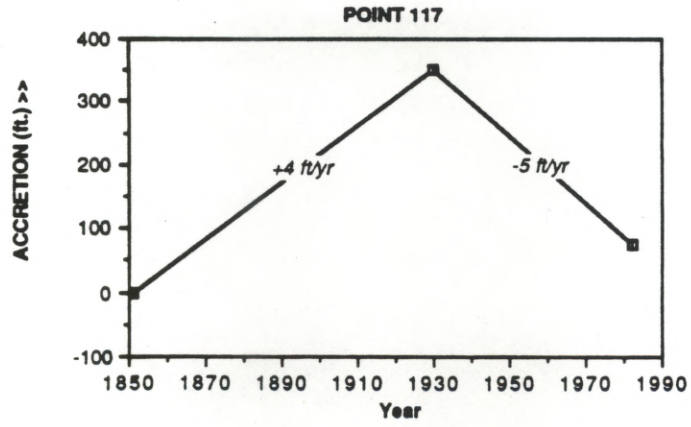
POINT 117
ACCRETION (ft.) >>
400
300
200
100
0
-100
+4 ft/yr
-5 ft/yr
1850 1870 1890 1910 1930 1950 1970 1990
Year

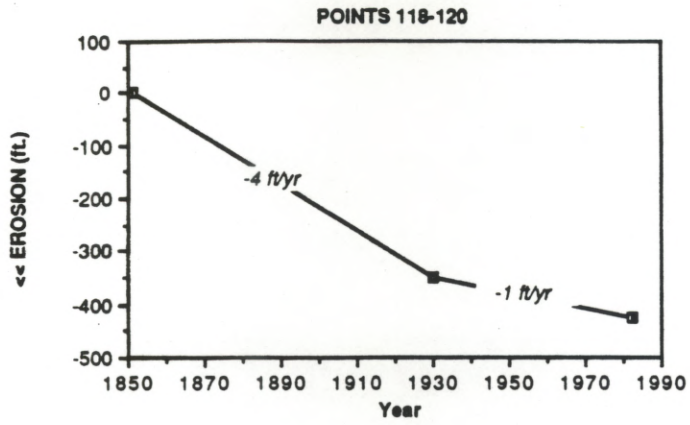
POINTS 118-120
<< EROSION (ft.)
100
0
-100
-200
-300
-400
-500
-4 ft/yr
-1 ft/yr
1850 1870 1890 1910 1930 1950 1970 1990
Year

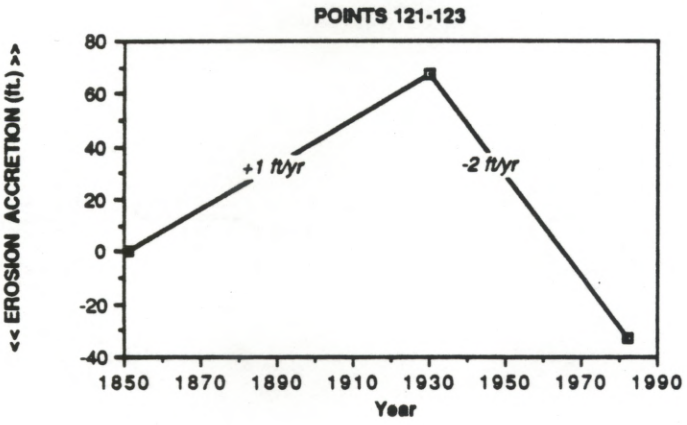
POINTS 121-123
<< EROSION ACCRETION (ft.) >>
80
60
40
20
0
-20
-40
+1 ft/yr
-2 ft/yr
1850 1870 1890 1910 1930 1950 1970 1990
Year

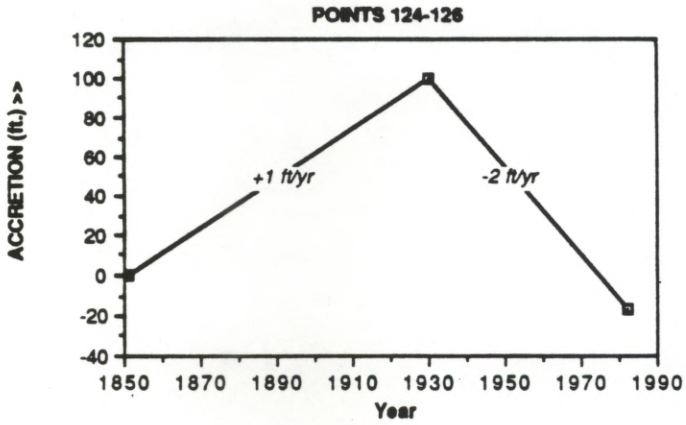
POINTS 124-126
ACCRETION (ft.) >>
120
100
80
60
40
20
0
-20
-40
+1 ft/yr
-2 ft/yr
1850 1870 1890 1910 1930 1950 1970 1990
Year

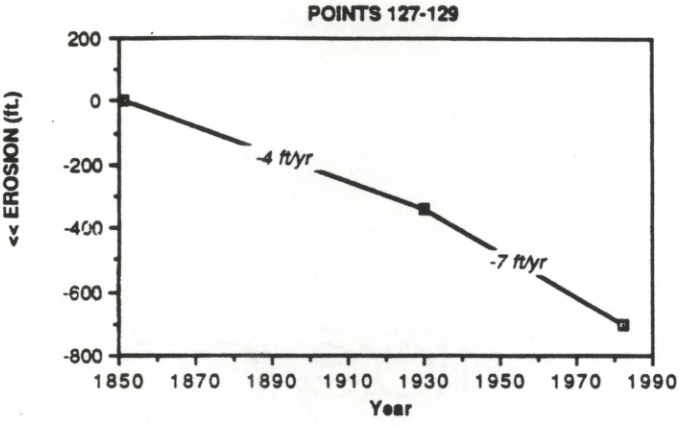
POINTS 127-129
<< EROSION (ft.)
200
0
-200
-400
-600
-800
-4 ft/yr
-7 ft/yr
1850 1870 1890 1910 1930 1950 1970 1990
Year

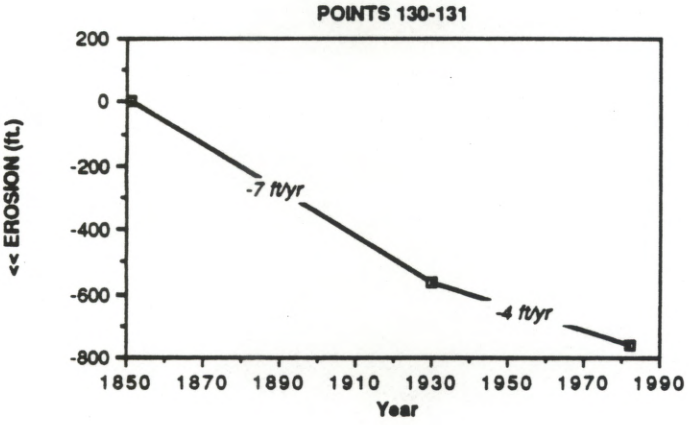
POINTS 130-131
<< EROSION (ft.)
200
0
-200
-400
-600
-800
-7 ft/yr
-4 ft/yr
1850 1870 1890 1910 1930 1950 1970 1990
Year

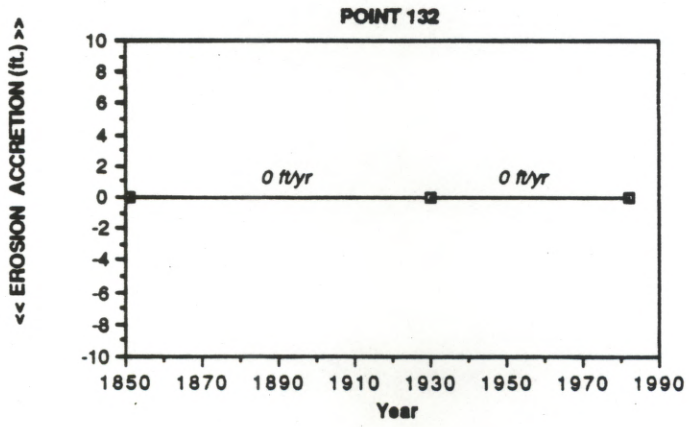
POINT 132
<< EROSION ACCRETION (ft.) >>
10
8
6
4
2
0
-2
-4
-6
-8
-10
0 ft/yr
0 ft/yr
1850 1870 1890 1910 1930 1950 1970 1990
Year

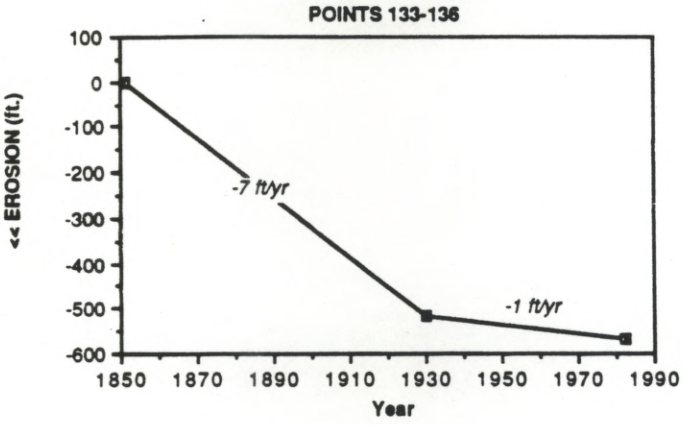
POINTS 133-136
<< EROSION (ft.)
100
0
-100
-200
-300
-400
-500
-600
-7 ft/yr
-1 ft/yr
1850 1870 1890 1910 1930 1950 1970 1990
Year

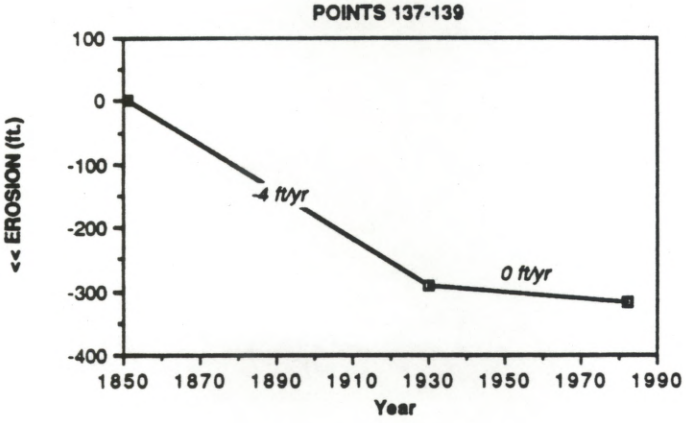
POINTS 137-139
<< EROSION (ft.)
100
0
-100
-200
-300
-400
-4 ft/yr
0 ft/yr
1850 1870 1890 1910 1930 1950 1970 1990
Year

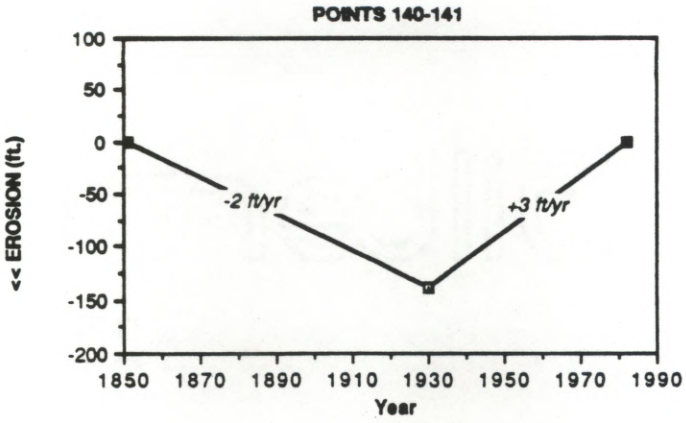
POINTS 140-141
<< EROSION (ft.)
100
50
0
-50
-100
-150
-200
-2 ft/yr
+3 ft/yr
1850 1870 1890 1910 1930 1950 1970 1990
Year

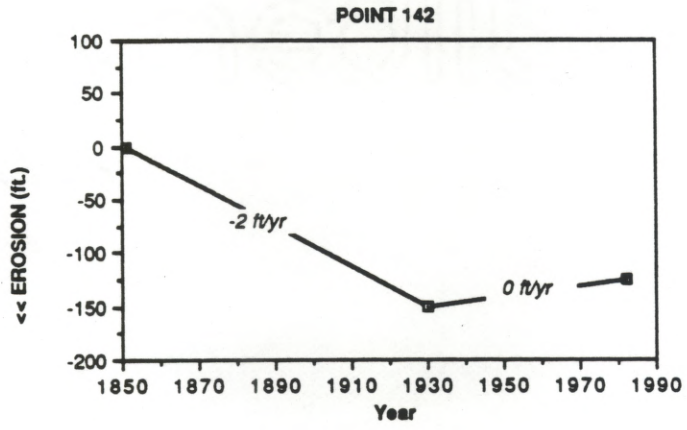
POINT 142
100
50
0
-50
-100
-150
-200
<< EROSION (ft.)
-2 ft/yr
0 ft/yr
1850
1870
1890
1910
1930
1950
1970
1990
Year

7.4 Appendix 4. Planimeter data for areal changes (acres) in the coastline between Sabine Pass and Bolivar Roads. (Unpublished data from R.A. Morton, 1988). Note: 1 acre = 4.047E-3 km2; 1 km2 = 247 acres

Section from points	Areal change (acres) 1930-1955/7	Areal change (acres) 1955/7-1974	Areal change (acres) 1930-1974
1 - 2	-52.3	-	-
2 - 3	-50.5	-	-
3 - 4	-29.7	-	-
4 - 5	0.0	-	-
5 - 6	-22.3	-41.6	-63.9
6 - 7	-48.9	-41.6	-90.5
7 - 8	-77.4	-21.4	-98.8
8 - 9	-89.7	-68.2	-157.9
9 - 10	-133.4	-40.1	-173.5
10 - 11	-146.3	-35.8	-182.1
11 - 12	-115.4	-32.1	-147.5
12 - 13	-59.4	-17.7	-77.1
13 - 14	-15.6	-15.0	-30.6
14 - 15	22.7	-25.7	-3.0
15 - 16	23.0	-11.9	11.1
16 - 17	0.0	-8.3	-8.3
17 - 18	14.4	0.0	14.4
18 - 19	16.8	0.0	16.8
19 - 20	20.5	-14.4	6.1
20 - 21	23.6	-23.2	0.4
21 - 22	20.2	-19.9	0.3
22 - 23	15.9	-15.6	0.3
23 - 24	17.4	-17.4	0.0
24 - 25	11.3	-23.0	-11.7
25 - 26	11.0	-21.4	-10.4
26 - 27	0.0	-13.1	-13.1
27 - 28	-57.9	-12.9	-70.8
28 - 29	-23.6	-12.2	-35.8
29 - 30	-23.0	-14.7	-37.7
30 - 31	-22.0	-13.5	-35.5
31 - 32	-5.0	-14.4	-19.4
32 - 33	5.0	-15.3	-10.3
33 - 34	8.3	-23.2	-14.9

Appendix 4 (cont.). Planimeter data for areal changes (acres) in the coastline between Sabine Pass and Bolivar Roads. (Unpublished data from R.A. Morton, 1988). Note: 1 acre = 4.047E-3 km2; 1 km2 = 247 acres

Section from points	Areal change (acres) 1930-1955/7	Areal change (acres) 1955/7-1974	Areal change (acres) 1930-1974
34 - 35	0.0	-24.8	-24.8
35 - 36	0.0	-38.8	-38.8
36 - 37	7.6	-42.0	-34.4
37 - 38	13.1	-45.3	-32.2
38 - 39	0.0	-42.2	-42.2
39 - 40	15.9	-30.0	-14.1
40 - 41	11.0	-40.1	-29.1
41 - 42	0.0	-34.6	-34.6
42 - 43	0.0	-31.5	-31.5
43 - 44	0.0	-36.5	-36.5
44 - 45	14.7	-36.7	-22.0
45 - 46	0.0	-25.4	-25.4
46 - 47	0.0	-20.2	-20.2
47 - 48	5.0	-24.2	-19.2
48 - 49	0.0	-23.6	-23.6
49 - 50	0.0	-21.4	-21.4
50 - 51	5.0	-15.6	-10.6
51 - 52	13.5	-13.5	0.0
52 - 53	16.3	-15.3	1.0
53 - 54	15.0	-5.0	10.0
54 - 55	23.2	-24.5	-1.3
55 - 56	23.2	-35.2	-12.0
56 - 57	17.2	-28.5	-11.3
57 - 58	22.3	-32.8	-10.5
58 - 59	42.0	-34.6	7.4
59 - 60	40.1	0.0	40.1
60 - 61	58.8	19.0	77.8
61 - 62	94.9	42.2	137.1
62 - jetty	94.9	42.2	137.1

8.0 References:

Ambach, W., and Kuhn, M., 1985, The shift of equilibrium-line altitude on the Greenland Ice Sheet following climatic changes, pp. 255-257, *in* Glaciers, Ice Sheets and Sea Level: Effect of a CO_2-Induced Climatic Change. Polar Research Board, National Research Council: Washington D.C., National Academy Press, 348 p.

Baker, E.T., 1979, Stratigraphic and hydrogeologic framework of the Coastal Plain of Texas: Texas Department of Water Resources Report 236. 43 p.

Balazs, E.I., 1980, The 1978 Houston-Galveston and Texas Gulf Coast vertical control surveys: NOAA Tech. Memorandum NOS NGS 27. 61 p.

Barnett, T.P., 1984, The estimation of 'global' sea level change: a problem of uniqueness: Journal of Geophysical Research, v. 89, pp. 7980-7988.

Barton, D.C., 1930, Deltaic coastal plain of southeast Texas: Geological Society of America Bull., v. 41, pp. 359-382.

Bentley, C.R., 1985, Glaciological evidence: The Ross Sea sector, pp. 178-196, *in* Glaciers, Ice Sheets and Sea Level: Effect of a CO_2-Induced Climatic Change. Polar Research Board, National Research Council: Washington D.C., National Academy Press, 348 p.

Bentley, M.E., 1980, Hydrogeology of the Beaumont Formation (Pleistocene) Brazoria County, Texas: unpub. M.A. thesis, Univ. of Texas at Austin, 105 p.

Bernard, H.A. and LeBlanc, R.J., 1965, Resume of the Quaternary geology of the northwest Gulf of Mexico Province: reprinted in Univ. of Texas at Austin, Bureau of Economic Geology Guidebook 11 - Recent sediments of Southeast Texas (1970), 64 p.

Bindschandler, R.A., 1985, Contribution of the Greenland Ice Cap to changing sea level: Present and future, pp. 258-266, *in* Glaciers, Ice Sheets and Sea Level: Effect of a CO_2-Induced Climatic Change. Polar Research Board, National Research Council: Washington D.C., National Academy Press, 348 p.

Bonnet, C.W. and Gabrysch, R.K., 1982, Development of groundwater resources in Orange County, Texas, and adjacent area of Texas and Louisiana, 1971-80: USGS Open File Report 82-330. 46 p.

Budd, W.F., and Smith, I.N., 1985, The state of balance of the Antarctic Ice Sheet - an updated assessment 1984, pp. 172-177, *in* Glaciers, Ice Sheets and Sea Level: Effect of a CO_2-Induced Climatic Change. Polar Research Board, National Research Council: Washington D.C., National Academy Press, 348 p.

Carr, J.E., Meyer, W.R., Sandeen, W.M., and McLane, I.R., 1985, Digital models for simulation of groundwater hydrology of the Chicot and Evangeline aquifers along the Gulf Coast of Texas: Texas Department of Water Resources report 289. 10 p.

Curray, J.R., 1960, Sediments and history of Holocene transgression, coast shelf, northwest Gulf of Mexico, pp. 221-266, *in* Shepard, F.P., et al, eds., Recent Sediments, northwest Gulf of Mexico, 1951 - 1958: AAPG, 394 p.

Dickinson, R.E., 1986, How will climate change?, pp. 207-270, *in* Greenhouse Effect, Climate Change, and Ecosystems, B. Bolin et al, eds. Scientific Committee on Problems of the Environment (SCOPE) of the International Council of Scientific Unions (ICSU). Chichester. John Wiley and Sons, 541 p.

Doake, C.S.M., 1985, Antarctic mass balance: Glaciological evidence from the Antarctic peninsula and Weddell Sea sectors, pp. 197-209, *in* Glaciers, Ice Sheets and Sea Level: Effect of a CO_2-Induced Climatic Change. Polar Research Board, National Research Council: Washington D.C., National Academy Press, 348 p.

Ewing, T.E., 1985, Subsidence and surface faulting in the Houston-Galveston area, Texas--related to deep fluid withdrawal?, *in* Geopressured-Geothermal Energy: Proceedings of the 6th U.S. Gulf Coast Geopressured-Geothermal Energy Conference, Dorfman, M.H., and Morton, R.A., eds. 344 p.

Fairbridge, R.W., and Krebs, O.A., 1962, Sea level and the southern oscillation: Geophysical Journal of the Royal Astronomical Society, v. 6, pp. 532-545.

Fisher, W.L., McGowen, J.H., Brown, L.F., and Groat, C.G., 1972, Environmental Geologic Atlas of the Texas Coastal Zone - Galveston-Houston area. University of Texas, Bureau of Economic Geology. 91 p.

Fisher, W.L., Brown, L.F., McGowen, J.H., and Groat, C.G., 1973, Environmental Geologic Atlas of the Texas Coastal Zone - Beaumont-Port Arthur area. University of Texas, Bureau of Economic Geology. 93 p.

Gabrysch, R.K., 1982, Groundwater withdrawals and land surface subsidence in the Houston-Galveston region, Texas, 1906-1980: USGS Open File Report 82-571, 68 p.

_____, 1984, Case history No. 9.12. The Houston-Galveston region, Texas U.S.A., *in* Guidebook to studies of land subsidence due to ground-water withdrawal, Poland, J.F., ed., UNESCO. 305 p.

Galloway, W.E., Ewing, T.E., Garrett, C.M., Tyler, N., and Bebout, D.G., 1983, Atlas of Major Texas Oil Reservoirs. Univ. of Texas at Austin, Bureau of Economic Geology.

Geertsma, J., 1973, Land subsidence above compacting oil-and-gas reservoirs: Journal of Petroleum Technology, v. 25, pp. 734-744.

Gornitz, V., Lebedeff, S., and Hansen, J., 1982, Global sea level trend in the past century: Science, v. 215, pp. 1611-1614.

Gornitz, V. and Lebedeff, S., 1987, Global sea-level changes during the past century, pp. 3-16, *in* Sea-Level Fluctuations and Coastal Evolution, Society of Economic Paleontologists and Mineralogists special pub. no. 41. Nummedal, D., et al, eds. 267 p.

Gould, H.R. and McFarlan, E., 1959, Geologic history of the Chenier Plain, southwestern Louisiana: Gulf Coast Association of Geological Societies Trans., v. 9, pp. 261-270.

Hansen, J., Johnson, D., Lacis, A., Lebedeff, S., Lee, P., Rind, D., and Russell, G., 1981, Climate impact of increasing atmospheric carbon dioxide: Science, v. 213, pp. 957-966.

_____, Lacis, A., Rind, D., Russell, G., Stone, P., Fung, I., Ruedy, R., and Lerner, J., 1984, Climate processes and climate sensitivity: Geophysical Monograph 29, American Geophysical Union, pp. 130-163.

Harris-Galveston Coastal Subsidence District, 1980, Harris-Galveston Coastal Subsidence District Water Management Program Phase 1. Prepared by: Espey-Huston and Assoc., Brown and Root, Inc., McClelland Engineers, Inc., Turner Collie and Braden, Inc., and William F. Guyton and Assoc.

Hicks, S.D., 1978, An average geopotential sea level series for the United States: Journal of Geophysical Research, v. 83, pp. 1377-1379.

Hoffman, J.S., Wells, J.B., and Titus, J.G., 1986, Future global warming and sea level rise, pp. 245-266, *in* Iceland Coastal and River Symposium, T. Sigbjarnarson, ed. Iceland National Energy Authority.

Holdahl, S.R., and Morrison, N.L., 1974, Regional investigations of vertical crustal movements in the U.S., using precise relevelings and mareograph data: Tectonophysics, v. 23, pp. 373-390.

Holzer, T.L., and Bluntzer, R.L., 1984, Land subsidence near oil and gas fields, Houston, texas: Groundwater, v. 22, pp. 450-459.

Jelgersma, S., 1966, Sea-level changes during the past 10,000 years, pp. 54-69, *in* Shepard, P.A., and Sawyer, J.S., eds., World Climate from 8000 to 0 B.C., Proceedings of the International Symposium at the Imperial College, London, April 1966, 355 p.

Jensen, R., 1985, Stopping the sinking: Texas Water Resources, v.11, no. 3, Texas Water Resources Institute, Texas A & M University, 4 p.

Jones, L.J., 1976, External costs of surface subsidence - Upper Galveston Bay, Texas: Publication no. 121 of the International Association of Hydrological Sciences: Proceedings of the Anaheim Symposium, December 1976, pp. 617-627.

Jones, P.H., Turcan, A.N., and Skibitzke, H.E., 1954, Geology and groundwater resources of southwestern Louisiana: Louisiana Geologic Survey Bull. 30, 285 p.

Kane, H.E., 1959, Late Quaternary geology of Sabine Lake and vicinity, Texas and Louisiana: Gulf Coast Association of Geological Societies Trans., v. 9, pp. 225-235.

Kaye, C.A. and Stuckey, G.W., 1973, Nodal tidal cycle of 18.6 yr. - Its importance in sea-level curves of the East Coast of the U.S. and its value in explaining long-term sea-level changes: Geology, v. 2, pp. 141-144.

Keepin, W., Mintzer, I., and Kristoferson, L., 1986, Emission of CO_2 into the atmosphere, *in* Greenhouse Effect, Climate Change, and Ecosystems, B. Bolin et al, eds. Scientific Committee on Problems of the Environment (SCOPE) of the International Council of Scientific Unions (ICSU). Chichester. John Wiley and Sons, 541 p.

Koerner, R.M., 1985, Canadian Arctic Islands: Glacier mass balance and global sea level rise, pp. 145-154, *in* Glaciers, Ice Sheets and Sea Level: Effect of a CO_2-Induced Climatic Change. Polar Research Board, National Research Council: Washington D.C., National Academy Press, 348 p.

Kreitler, C.W., 1977, Faulting and land subsidence from groundwater and hydrocarbon production, Houston-Galveston, Texas, *in* 2nd International Land Subsidence Symposium Proceedings, Anaheim, CA, 1976. International Association of Hydrological Sciences Pub. no. 121, pp. 435-445.

_____, Guevera, E., Granata, G., and McKalips, D., 1977, Hydrogeology of Gulf Coast aquifers, Houston-Galveston area, Texas: Univ. of Texas at Austin, Bureau of Economic Geology Geological Circular 77-4, pp. 72-89.

Lacis, A., Hansen, J., Lee, P., Mitchell, T., and Lebedeff, S., 1981, Greenhouse effect of trace gasses: Geophysical Research Letters, v. 8, pp. 1035-1038.

LeBlanc, R.J. and Hodgson, W.D., 1959, Origin and development of the Texas shoreline: Gulf Coast Association of Geological Societies Trans., v. 9, pp. 197-220.

Lisitzin, E., 1958, *in* Lisitzin, E., 1974, Sea Level Changes, p. 182: Elsevier Oceanography Series, 8, Amsterdam, Elsevier Scientific Publishing Co. 286 p.

Machta, L.,1983, Effects of non-CO_2 greenhouse gasses, pp. 285-291, *in* Changing Climate. Washington D.C. National Academy Press. 495 p.

Manabe, S. and Wetherald, R.J., 1975, The effects of doubling the CO_2 concentrations on the climate of a general circulation model: Journal of Atmospheric Sciences, v. 32, pp 3-15.

Marine Board, Committee on Engineering Implications of Changes in Relative Mean Sea Level, National Research Council, 1987, Responding to changes in sea level. Washington D.C. National Academy Press. 148 p.

Mc Farlan, E., 1961, Radiocarbon dating of late Quaternary deposits, South Louisiana: Geological Society of America Bull., v. 72, pp. 129-158.

McGowen, J.H., Garner, L.E., and Wilkinson, B.H., 1977, The Gulf Shoreline of Texas - processes, characteristics, and factors in use: Univ. of Texas at Austin, Bureau of Economic Geology Geologic Circular 77-3. 27 p.

Meade, R.H. and Parker, R.S., 1985, Sediment in rivers of the United States, pp. 49-60, *in* National Water Summary 1984: USGS Water Supply Paper 2275.

Meier, M.F., 1984, Contribution of small glaciers to global sea level: Science, v. 226, pp. 1418-1421.

Morton, R.A., 1975, Shoreline changes between Sabine Pass and Bolivar Roads - an analysis of historical changes of the Texas Gulf Shoreline: Univ. of Texas at Austin, Bureau of Economic Geology Geologic Circular 75-6. 43 p.

_____, 1977, Historical shoreline changes and their causes, Texas Gulf Coast: Gulf Coast Association of Geological Societies Trans., v. 27, pp. 352-364.

_____, 1979, Temporal and spatial variations in shoreline changes and their implications, examples from the Texas Gulf Coast: Journal of Sedimentary Petrology, v. 49, pp. 1101-1112.

_____ and Nummedal, D., 1982, Regional geology of the N.W. Gulf Coastal Plain, pp. 3-25, *in* Sedimentary processes and environments along the Louisiana-Texas Coast. 1982 Geological Society of America Annual Meeting Fieldtrip Guidebook. Nummedal, D., ed. 92 p.

_____ and Price, W.A., 1987, Late Quaternary sea-level fluctuations and sedimentary phases of the Texas coastal plain and shelf, pp. 181-196, *in* Sea-Level Fluctuations and Coastal Evolution, Society of Economic Paleontologists and Mineralogists special pub. no. 41. Nummedal, D., et al, eds. 267 p.

National Ocean Service, 1974, Report of the 1973 releveling of the Houston-Galveston Area, Texas. U.S. Dept. of Commerce. 48 p.

National Research Council. Climate Research Board, 1979, Carbon Dioxide and Climate Change: A Scientific Assessment. Washington D.C. National Academy Press. 233 p.

_____. CO_2/Climate Review Panel, 1982, Carbon Dioxide and Climate: A Second Assessment. Washington D.C. National Academy Press. 72 p.

_____. Carbon Dioxide Assessment Committee, 1983, Changing Climate. Washington D.C. National Academy Press. 495 p.

_____. Polar Research Board, 1985, Glaciers, Ice Sheets and Sea Level: Effect of a CO_2-Induced Climatic Change. Washington D.C., National Academy Press, 348 p.

Nelson, H.F. and Bray, E.E., 1970, Stratigraphy and history of the Holocene sediments in the Sabine - High Island area, Gulf of Mexico, *in* Morgan, J.P. and Shaver, R.H., eds., Deltaic Sedimentation - Modern and Ancient: Society of Economic Paleontologists and Mineralogists special pub. no. 15, 312 p.

Nordhaus, W.D. and Yohe, G.W., 1983, Future carbon dioxide emissions from fossil fuels, pp. 87-152, *in* Changing Climate. Washington D.C. National Academy Press. 495 p.

Orheim, O., 1985, Iceberg discharge and the mass balance of Antarctica, pp. 210-215, *in* Glaciers, Ice Sheets and Sea Level: Effect of a CO_2-Induced Climatic Change. Polar Research Board, National Research Council: Washington D.C., National Academy Press, 348 p.

Paine, J.G. and Morton, R.A., 1986, Historical shoreline changes in Trinity, Galveston, West, and East Bays, Texas Gulf Coast: Univ. of Texas at Austin, Bureau of Economic Geology Geological Circular 86-3. 58 p.

Pratt, W.E. and Johnson, D.W., 1926, Local subsidence of the Goose Creek oil field: Journal of Geology, v. 34, pp. 577-590.

Price, W.A., 1933, Role of diastrophism in the topography of the Corpus Christi area, South Texas: AAPG Bull., v. 17, pp. 907-962.

_____, 1947, Equilibrium of form and forces in tidal basins of the coasts of Texas and Louisiana: AAPG Bull., v. 31, pp. 1619-1663.

Ramsey, K.E. and Moslow, T.F., 1987, A numerical analysis of subsidence and sea-level rise in Louisiana, pp. 1673-1688, *in* Coastal Sediments '87. ASCE.

Ratzlaff, K.W., 1982, Land-surface subsidence in the Texas coastal region: Texas Department of Water Resources Report 272. 26 p.

Reeh, N., 1985, Greenland Ice Sheet mass balance and sea level change, pp. 155-171, *in* Glaciers, Ice Sheets and Sea Level: Effect of a CO_2-Induced Climatic Change. Polar Research Board, National Research Council: Washington D.C., National Academy Press, 348 p.

Revelle, R.R., 1983, Probable future changes in sea level from increased atmospheric CO_2, pp. 433-448, *in* Changing Climate. Washington D.C. National Academy Press. 495 p.

Robin, G. de Q., 1986, Changing the sea level, pp. 323-359, *in* Greenhouse Effect, Climate Change, and Ecosystems, B. Bolin et al, eds. Scientific Committee on Problems of the Environment (SCOPE) of the International Council of Scientific Unions (ICSU). Chichester. John Wiley and Sons, 541 p.

Rose, N.A., 1943, Progress report on the ground water resources of the Texas City area, Texas: USGS open-file report, 45 p.

Schlesinger, M.E., 1983, A review of climate models and their simulation of CO_2-induced warming: International Journal of Environmental Studies, v. 20, pp. 103-114.

Shepard, F.P., 1960, Rise of sea level along the northwest Gulf of Mexico, pp. 338-343, *in* Shepard, F.P., et al, eds., Recent Sediments, northwest Gulf of Mexico, 1951 - 1958: AAPG, 394 p.

_____, 1963, Thirty-five thousand years of sea level, pp. 1-9, *in* Essays in Marine Geology. University of Southern California Press. 201 p.

Swanson, R.L., and Thurlow, C.I., 1973, Recent subsidence rates along the Texas and Louisiana coasts as determined from tide measurements: Journal of Geophysical Research, v. 78, pp. 2665-2671.

Thomas, R.H., 1985, Responses of the polar ice sheets to climatic warming, pp. 301-316, *in* Glaciers, Ice Sheets and Sea Level: Effect of a CO_2-Induced Climatic Change. Polar Research Board, National Research Council: Washington D.C., National Academy Press, 348 p.

Vail, P.R., Mitchum, R.M., and Thompson, S., 1977, Seismic stratigraphy and global changes of sea level, part 4: Global cycles of relative changes of sea level, pp. 83-97, *in* Seismic Stratigraphy - Applications to Hydrocarbons: AAPG Memoir 26, 212 p.

Washington, W.M. and Meehl, G.A., 1983, General circulation model experiments on the climatic effects due to doubling and quadrupling of carbon dioxide concentration, Journal of Geophysical Research, v. 88, pp. 6600-6610.

_____, 1984, Seasonal cycling experiment on the climate sensitvity due to a doubling of CO_2 with an atmospheric general circulation model coupled to a simple mixed layer ocean model, Journal of Geophysical Research, v. 89, pp. 9475-9503.

Washington, W.M. and Williamson, D.L., 1977, A description of the NCAR global circulation models of the atmosphere in methods of computational physics, pp. 111-172,*in* Global Circulation Models of the Atmosphere, J. Chang, ed. New York. Academic Press. 348 p.

Wesselman, J.B. and Aronow, S., 1971, Groundwater resources of Chambers and Jefferson Counties, Texas: Texas Water Development Board Report 133. 173 p.

Wigley, T.M.L., Jones, P.D., and Kelly, P.M., 1986, Empirical climate studies, pp. 271-322, *in* Greenhouse Effect, Climate Change, and Ecosystems, B. Bolin et al, eds. Scientific Committee on Problems of the Environment (SCOPE) of the International Council of Scientific Unions (ICSU). Chichester. John Wiley and Sons, 541 p.

Williams, J.F. and Ranzau, C.E., 1985, Approximate water level changes in wells in the Chicot and Evangeline aquifers 1977-1985 and 1984-5, and measured compaction 1973-85 in the Houston-Galveston region, Texas: USGS Open File Report 85-158.

Winker, C.D., 1979, Late Pleistocene fluvial-deltaic deposition of the Texas coastal plain and shelf: Unpublished M.A. thesis. University of Texas at Austin. 187 p.

Winslow, A.G., and Wood, L.A., 1959, Relation of land subsidence to groundwater withdrawals in Upper Gulf Coast region, Texas: Mining Engineering, v.11, pp. 1030-1040.

Wood, L.A., and Gabrysch, R.K., 1965, An analog-model study of ground water in the Houston district, Texas, with a section on design, construction and use of analog models by E.P. Patten Jr.: Texas Water Commission Bulletin 6508, 103 p.

Yerkes, R.F., and Castle, R.O., 1969, Surface deformation associated with oil and gas field operations in the United States, pp. 55-66, *in* 1st International Land Surface Symposium Proceedings, Tokyo, 1969. International Assoc. of Hydrological Sciences pub. no. 88. 407 p.

The vita has been removed from the digitized version of this document.

PLATE 1. TOPOGRAPHIC MAP OF STUDY AREA (DIGITIZED FROM ENVIRONMENTAL GEOLOGIC ATLAS OF THE TEXAS COASTAL ZONE).

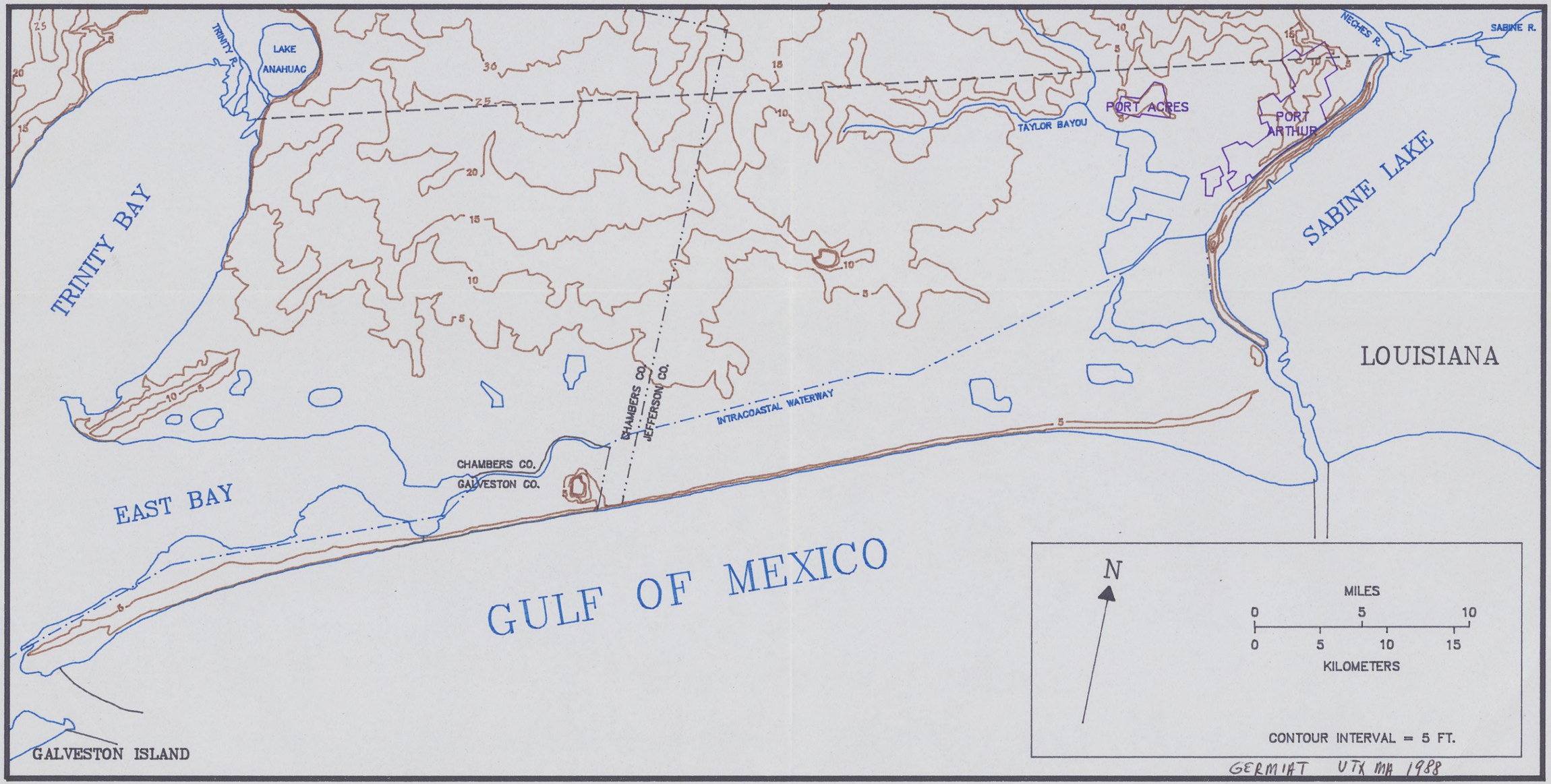

GERMIAT UTX MA 1988